Application of *in vitro*, *in silico*, and *in vivo* methodologies to quantitatively study maternal-fetal disposition of xenobiotics

Sara (Hiu Man) Shum

A dissertation

submitted in partial fulfillment of the

requirements for the degree of

Doctor of Philosophy

University of Washington

2020

Reading Committee:

Nina Isoherranen, Chair

Edward J. Kelly

Qingcheng Mao

Program Authorized to Offer Degree:

Pharmaceutics

University of Washington

Abstract

Application of *in vitro*, *in silico*, and *in vivo* methodologies to quantitatively study maternal-fetal disposition of xenobiotics

Sara (Hiu Man) Shum

Chair of the Supervisory Committee:

Nina Isoherranen

Department of Pharmaceutics

Ninety-seven percent of pregnant women in the US use at least one medication during pregnancy, yet maternal-fetal disposition of xenobiotics is under-studied. Maternal-fetal disposition of xenobitoics is determined by the maternal disposition, fetal disposition, and transplacental distribution processes which depend on the physicochemical properties of the xenobiotics and the physiological factors of the mother and the fetus. However, due to ethical concerns and to avoid unnecessary risks pose to the developing fetus, only limited maternal-fetal disposition information can be ascertained through clinical studies. Therefore, alternative experimental approaches including *in vitro*, *in silico*, and *in vivo* methodologies are required to study the maternal-fetal disposition of xenobiotics. In this dissertation, the maternal-fetal disposition of domoic acid (DA), oxycodone, and fentanyl were quantitatively studied using *in*

vitro, *in silico*, and *in vivo* methodologies. In chapter 2 and 3, the maternal-fetal disposition of DA, a hydrophilic algal toxin, was studied *in vivo* using cynomolgus monkeys as the preclinical model species. The toxicokinetics (TK) following repeated oral doses of DA before, during, and after pregnancy was measured and compared and the fetal disposition at term was described using a maternal-fetal TK model. The study showed that the renal clearance (CL_r) of DA was increased by 30-90% during pregnancy, similar to the increase in creatinine clearance which suggested that the increase in CL_r is likely mediated by the increase in glomerular filtration rate (GFR). The fetal-to-maternal plasma concentration (F/M) ratio at birth ranged between 0.3 to 0.6 and changed as a function of time. Using the maternal-fetal TK model, placental transport and recirculation of DA between the fetus and amniotic fluid were suggested to be the major determining factors of the maternal-fetal disposition of DA. In chapter 4, the fetal hepatic clearance of oxycodone, a CYP3A4 and CYP2D6 substrate, was studied *in vitro* using fetal liver microsomes (FLM) extracted from individual livers (n=18). The results of this study demonstrated that CYP3A7 metabolizes oxycodone to noroxycodone in the fetal liver, similar to the reaction mediated by CYP3A4 in the adult liver. The CYP3A7 expression in the FLMs was measured by HPLC-MS/MS to be 191-409 pmol/mg and the intersystem extrapolation factor (ISEF) was estimated to be 0.016-0.066 using 6β-OH-testosterone formation as the probe reaction. The noroxycodone formation clearance ($CL_{int,FLM}$) predicted using the recombinant CYP3A7 activity together with the CYP3A7 expression and the ISEF of each FLM successfully predicted the observed $CL_{int,FLM}$ (0.15-1.13 μL/min/mg protein) with an average fold-error of 1.24-fold. To quantitatively predict the fetal hepatic clearance (CL_h), the observed $CL_{int,FLM}$ was extrapolated using *in vitro*-to-*in vivo* extrapolation (IVIVE). The prediction suggested that the fetal liver plays a minimal role in maternal and fetal disposition of oxycodone. In chapter 5, the

maternal-fetal disposition of fentanyl, a lipophilic opioid analgesic, following epidural dosing to parturient women was studied *in silico* using a maternal-fetal physiologically-based pharmacokinetic (mf-PBPK) model. To capture the disposition of fentanyl following epidural dosing, an epidural dosing site model was developed based on the physiology of the epidural space and verified using alfentanil as a model compound. Since fentanyl is predominantly metabolized by CYP3A4 in the adult, the fetal liver metabolism of fentanyl was measured in FLM to be 0.20 ± 0.05 μL/min/mg protein and extrapolated to predict the whole fetal liver intrinsic clearance ($CL_{int,u}$) using IVIVE as established in chapter 4. The mf-PBPK model of fentanyl successfully predicted the maternal venous, umbilical venous and umbilical arterial plasma concentrations in parturient women and newborns following epidural dosing during labor and delivery with the average absolute fold errors (AAFEs) within 2-fold of the observed plasma concentrations. Using the verified mf-PBPK model, the impact of maternal, fetal, and transplacental distribution kinetics on the F/M ratio of fentanyl was demonstrated, highlighting the importance of these distribution kinetics on the interpretation of maternal-fetal disposition of xenobiotics. In conclusion, this dissertation demonstrated that the maternal-fetal disposition of xenobiotics can be quantitatively studied using *in vitro*, *in silico*, and *in vivo* methodologies and a framework was established to study the maternal-fetal disposition of other xenobiotics using these methodologies.

Dedication

To my husband, Ting,

who supports me unconditionally and loves me as I am.

To my parents, Matthew and Joannie,

who give me a wonderful family and are always proud of me.

To the almighty God,

who blesses me with the best in life and reminds me to be strong and courageous.

Acknowledgement

I would like to express my deepest gratitude to everyone who have walked with me and guided me on this journey to become an independent scientist. My doctoral advisor, Dr. Nina Isoherranen, thank you for always believing in me and encouraging me to aim high and step outside of my comfort zone. You are my role model. You showed me how to be a prudent scientist with high integrity. I will always remember everything you have taught me through words and life. My advisory committee, Dr. Danny Shen, Dr. Edward Kelly, Dr. Qingcheng Mao, and Dr. Gail Anderson, thank you for your guidance and the inspiring scientific discussions through the years. My collaborators, Dr. Mary Hebert, Dr. Tom Burbacher, Dr. Kimberly Grant, Dr. Kathi Lefebvre, and Dr. Cathy Yeung, thank you for giving me the opportunity to collaborate with you on these exciting projects and for your trust and encouragements. My past and present mentors, Dr. Stanley McKnight, Dr. Aaron Moss, Dr. Jing Yang, Dr. Greg Slatter, Dr. Terry Podoll, and Mr. Mike Zientek, thank you for the time you generously spent to guide me in many aspects of career and life. My most treasured peers, my cohort, the past and present Isoherranen's lab members and my fellow pharmaceutics graduate students, thank you for always being there to pick me up, to share my joy, and to laugh at my jokes. This journey would not have been the same without you. My parents, my grandparents, my family, and my in-laws, thank you for the unconditional love and support you have given me. Your support is my biggest motivation. My husband, Ting, thank you for loving me as I am. You are always here with me to share my success and to pick me up when I feel defeated. You are my life coach and my best friend. And my God, thank you for watching over me and being my strength and shield. You blessed me with the best people in my life and I rejoice in you.

TABLE OF CONTENTS

LIST OF TABLES

LIST OF FIGURES

Chapter 1.

Introduction

1.1 BACKGROUND

About 60 years ago, the thalidomide tragedy[1,2] raised global awareness on the need to thoroughly evaluate potential developmental toxicity of drugs before human consumption as pregnant women may have different sensitivity to drugs than nonpregnant women or men. To date, more drugs have been shown to cause various types of toxicities in human fetuses.[3–5] Some drugs interfere with early organogenesis and cause major congenital malformations if used early in gestation. For example, valproic acid and angiotensin-converting enzyme (ACE) inhibitors have been shown to cause morphological damages in the cardiovascular and neurological systems in newborns exposed prenatally.[6–8] Other drugs interfere with critical biochemical processes during fetal development and cause organ toxicity if used late in gestation. For example, learning capacity has been shown to be decreased in juvenile animals following prenatal exposure to phenobarbital.[3]

A recently published prospective longitudinal cohort study in the United States reported that 97% of pregnant women used at least one medication during pregnancy and 31% had used more than five medications during pregnancy.[9] The most used medications were antiemetic agents followed by antibiotics and analgesics including opioid analgesics. Pregnant women use drugs to treat their existing medical conditions or conditions that arise during pregnancy including epilepsy, gestational diabetes, and hypertension, which, if left untreated, can be harmful to the pregnant woman and cause detrimental effects on the health of the fetus.[10–12] Hence, drug use cannot be avoided during pregnancy and instead, the risk-to-benefit ratio must be carefully evaluated for pregnant women. Establishment of a good understanding of maternal-fetal disposition is a crucial step in determining drug safety and efficacy for this special population.

1.2 MATERNAL-FETAL DISPOSITION

1.2.1 *Xenobiotic disposition during pregnancy*

Pregnancy induces physiological changes in pregnant women to support the growth of the fetus. The most profound changes are in the cardiovascular system. The cardiac output increases substantially during pregnancy to as high as 1.5-fold of that of nonpregnant women.[13] Although the majority of this increased blood flow is to supply the placenta for fetal growth, significant renal vasodilatation during pregnancy also leads to a 40-65% increase in renal blood flow and a 50-85% increase in glomerular filtration rate (GFR).[14,15] The plasma volume also increases during pregnancy which decreases plasma protein concentrations and hematocrit. In addition to the physiological changes, glucose, lipid, and protein catabolism and homeostasis are altered during pregnancy to promote fetal development leading to altered serum biochemistry.[13] Associated with these biochemical changes, the drug metabolizing enzyme and transporter activities have also been shown to be altered during pregnancy.[16,17]

There are numerous examples in the literature that the physiological changes during pregnancy alter the pharmacokinetics (PK) of drugs.[18] For compounds that are typically eliminated unchanged in the urine through glomerular filtration and active secretion by the proximal tubule epithelial cells (PTEC), the increased renal blood flow, GFR, and drug transporter expression in the PTEC during pregnancy increases the clearance and decreases the AUC of these compounds in pregnant women. For example, the renal filtration and secretion clearances of digoxin, an antiarrhythmic that is a P-gp substrate, were increased by 1.5- to 2-fold and the AUC was decreased by 20% during pregnancy.[16] Similarly, the renal and secretion clearances of metformin, an antidiabetic drug that is an OCT2 substrate, were increased by 1.7-fold and the AUC was decreased by 20% during pregnancy.[19] For compounds that are typically

eliminated through hepatic metabolism, their clearance and AUC are altered in pregnant women due to the induction and downregulation of drug metabolizing enzymes during pregnancy. For example, the AUC of metoprolol, a beta blocker that is mainly metabolized by CYP2D6, decreased by 80% after oral administration during pregnancy.[20] The AUC of midazolam, a sedative that is eliminated through CYP3A4 metabolism, decreased by 46% after oral administration during pregnancy.[16] In contrast, the AUC of caffeine, which is mainly metabolized by CYP1A2, increased 1.5- to 2.9-fold during pregnancy.[21] Some PK changes during pregnancy are more complex. For example, decreased plasma protein concentration leads to increased fraction unbound (f_u) of valproic acid. The increased f_u increases the hepatic clearance and decreases the AUC of valproic acid in pregnant women. However, the unbound AUC of valproic acid remains unchanged because the decreased AUC is offset by the increased f_u.[22]

The altered PK during pregnancy could lead to a decrease in efficacy for some narrow therapeutic index drugs. As demonstrated for the antiepileptic drugs, lamotrigine and levetiracetam, the clearance was increased by 1.5- to 2.5-fold due to UGT1A4 induction and increased renal clearance which substantially decreased the AUC and increased the seizure frequency in pregnant women.[23] Hence, dose adjustment is required in pregnant women to ensure optimal level of seizure control is reached.

1.2.2 *Placenta transfer*

The placenta is the interface of nutrients and waste exchange between maternal and fetal circulation. The human placenta is divided into 10-40 cotyledons that are perfused with maternal and fetal blood.[24] About 10% of the maternal blood and 40% of the fetal blood perfuse the placenta. The maternal and fetal blood is separated by layers of cytotrophoblasts, a single layer

of syncytiotrophoblast, and the fetal endothelium. Xenobiotics in maternal circulation are distributed to the fetal circulation (and vice versa) across these cellular barriers through passive and active mechanisms. The passive diffusion clearance depends on the physicochemical properties of the compound (e.g. pKa, logP, MW), as demonstrated by the correlation between BeWo monolayer permeability and *ex vivo* human placental transfer.[25] The *ex vivo* human placental transfer has been shown to be more rapid for lipophilic compounds than hydrophilic compounds.[26] On the other hand, the active transport clearance is mediated by drug transporters expressed in the syncytiotrophoblast.[27] As demonstrated *in vivo* in rats and *ex vivo* in human placenta perfusion experiment for abacavir, an antiretroviral drug to prevent vertical HIV transmission from the mother to the child, the transplacental clearance is facilitated by a bidirectional transporter, ENT1.[28] Also using rat placenta, the fetal to maternal transplacental clearance (CL_{fm}) of glyburide, an antihyperglycemic, was demonstrated to be mediated by the efflux transporters P-gp and BCRP expressed in the placenta.[29] In addition to the increased rate of transplacental distribution, the asymmetrical CL_{fm} and the CL_{mf} impact the extent of fetal exposure in relationship to the maternal exposure (i.e. fetal to maternal AUC ratio). As demonstrated in rats, the fetal-to-maternal AUC ratio of metformin, an antihyperglycemic, was decreased in $OCT3^{-/-}$ pregnant mice compared to the wildtype control.[30] Similarly, the fetal-to-maternal AUC ratio of nitrofurantoin, an antibiotic for treatment of urinary tract infection, has been shown to be increased in $BCRP^{-/-}$ pregnant mice compared to the wildtype control.[31] Furthermore, the risk of congenital anomalies of infants exposed to more than one drugs that could potentially interact with P-gp or BCRP prenatally has shown to be increased which demonstrated the importance of placental transport in the maternal-fetal disposition.[32]

1.2.3 *Fetal hepatic metabolism*

Anatomically, the fetal liver is situated between the placenta and the fetal systemic circulation, giving it an important role in drug disposition in the fetus. The oxygenated fetal blood, together with drug or xenobiotics that crosses the syncytiotrophoblast barrier, returns from the placenta through the umbilical vein. Before the blood reaches the fetal systemic circulation, it is first routed through the fetal liver. Hence, the fetal liver acts as a first-pass organ for the fetus to metabolize the drug or xenobiotics that crosses the placental barrier and distributes to the fetus.[33] However, in contrast to the liver anatomy of adult that 100% of the blood from the hepatic portal vein perfuse the liver, about 20-70% of the umbilical venous blood flow is shunted through the ductus venosus bypassing the hepatic sinusoids directly to the inferior vena cava.[33,34] This direct connection between the umbilical vein and the inferior vena cava limits the fetal liver function as a partial first-pass barrier.[35]

The metabolic capacity of the fetal liver has been amply demonstrated in the literature through gene and protein expression of drug metabolizing enzymes and drug metabolism activities in fetal liver microsomes (FLM) and hepatocytes.[36,37] The drug metabolizing enzyme expression and abundance is markedly different between the fetal liver and the adult liver. Developmental transition of isozymes at birth have been shown for drug metabolizing enzymes, for example, the expression of CYP3A4, the most abundant CYP in adult liver (~50 pmol/mg protein), has been shown to be low in the fetal liver (<1 pmol/mg protein).[38] In contrast, CYP3A7 has been shown to be abundantly expressed in the fetal liver (~200 pmol/mg protein). After birth, the expression of CYP3A7 gradually decreases and the expression of CYP3A4 gradually increases until they reach the adult expression levels.[38] Similarly, developmental transition has been shown for FMO1 in fetal liver to FMO3 in adult liver, and from GSTP in

fetal liver to GSTM in adult liver.[37] Some enzymes that are expressed in adult liver including CYP1A2, 2C8, 2D6, 2E1 and UGT1A1, 1A4, 2B7, 2B15 have been detected in the fetal liver but the expression is minimal.[36,37,39] Other enzymes including SULT1A1 and UGT2B4 have been shown to express at similar level in fetal and adult liver.[37,39] These unique drug metabolizing enzyme expression patterns in the fetal liver suggest that the metabolic profile of xenobiotics is substantially different between fetal and adult liver, and that the fetal liver metabolism cannot be simply scaled using adult liver metabolism based on bodyweight.

1.2.4 *Fetal renal clearance and amniotic fluid*

Kidney is a major elimination organ for hydrophilic compounds which are not extensively metabolized and not highly bound to plasma protein. These compounds are mainly eliminated in the urine through passive filtration at the glomerulus or active secretion by drug transporters expressed in the PTECs. The blood flow to the kidney is about 20% of the total cardiac output and the glomerular filtration rate (GFR) is about 120 mL/min in adult. Similar processes are also present in the fetal kidney as it develops over the gestational period.[40] However, the role of the fetal kidney in homeostasis maintenance and xenobiotic elimination is different from that in adult. The blood flow to the kidney is about 4-5% of the total cardiac output in the fetus[41] and the GFR is significantly less than adult even at term (~2 mL/min) due to the lower fetal blood pressure (40 – 60 mm Hg).[40,42] The drug transporters and ion channels are also not fully developed in the fetus resulting in hypotonic fetal urine.[40]

Instead of elimination, xenobiotics excreted through fetal urine end up in the amniotic fluid which is subsequently reabsorbed to the fetal circulation through deglutition and intramembranous absorption.[43] This physiology creates a recirculating pathway of xenobiotics between the fetus and the amniotic fluid. For compounds that are highly bound to plasma

protein, this recirculation is likely not quantitatively significant. However, for polar compounds that are not highly bound to plasma proteins, they are likely eliminated through urine to the amniotic fluid. And because of their polarity, the reabsorption to the fetal circulation will be slow resulting in a long residence time in amniotic fluid.[44] For example, the amniotic fluid concentration of lamivudine, an antiretroviral drug that is mainly eliminated unchanged in urine, has been shown to be 12-fold higher than maternal plasma concentration.[45] This long residence time in amniotic fluid could increase the residence time in the fetus.

1.3 METHODOLOGIES TO STUDY MATERNAL-FETAL DISPOSITION

1.3.1 *Clinical study of maternal-fetal disposition*

Maternal-fetal disposition can be studied through clinical studies. However, because of ethical considerations, clinical studies in pregnant women are limited to opportunistic studies. In fact, a meta-analysis showed that out of the 502 clinical studies in pregnant women reported between 2000 and 2009, 53% were preventive studies in maternal and fetal conditions and 47% were therapeutic trials of pharmacological interventions on existing conditions in the mother or the fetus.[46] Although clinical studies in pregnant women are mostly restricted to opportunistic studies, they provide valuable maternal-fetal disposition knowledge. First, PK of drugs in pregnant women can be measured at various time points over gestation period. For example, the clearances of several antiepileptic agents were measured in pregnant women at each trimester to monitor for changes from nonpregnant baseline.[47] These clinical studies not only yield information on disposition of the studied drugs during pregnancy, but more importantly, they provide information on pregnancy-induced physiological changes.[16,20] Second, fetal disposition can be measured in these studies. Typically, umbilical cord (umbilical vein and umbilical arteries) plasma concentration can be obtained at birth which provides information on fetal drug

disposition relative to maternal drug disposition (i.e. F/M plasma concentration ratio). However, information obtained from a single plasma concentration time point is limited. Depending on the sampling time point, the plasma concentration ratio might not represent fetal exposure relative to maternal exposure (i.e. AUC_f/AUC_m ratio), especially before the maternal and fetal plasma reaches distribution equilibrium.[48] Also, since umbilical cord samples are usually taken at birth, fetal disposition at different time points over gestation cannot be ascertained.

1.3.2 *Preclinical studies of maternal-fetal disposition*

Maternal-fetal disposition can be studied in preclinical animal species when clinical studies are not feasible. Since more invasive procedures can be done in preclinical studies, more information can be obtained. For example, fetal baboons were cannulated for fetal dosing and plasma sampling to measure placental transfer clearance and fetal clearance of morphine.[49] Although animal model is a viable alternative to study maternal-fetal disposition, a major disadvantage of studying animals is that species differences could substantially affect mechanistic understanding of maternal-fetal disposition. Hence, these differences have to be carefully considered when maternal-fetal disposition measured in animals is extrapolated to the maternal-fetal disposition in humans. For example, the rodent placenta is trichorial (multiple layers of syncytiotrophoblast) but the human placenta is monochorial (single layer of syncytiotrophoblast)[50] which might result in different rate and extent of placental transfer. Also, the expression of drug metabolizing enzymes can be different from species to species. For example, the fetal metabolism of morphine in baboon fetus has been shown to be higher than that in human fetus.[51]

1.3.3 *In vitro methods to study fetal liver metabolism*

Like adult liver metabolism, fetal liver metabolism can be studied using fetal liver microsomes (FLM). Limited number of xenobiotics including codeine,[52] dextromethorphan,[53] ethylmorphine,[54] morphine,[55] glyburide,[56] and retinoic acid,[57] have reported FLM metabolism in the literature. The FLM intrinsic clearances ($CL_{int,FLM}$) measured in the above studies were 10 – 40% of the intrinsic clearance ($CL_{int,HLM}$) obtained adult HLM. These results suggest a significant metabolic capacity of the fetal liver. Although measuring fetal metabolism using FLM is one of the most direct ways to characterize fetal metabolism of xenobiotics, one major limitation of this approach is the scarcity of fetal liver tissue.

Another approach to measure fetal liver metabolism is to use recombinant enzymes for enzymes that are known to be abundantly expressed in the fetal liver. For example, an extended list of xenobiotics has been tested and shown to be substrates of CYP3A7 including midazolam, tacrolimus, carbamazepine, alfentanil, and glyburide.[56,58,59]

1.3.4 *Quantitative prediction of fetal hepatic clearance (CL_h) by in vitro to in vivo extrapolation (IVIVE)*

The ultimate goal of measuring fetal hepatic metabolism *in vitro* is to predict how the fetal hepatic metabolism impacts *in vivo* maternal-fetal disposition. Theoretically, fetal hepatic metabolism can affect maternal-fetal disposition in two ways: 1) decreases maternal and fetal exposure by increasing the total body clearance in pregnant women, although it is highly unlikely because of the significant size difference between adult and fetal liver (1.8 kg vs 0.13 kg) and 2) decreases fetal exposure as the fetal liver functions as a first-pass barrier organ for xenobiotics that cross the placenta. Hence, it is important to quantitatively evaluate the fetal hepatic clearance by predicting the fetal CL_h.

To predict the fetal CL_h, the *in vitro* measured $CL_{int,FLM}$ can be extrapolated to predict the *in vivo* whole fetal hepatic clearance (CL_h) through IVIVE. Although this method is commonly used to predict adult CL_h, this quantitative prediction has not been done to predict fetal CL_h until recently for retinoic acid.[57] The fetal CL_h can be predicted from the $CL_{int,FLM}$ together with the microsomal protein yield (i.e. MPPGL), the liver size, and hepatic blood flow. Basically, scaling the $CL_{int,FLM}$ to the whole liver CL_{int} based on the liver size and predicting the CL_h using the well-stirred model.[60] The advantage of this method is that minimal characterization of the enzymes is needed, the $CL_{int,FLM}$ can be scaled directly with limited kinetics knowledge (e.g. K_m, V_{max}). The disadvantage of this method is the scarcity of fetal tissues as they are not readily accessible like HLM for research.

Alternatively, fetal CL_h can be predicted from the $CL_{int,enzyme}$ together with enzyme abundance and hepatic blood flow. Similar to the prediction using $CL_{int,FLM}$, the $CL_{int,enzyme}$ can be scaled to the whole fetal liver CL_{int} based on enzyme abundance in the fetal liver. The resulting CL_{int} can then be used to predict the CL_h using the well-stirred model. Scaling using activities measured in recombinant enzymes requires knowledge of enzyme abundance in the fetal liver. Efforts have been made over the years to estimate the metabolizing enzyme, CYP3A7 in particular, abundance in the fetal liver using indirect measurement methods including gene expression[36,61] or probe substrate metabolism.[38] In light of the advancement in technology, direct quantitative measurement of enzyme abundance in the fetal liver have been done in the recent years through proteomics.[56] The advantage of scaling fetal CL_h from the $CL_{int,enzyme}$ is that most recombinant enzymes are relatively easy to express and are readily accessible for research. The disadvantage is that the recombinant enzyme expression systems typically are of insect cell or bacterial origin, hence, the cellular membrane environment of these systems is different from the

mammalian system that has been shown to affect the catalytic capacity (i.e. k_{cat}) of the enzymes.[62]

1.3.5 *Physiologically-based pharmacokinetic (PBPK) model*

PBPK models are multicompartmental PK models that incorporate physiological parameters to predict drug or xenobiotics disposition in the population of interest. The development of a PBPK model consists of three independent components: 1) physiology or system component, 2) drug-specific component, and 3) study design component.[63] The system component includes the physiological parameters in the population of interest, for example, organ volume, organ blood flow, and hepatic enzyme expression.[64] The drug-specific component includes the physicochemical and PK properties of the drug, for example, plasma protein binding and enzyme kinetics which can be obtained from *in vitro* studies. The study design component describes the specific trial design, for example, route of administration, dosing regimen, and sampling schedule. Theoretically, PBPK model can be built using a bottom-up approach with experimentally determined parameters (e.g. protein binding, blood to plasma partitioning, HLM metabolism) or parameters predicted using mechanistic modeling[65] to predict *in vivo* PK in humans. Alternatively, the model can be built using a top-down approach, for example, back-calculation of hepatic CL_{int} from the systemic clearance observed following IV dose using the hepatic well-stirred model.[60] However, pragmatically, a hybrid middle-out approach combining bottom-up and top-down approaches is often used.[66]

PBPK modeling has gained tremendous popularity in recent years in pharmaceutical research. It has been applied to research at various stages of drug discovery and development,[67] prediction of drug-drug interactions (DDI),[68] and pediatric drug development.[69] PBPK modeling offers several key advantages over other PK modeling tools including static predictions and

compartmental PK models. First, PBPK models are predictive. Since PBPK models are built mechanistically using physiological and experimentally obtained parameters, they can predict human PK without prior knowledge.[70] Second, PBPK model allows dynamic simulation of the time course of drug disposition. Dynamic predictions are superior to static predictions because they take into account other PK properties of the drug. For example, the half-lives of the perpetrator and the victim drugs are taken into account to predict a DDI, which avoids overprediction of a DDI by static prediction using the C_{max}.[71] Third, the mechanistic information of drug disposition allows extrapolation from one population to another. It provides an *in silico* alternative to clinical studies which is especially valuable for vulnerable special populations (for example, pediatric and pregnant women) where clinical studies are hampered.[69]

1.3.6 *Maternal-fetal PBPK (mf-PBPK) model*

PBPK modeling is especially useful in the context of predicting maternal-fetal disposition in humans because of the dynamic simulation of the time course of the plasma concentration for both the mother and the fetus when this information is difficult to ascertain through clinical studies. Starting from the early 1980s, mf-PBPK models with different levels of complexity have been developed to describe maternal-fetal drug disposition in humans and preclinical animal species.[72] As more information on the physiological and metabolic changes during pregnancy becomes available, new mf-PBPK models are developed to incorporate these changes.[73] For example, CYP induction and downregulation are captured and verified in these newly developed mf-PBPK models.[74–76] On top of maternal physiology, placental and fetal physiology have also been incorporated into mf-PBPK models.[77–79] These added complexities will allow more mechanistic prediction of maternal-fetal disposition. For example, fetal hepatic metabolism and exchange between the fetus and the amniotic fluid can be captured with these new mf-PBPK

models. On the downside, the verification of the fetal physiological parameters is challenging as limited clinical fetal drug disposition information is available.

1.4 NEUROLOGICALLY ACTIVE XENOBIOTICS

Brain development starts as early as the third gestational week and continues postnatally into early childhood.[80] The neurodevelopmental events are highly complex and that the expression of neurotransmitter receptors, transporters, and enzymes is tightly coordinated and dynamic during development.[5] Hence, fetal exposure to neurologically active xenobiotics that modulate neurotransmission processes can interrupt brain development and cause neurotoxicity including altered neuroanatomical morphology, decreased cognitive functions, and behavioral problems that manifested later in life.[5,81] Some commonly used prescription or recreational drugs including opioids, amphetamines, and cocaine are known to cause fetal neurotoxicity.[82] For example, opioids interact with opiate receptors in the brain and their use during pregnancy has been shown to be associated with neonatal opioid withdrawal syndrome (NOWS), neurological disorders, and impairment of psychomotor developments.[83,84] In addition to drug use during pregnancy, pregnant women may be exposed to environmental toxins that may cause neurotoxicity. For example, methylmercury is well-recognized to cause blindness, deafness, and mental retardation in children who are exposed prenatally.[85,86]

1.4.1 *Domoic acid (DA)*

DA is a neurotoxin produced by species of marine algae, *pseudo-nitzschia*, that humans get exposed to through consumption of contaminated seafood.[87] DA activates glutamate receptors[88] and potentiates NMDA receptors[89] which prolongs neuronal excitation that causes brain lesions in some severe cases of acute neurotoxicity in humans and animals.[90,91] Chronic

exposure to DA has been shown to cause oxidative stress, alter glutamatergic transmission, and alter neuronal connectivity in the brain in multiple animal species[92–94], and was associated with impaired daily memory in humans.[95] These excitotoxicities of DA have been shown to impair cognitive and behavioral development in juvenile animals exposed to DA prenatally.[96–100] Despite the fetal neurotoxicity observed in animals, little is known about the maternal-fetal disposition of DA following oral administration, a relevant route of exposure for humans. Knowledge of the maternal-fetal disposition of DA is essential to understand the dose-toxicity relationship of DA for pregnant women, which is critical to establish safety guidelines for pregnant women who are at risks of DA exposure.

DA is a hydrophilic (LogP: -0.23) small molecule that is ionized with three negative charges and one positive charge at physiological pH.[101] Consistent with these physicochemical properties, DA is mainly excreted unchanged in urine following intravenous administration in monkeys and rats[102,103] and it follows flip flop kinetics following oral dose as a result of a slow absorption rate.[103] Based on these PK properties of DA, the maternal-fetal distribution of DA is expected to be slow and DA is expected to accumulate in the amniotic fluid. This is supported by the observation in the California sea lions that DA accumulates in the amniotic fluid which was suggested to prolong fetal exposure.[104]

In this dissertation, the maternal-fetal disposition of DA following repeated oral doses was studied in cynomolgus monkeys. Changes of toxicokinetics (TK) of DA were studied at multiple time points before, during, and after pregnancy. Fetal disposition of DA at delivery was studied through infant plasma sampling and maternal-fetal PK modeling.

1.4.2 *Oxycodone*

Oxycodone is an oral opioid analgesic that is commonly prescribed to pregnant women to treat moderate and severe pain.[105,106] The use of opioids during pregnancy, particularly during synaptogenesis at the third trimester, has been shown to be associated with neonatal opioid withdrawal syndrome (NOWS).[82,107] Further, NOWS has been shown to be associated with impaired childhood neurodevelopment.[83,84] Oxycodone is a lipophilic (LogP: 0.7) weak base (pKa of 8.53) that is widely distributed in the body (V_{ss} = 2 L/kg). Based on the physicochemical properties, oxycodone is expected to cross the placenta and distribute to the fetus. This is supported by two clinical studies reporting similar plasma concentrations in umbilical cord plasma and in maternal arm vein plasma at delivery following intravenous and subcutaneous administration of oxycodone to parturient women.[108,109]

Oxycodone is mainly metabolized in the liver by CYP3A4 and CYP2D6.[110] It is N-demethylated by CYP3A4 into noroxycodone, the major metabolite, and O-demethylated by CYP2D6 into oxymorphone, an active metabolite in adult.[111] Based on the overlapping substrate specificity between CYP3A4 and CYP3A7[112] and the abundance of CYP3A7 expression in the fetal liver,[38] the fetal liver is expected to metabolize oxycodone to noroxycodone. In contrast, because the minimal expression of CYP2D6 in the fetal liver,[36] the fetal liver is not likely to form oxymorphone.

In this dissertation, the fetal metabolism of oxycodone was studied. Metabolite formed and the main enzyme mediating the reaction was characterized. The quantitative contribution of fetal liver in maternal-fetal disposition was predicted using IVIVE.

1.4.3 *Fentanyl*

Fentanyl is a potent synthetic opioid that is commonly used as an analgesic agent given through IV and epidural administrations to pregnant women during labor and delivery.[113,114] Its use during labor is generally considered safe as limited adverse fetal outcomes have been observed following intravenous or epidural administration of fentanyl to parturient women.[114,115] Maternal-fetal disposition of fentanyl following epidural administration has been reported in parturient women with the umbilical vein to maternal vein plasma concentration ratio ranging between 0.5 to 0.94[116,117] suggesting that the fetus is exposed to similar concentrations of fentanyl as the mother.

Fentanyl is a lipophilic (LogP: 4.05) weak base (pKa of 8.99)[118] that is widely distributed in the body (V_{ss} = 4 L/kg). Fentanyl is mainly eliminated through hepatic metabolism mediated by CYP3A4 with less than 5% of the IV dose excreted unchanged in urine.[119] The systemic clearance of fentanyl has not been reported in pregnant women, but is expected to increase in pregnant women based on the CYP3A4 mediated metabolism increase observed in pregnant women.[16] Similar to oxycodone, the fetal liver is expected to metabolize fentanyl because of the overlapping substrate specificity of CYP3A4 and CYP3A7.

In this dissertation, the maternal-fetal disposition of fentanyl following IV and epidural doses was studied using mf-PBPK modeling. A novel epidural model was developed based on physiology of the epidural space and verified using alfentanil as the model compound. The maternal-fetal disposition of fentanyl following IV and epidural doses were simulated and compared.

1.5 HYPOTHESIS AND SPECIFIC AIMS

The overarching hypothesis of this dissertation is that the maternal-fetal disposition of drugs and xenobiotics can be quantitatively predicted using *in vivo*, *in vitro*, and *in silico* methodologies. To test this hypothesis, the maternal-fetal disposition of DA, oxycodone, and fentanyl was studied using *in vivo*, *in vitro*, and *in silico* approaches.

The first aim of this dissertation was to study the maternal-fetal disposition of DA following repeated oral doses using cynomolgus monkeys as the model species. Female monkeys were dosed orally with DA daily before, during, and after pregnancy. The maternal PK was measured at various time points to elucidate the effect of pregnancy on DA disposition and the maternal-fetal disposition was measured at delivery. Two steps were taken to accomplish this aim. First, an HPLC-MS/MS method was developed and validated to quantify DA in monkey plasma and urine. The method validation was performed according to the FDA bioanalytical method validation guidance. This method was also cross validated to quantify DA in human plasma and urine which can be applied to precisely quantify DA in preclinical and clinical samples (**Chapter 2**). Second, plasma, urine, and amniotic fluid samples were measured using the validated HPLC-MS/MS method. The PK of DA before, during, and after pregnancy and the maternal-fetal disposition of DA was quantitatively described using a maternal-fetal PK model (**Chapter 3**).

The second aim of this dissertation was to quantitatively predict the contribution of fetal hepatic clearance on the maternal-fetal disposition of oxycodone. The intrinsic clearance of oxycodone was measured in FLM and recombinant CYP3A7 and the measured intrinsic clearance was used to predict the fetal CL_h by IVIVE (**Chapter 4**).

The third aim of this dissertation was to quantitatively predict the time course of maternal-fetal disposition of fentanyl following epidural and IV dosing to parturient women using a maternal-fetal PBPK model with a novel epidural dosing site model (**Chapter 5**).

Chapter 2.

A validated HPLC-MS/MS method to quantify low level domoic acid in biological samples

A version of this chapter was published as a research article: ACS Omega (2018) 3(9):12079-12088

Authors: Sara Shum, Jay S. Kirkwood, Jing Jing, Rebekah Petroff, Brenda Crouthamel, Kimberly S. Grant, Thomas M. Burbacher, Wendel L. Nelson, and Nina Isoherranen

2.1 ABSTRACT

Domoic acid (DA) is a marine neurotoxin produced by several species of *Pseudo-nitzschia*. DA causes severe neurological toxicity in humans and animals. To address the current analytical need to quantify low levels of DA in human and animal body fluids, a sensitive and selective high performance liquid chromatography-tandem mass spectrometry method was developed to measure DA in plasma and urine. This method was fully validated to accurately and precisely quantify DA between 0.31 and 16 ng/mL in plasma and between 7.8 and 1000 ng/mL in urine. Our group introduced the use of a novel internal standard, tetrahydrodomoic acid to control for matrix effects and other sources of variability. The validated method will be useful to assess DA concentrations in biological samples of human or animal origin after suspected DA exposure from contaminated food. It will also be applicable to sentinel programs and research studies to analyze body fluids with low levels of DA.

2.2 INTRODUCTION

Domoic acid (DA) is a marine neurotoxin produced by several species of diatoms of *Pseudo-nitzschia*.[87] DA is readily filtered and taken up by shellfish that is subsequently consumed by predators and humans. Exposure to DA via consumption of contaminated shellfish is a risk to human health. During a marked algal bloom in 1987, 107 people experienced acute neurological symptoms, and three died shortly after eating mussels contaminated with DA.[90,120] To protect human health, DA monitoring programs have been established, and extensive efforts have been made to develop sensitive and selective methods to measure DA concentrations in seafood and seawater.[121] The recently developed methods include indirect measurement of DA via competitive enzyme-linked immunosorbent assay (ELISA)[122] and direct measurement of DA

via liquid chromatography-tandem mass spectrometry (LC-MS/MS)[123–131] or laser ablation-MS.[132] These methods have been successful in monitoring DA in matrices that are available in large quantities, such as seawater and mussels. However, no methods have been published to determine DA concentrations in human blood or urine after potential exposures to subacute doses of DA, and plasma DA concentrations have not been reported in humans following contaminated shellfish consumption.[133,134] DA exposures have, however, been measured using indirect competitive ELISA followed by confirmatory LC-MS/MS in marine mammals, such as California sea lions (CSLs),[135] exposed to DA via food and showing neurological symptoms of acute or chronic toxicity. The DA concentrations ranged from undetectable to 200 ng/mL in serum and from undetectable to 3,700 ng/mL in urine. On the basis of estimates of DA exposure and toxic effects observed therein, and from results of laboratory studies in nonhuman primates, researchers and environmental health agencies have proposed estimates for tolerable daily intake (TDI) of DA from 0.075 to 0.1 mg/kg/day.[136–139] However, recent studies have shown that some recreational harvesters consume DA in excess of the proposed TDI[133] and that chronic low-level exposure to DA is associated with memory loss.[134] On the basis of the dose-exposure relationship in nonhuman primates and physiologically-based pharmacokinetic (PBPK) modeling and simulations,[103] we predicted that a bioanalytical method with a lower limit of quantification (LLOQ) around 0.2-0.4 ng/mL is needed to detect DA in human or nonhuman primate plasma after exposure to DA at or above the proposed TDI. None of the currently available methods to detect DA in serum by LC-MS/MS reaches this sensitivity, and a single method has been reported to detect DA in urine at this level (**Table 2.1**). Hence, more sensitive, validated, LC-MS/MS methods are needed to assess human DA exposures.

DA is a hydrophilic molecule (clogP = -0.23, value obtained from Drug Bank on June 12, 2018, https://www.drugbank.ca/drugs/DB02852) with three carboxyl groups (pKa: 1.85, 4.47, 4.75) and an amine group (pKa: 10.60)[101] as shown in **Figure 2.1A**. The ionized and polar nature of DA makes extraction from biological matrices challenging. Solid phase extraction (SPE) has been used to obtain DA from complex samples,[123,140–143] but this step can introduce variability into the assay via sample recovery.

Several bioanalytical methods have been developed or optimized to measure DA concentrations directly or indirectly in serum and urine samples from various mammalian species as listed in **Table 2.1**. However, validation data have not been provided for any of the LC-MS methods for serum analysis and for only one of the urine analysis methods.[143] Despite the extraction methods used in the published assays and the known variability in analyte ionization in LC-MS/MS methods, none of these published methods for serum and urine analyses includes an internal standard. In mussel and seawater analyses, the deuterated dansyl chloride derivative of DA,[144] kainic acid (KA),[145] and leucine-enkephalin (ENK)[124,126] have been used as internal standards of LC-MS/MS methods. These internal standards have distinctly different chromatographic and spectrometric properties than DA, which decrease their usefulness. They have also not been applied to plasma, serum or urine analysis. To address the lack of internal standards in published methods, we explored the feasibility to use fully reduced tetrahydrodomoic acid (THDA) (**Figure 2.1B)** as a suitable internal standard for DA measurement by LC-MS/MS.

The goal of this study was to develop and validate a high performance liquid chromatography-tandem mass spectrometry (HPLC-MS/MS) method for quantification of DA in urine and plasma with sufficient sensitivity to measure DA following low level exposure to DA.

The applicability of this method was confirmed in a cohort of *Macaca fascicularis* (cynomolgus) monkeys following a single oral dose of 0.075 mg/kg DA (proposed human TDI for DA). To further enhance the applicability, the method was cross-validated in human plasma.

2.3 Materials and Methods

2.3.1 *Chemicals and reagents*

A certified calibration standard of DA (332 μM) in acetonitrile/water (1:19, v/v) was purchased from National Research Council Canada (Halifax, NS, Canada). HPLC solvents including Optima LC/MS grade water, acetonitrile, methanol and formic acid were purchased from Fisher Scientific (Pittsburgh, PA). DA, dihydrokainic acid (DHKA), acetaldehyde, sodium nitroprusside, sodium carbonate, and sodium bicarbonate were purchased from Millipore Sigma (St. Louis, MO). Frozen treatment-naïve monkey plasma and urine were obtained from the Washington National Primate Research Center (WaNPRC) at the University of Washington (Seattle, WA). Frozen human plasma and urine were obtained from banked tissue at the University of Washington (Seattle, WA).

The internal standard THDA was synthesized as previously described.[146] Briefly, 1.5 mg of DA powder was dissolved in 5 mL of aqueous methanol (90%, v/v) prior to the addition of 10 mg platinum dioxide. The mixture was placed in a round bottom flask evacuated on a Schlenk line flushing repeatedly with argon. Hydrogen, generated by drop-wise addition of aqueous 10% sulfuric acid to an aqueous solution of sodium borohydride (37 mg, l.0 mmole, in 1.5 mL of water), was introduced to the DA-containing flask via a hypodermic needle. After 5 h, the reaction mixture was flushed with argon a few times, filtered through Celite, followed by two methanol washes. The product is a mixture of two diastereomers because the reduction process

introduces a new chiral center. This stock solution of THDA was stored at 4°C to be used as an internal standard.

The concentration of THDA was determined by a colorimetric assay using a mixture of acetaldehyde and sodium nitroprusside, commonly referred to as Simon's reagent.[147,148] This assay is used to detect certain secondary amines based on their reaction with acetaldehyde and sodium nitroprusside.[148] On the basis of their structural similarity, DHKA was chosen as the reference standard to quantify THDA. The colorimetric response at 590 nm was linear between 100 and 500 μM of DHKA under the assay conditions. For the assay, duplicate 100 μL samples of DHKA in water or THDA in 10% aqueous methanol were added to 100 μL of 50 mM sodium carbonate-bicarbonate buffer at pH 9.8 in a clear-bottom 96-well plate. To initiate the reactions, 50 μL of Simon's reagent containing 10% w/w acetaldehyde and 1% w/w sodium nitroprusside in water were added to each well. Absorbance at 590 nm was determined on a Tecan Infinite 200 PRO spectrophotometer (San Jose, CA) between 8 and 20 min following spiking of the reagent. The experiment was repeated on three different days. The purity of the product was assessed by HPLC-MS/MS to be greater than 98%. Ultraviolet absorbance was determined on Olis Modernized Aminco DW-2 spectrophotometer (Bogart, GA) and the UV spectra are shown in **Figure 2.1**.

2.3.2 *HPLC-MS/MS*

Aqueous stock solutions of the certified DA standard and THDA stock at 3.1 ng/mL (10 nM) and 0.63 ng/ml (2 nM), respectively, were used to characterize their fragmentation patterns and to optimize their MS/MS detection parameters on a Sciex 6500 QTRAP system (Foster City, CA) by positive ion electrospray ionization. The optimized MS parameters for both DA and THDA were ion source temperature at 550, curtain gas at 50, nebulizing gas (GS1) at 70, drying

gas (GS2) at 70, collision activated dissociation gas at -2, ion-spray voltage at 5500, declustering potential at 15, and entrance potential at 10. Collision energy (CE) for MS^2 analysis was set as 24 and excitation energy (AF2) for MS^3 EPI scans was set at 0.05. For MS^2 EPI scans, Q1 was set to filter for the precursor ions $[M + H]^+$ m/z 312 for DA and m/z 316 for THDA. For MS^3 EPI scans, the QTRAP function was used and Q3 filter was set up to filter for m/z 312 > 294 (CE 15) and m/z 312 > 266 (CE 20) for DA, and m/z 316 > 298 (CE 15) and m/z 316 > 270 (CE 20) for THDA.

The LC-MS method was developed and validated using a Shimadzu UFLC XR DGU-20A5 (Kyoto, Japan) equipped with a Phenomenex Synergi™ Hydro-RP 100 Å (2.5 µm, 50 x 2 mm) LC column and a guard cartridge (2 x 2.1 mm, sub 2 µm) (Torrance, CA) coupled to a Sciex 6500 QTRAP system (Foster City, CA). A 9-minute gradient elution was employed using (A) water with 0.1% formic acid and (B) 95% acetonitrile with 0.1% formic acid at a flow rate of 0.5 mL/min. Sample injection volume was 10 µL. The gradient was initiated at 5% B for one1 min, increased to 100% B over the next 3 min, kept at 100% B for 30 s before decreasing to 5% B over 30 s, and re-equilibrating at 5% B for another 4 min. Three product ions for DA (m/z 312 > 266, m/z 312 > 248, m/z 312 > 220) and for THDA (m/z 316 > 270, m/z 316 > 252, m/z 316 > 224) were monitored to confirm the identity of the analytes. MRM conditions were optimized to collision energy (CE) at 24 eV and collision cell exit potential (CXP) at 10 eV.

The on-column LOD for DA was determined by injecting 10 µL of DA standard in water at concentrations ranging from 0.031 to 0.31 ng/mL (0.1 to 1 nM). The LOD was defined as the lowest amount of DA injected producing a S/N >3 for the DA transition m/z 312 > 266. The on-column LLOQ was defined as the lowest amount of injected DA producing a S/N >3 for all three DA mass transitions m/z 312 > 266, 248, 220. Calibration standards covering 4 orders of

magnitude at concentrations ranging from 0.031 to 310 ng/mL (0.1 to 1,000 nM) of DA were prepared in water to determine the linearity of response (peak area of DA mass transition m/z 312 > 266).

2.3.3 *DA extraction from plasma and urine samples*

DA was extracted from plasma by mixing 60 µL of plasma standards or samples with 120 µL LC/MS grade methanol containing 0.63 ng/mL (2 nM) THDA and vortexed for 30 s to precipitate proteins. The precipitated plasma standards and samples were centrifuged at 16 100 g for 60 min, and the supernatant was removed for HPLC-MS/MS analysis. DA was extracted from urine by mixing 10 µL of urine standards or samples with 490 µL of LC/MS grade water containing 0.63 ng/mL (2 nM) THDA and subsequently 500 µL of methanol. The urine was vortexed for 30 s to precipitate proteins and centrifuged at 16 100 g for 15 min. The supernatant was removed for HPLC-MS/MS analysis.

2.3.4 *Method Validation*

The method was validated according to the FDA Guidance for Industry Bioanalytical Method Validation[149] using pooled cynomolgus monkey plasma and urine. The plasma calibration standards were prepared by spiking plasma with the DA certified standard and serially diluting with plasma to nine concentrations ranging between 0.16 and 16 ng/mL (0.5-50 nM). The urine calibration standards were prepared by spiking urine with DA certified standard and serially diluting with urine to nine concentrations ranging between 7.8 and 1000 ng/mL (25-3,200 nM). The calibration standards were processed and analyzed by HPLC-MS/MS as described above. The MRM chromatograms were integrated using AB Sciex MultiQuant software version 2.1.1 (Foster City, CA). DA was quantified using the peak area ratio of m/z 312

> 266 (DA) and m/z 316 > 252 (THDA), and a weighted ($1/y^2$) calibration curve was fitted linearly to the data. The $1/y^2$ weighing was used as the simplest weighing scheme providing sufficient accuracy over the concentration range used. The $1/y^2$ weighing provided better accuracy over the concentration range studied in comparison to uniform weighing. The acceptance criteria for each calibration curve was defined as greater than 75% of all nonzero concentrations determined with less than 15% error from the nominal concentrations, except at the LLOQ, which was accepted with less than 20% error.

Plasma QCs were prepared by spiking blank plasma with DA certified standard to 0.31 ng/mL (LLOQ), 0.93 ng/mL (LQC), 7.8 ng/mL (MQC), 12 ng/mL (HQC) (1, 3, 25, 40 nM). Urine QCs were prepared by spiking blank urine with DA certified standard to 7.8 ng/mL (LLOQ), 23 ng/mL (LQC), 500 ng/mL (MQC), 780 ng/mL (HQC) (25, 75, 1600, 2500 nM). Blank plasma and urine from six treatment-naïve cynomolgus monkeys with and without internal standard were analyzed for potential interference. The accuracy and precision of the method were determined on three different days. Interday variability was calculated with at least 12 replicates of each QC analyzed on three different days. Intraday variability was determined with five replicates analyzed on the same day. Calibration standards were analyzed in duplicates along with blanks and replicates of QCs (LLOQ, LQC, MQC, HQC) in each run. The LLOQ was defined as the lowest concentration in plasma or urine with S/N >3 for DA transition m/z 312 > 266 that could be repeatedly determined with less than 20% error and within 20% CV. The % error and % CV were calculated according to equations 1 and 2.

$$\%\, error = \frac{measured\ concentration - nominal\ concentration}{nominal\ concentration} \times 100 \qquad (1)$$

$$\%\, CV = \frac{\sqrt{\sum_{i=1}^{n}(x_i - \bar{x})^2 / _{n-1}}}{\bar{x}} \times 100 \qquad (2)$$

The LOD was defined as the lowest concentration in plasma and urine with S/N > 3 for the DA transition m/z 312 > 266 but did not meet the LLOQ acceptance criteria for reproducibility. QCs with less than 15% error from the nominal concentration or less than 20% error at LLOQ were accepted.

Stability of extracted samples was determined by repeated injections of QC samples (LQC, MQC, HQC) stored either in the auto-sampler at 4°C for up to five days or on bench-top at room temperature for a day. Acceptance criterion of extracted sample stability was defined as less than 15% CV from repeated injections. Long-term stability was determined by repeated analysis of spiked plasma controls at 0.93, 1.9, 3.7 ng/mL (3, 6, 12 nM) and spiked urine controls at 16, 160, 620 ng/mL (50, 500, 2000 nM) stored at -20°C and that were subjected to at least five freeze-thaw cycles. Acceptance criterion of long-term stability was defined as less than 15% CV of measured concentration from repeated analysis.

Recovery of DA was determined at 0.31, 0.93, 7.8, 12 ng/mL (1, 3, 25, 40 nM) of DA in plasma and 7.8, 23, 500, 780 ng/mL (25, 75, 1600, 2500 nM) of DA in urine in triplicates. The recovery was calculated by comparing the DA/THDA peak area ratio of samples spiked with DA prior to methanol extraction to DA/THDA peak area ratio in samples extracted with methanol and subsequently spiked with the DA at matching amount. The THDA (0.32 ng/mL) was added to all samples following extraction. The percent recovery was reported as the percentage of peak area ratio of recovery samples divided by the mean peak area ratio of control samples.

Cross validation using human plasma and urine was performed in a single accuracy and precision validation run. Plasma and urine calibration standards and QCs were prepared as described for monkey standards and QCs. Plasma and urine were pooled from banked tissue from six individuals. Potential matrix interferences were assessed by analyzing blank plasma and

urine. Duplicates of calibration standards and five replicates of LQC, MQC, HQC and four replicates of LLOQ were included in the cross validation to assess variability.

2.3.5 *Animal study samples and application of the method*

Monkey plasma and urine samples from a DA toxicokinetic study were analyzed to evaluate the applicability of the assay to determine DA exposure after a single oral dose at the proposed TDI of 0.075 mg/kg. All animal procedures followed the guidelines set by the Animal Welfare Act and the Guide for Care and Use of Laboratory Animals of National Research Council. The research protocol was approved by the University of Washington Institutional Animal Care and Use Committee. Fresh blood and urine samples were obtained at 1, 2, 4, 6, 8, 10, 12, and 24 h from 20 healthy adult female cynomolgus monkeys following a single oral dose of 0.075 mg/kg DA in 5 % sucrose in water (n = 10) or a single oral dose of 5% sucrose in water (n = 10). Training protocols using positive reinforcement were implemented to collect blood without sedation. Fresh blood was collected from the peripheral vein using sodium heparin coated collection tubes and centrifuged at 3000g for 15 min within 1 h of collection to isolate plasma from blood cells. The plasma samples were stored at -20 °C until analysis. Urine was collected from the cage pans equipped with metabolic urine collection trays at the same time fresh blood was collected. The total volume of urine in the pan was measured and a 2 mL sample was collected before discarding the rest of the urine. The urine samples were stored at -20 °C until analysis.

2.3.6 *Pharmacokinetic analysis*

Pharmacokinetic parameters, including area under the plasma concentration-time curve (AUC) and maximum plasma concentration (C_{max}) were estimated by noncompartmental

analysis using Phoenix WinNonlin (St. Louis, MO). The plasma concentration was assigned to be 0.2 ng/mL when DA was detected but was below the LLOQ for AUC calculation. The cumulative amount of unchanged DA excreted in urine (A_e) was calculated from the determined concentration and the volume of urine at all collection time intervals using equation 3. Renal clearance (CL_r) was estimated from the cumulative amount excreted unchanged in urine and the plasma AUC using equation 4.

$$A_e = \sum_{i=1}^{n} volume_i * urine\ concentration_i \quad (3)$$

$$CL_r = \frac{A_{e,\ 0-24}}{AUC_{0-24}} \quad (4)$$

2.4 RESULTS

2.4.1 *Fragmentation patterns and HPLC-MS/MS optimization*

To characterize the ionization and fragmentation of DA and THDA, MS^2 scans of the precursor ions and MS^3 scans of the two product ions were collected. The enhanced product ion (EPI) mass spectra are shown in **Figure 2.2**. The product ions observed in the MS^2 spectra for DA ($[M + H]^+$ m/z 312) are consistent with published spectral data.[150,151] The MS^3 spectra of the two product ions of DA (m/z 312 > 294 and m/z 312 > 266) and THDA (m/z 316 > 298 and m/z 316 > 270) support the analogous fragmentation of the two compounds. HPLC-MS/MS multiple reaction monitoring (MRM) was optimized for quantification of DA. The three most sensitive MS^2 product ions for DA (m/z 312 > 266, m/z 312 > 248, and m/z 312 > 220) and THDA (m/z 316 > 270, m/z 316 > 252, and m/z 316 > 224) were chosen for each compound. The final MS/MS conditions are described in the Materials and Methods section. Representative chromatograms of DA and THDA are shown in **Figure 2.3**.

The on-column limit of detection (LOD) of DA was determined to be 0.52 pg (1.7 fmol) (**Figure 2.4A**). Signal-to-noise ratio (S/N) was greater than three for transition m/z 312 > 266, while the S/N was less than three for transitions m/z 312 > 248 and m/z 312 > 220 at LOD. The on-column lower limit of quantification (LLOQ) was 1.0 pg (3.3 fmol) (**Figure 2.4B**). The S/N was greater than three for all three transitions at LLOQ.

2.4.2 *Method validation*

Selectivity of the method was assessed by analyzing blank plasma and urine samples from six treatment-naïve monkeys to determine potential matrix interference. An interference peak was observed at 2.4 minutes in both plasma and urine chromatograms with the MRM transition m/z 316 > 270 and hence, this MRM transition was not used. No interference peak was observed in the chromatograms with the other MRM transitions (**Figure 2.5a,b**). Specificity of the method was assessed by analyzing plasma and urine samples with THDA as an internal standard and without DA to determine potential interference from the internal standard. No interference peak was observed at any of the DA MRM transitions. (**Figure 2.5c,d**). DA recovery was complete in all samples with measured recoveries of 105 ± 10%, 108 ± 2%, 107 ± 10%, and 101 ± 2% at 0.31, 0.93, 7.8, 12 ng/mL (1, 3, 25, 40 nM), respectively, in plasma and 113 ± 9%, 110 ± 8%, 107 ± 3% and 106 ± 5% at 7.8, 23, 500, 780 ng/mL (25, 75, 1600, 2500 nM), respectively, in urine. Extracted samples were stable for up to five days in the autosampler and up to a day on bench-top. Plasma and urine samples were stable at -20 °C storage for at least five freeze-thaw cycles and for up to 28 weeks in plasma and 34 weeks in urine.

The DA/THDA peak area ratio was linear between 0.31 and 16 ng/mL (1 and 50 nM) of DA in plasma and between 7.8 and 1,000 ng/mL (25 and 3,200 nM) of DA in urine. All calibration curves satisfied the predefined acceptance criteria with greater than 80% non-zero

calibration standards within 15% of nominal concentration. The LLOQ in plasma was 0.31 ng/mL (1 nM), at which concentration all three mass transitions (m/z 312 > 266, 248, 220) were detected with S/N > 3. The LOD in plasma was 0.16 ng/mL (0.5 nM), at which concentration only mass transition m/z 312 > 266 was detected with S/N > 3. The LLOQ in urine was 7.8 ng/mL (25 nM), at which concentration all three mass transitions were detected with S/N > 3. The representative LC-MS chromatograms at LLOQ in plasma and urine are shown in **Figure 2.5e,f**. The intraday and interday accuracy (% error) and precision (% CV) in plasma and urine are shown in **Table 2.2**.

Overall, the accuracy and precision parameters would have passed assay validation criteria if samples were quantified without an internal standard. However, the variability in the quantification of extracted samples nearly doubled in the absence of an internal standard, and in long LC-MS run batches spanning more than a day (>150 samples), the variability exceeded 15% across the run without internal standard normalization. In addition, occasional samples prepared from plasma of individual animals plasma had approximately 50% error in accuracy when quantified without internal standard normalization. This poor accuracy was corrected to 6% via the normalization to the internal standard. This error is likely due to matrix effects on DA and THDA. Based on an analysis of calibration curves of DA and THDA in solvent and matrix, matrix effects were present for both compounds, and the matrix effect was not different between the compounds.

This LC-MS method was also cross-validated in pooled human plasma and urine. Although different background peaks were detected in human plasma and urine when compared to monkey plasma and urine, none of these interfered with the quantification of DA or THDA. The human plasma LLOQ was 0.31 ng/mL (1 nM) and the urine LLOQ was 7.8 ng/mL (25 nM).

Plasma and urine calibration standards satisfied the predefined acceptance criteria with 89 and 100% non-zero calibration standards of plasma and urine, respectively, falling within 15% of nominal concentration. The accuracy and precision data are shown in **Table 2.2**.

2.4.3 *Measuring DA in monkey plasma and urine after oral exposure to DA*

Plasma and urine DA concentrations were determined in samples collected over a 24 h period from healthy female cynomolgus monkeys (n = 10) following single oral doses of DA at the human TDI of 0.075 mg/kg. Plasma and urine concentrations from these monkeys are shown in **Figure 2.6**. A total of 77 plasma samples were collected and analyzed to measure DA concentrations. Sixty-three samples (82%) contained DA above the LLOQ at 0.31 ng/mL (1 nM). The range of determined plasma concentrations was between 0.31 and 11 ng/mL (1 and 35 nM). In the remaining 18% of samples (n = 14), DA was detected, indicating that the concentration of DA in these samples was between 0.16 ng/mL (0.5 nM, LOD) and 0.31 ng/mL (1 nM, LLOQ). A total of 60 urine samples were collected and analyzed to measure DA concentrations and DA excretion into urine. All 60 samples contained DA above the LLOQ of 7.8 ng/mL (25 nM). The range of determined urine concentrations was between 9.4 and 745 ng/mL (30 and 2400 nM). Pharmacokinetic parameters were estimated from nine monkeys (n = 9) because the AUC could not be reliably estimated from one monkey, as more than 50% of the plasma concentrations were below LLOQ. A geometric mean peak plasma concentration (C_{max}) of 2.3 ng/mL (95% confidence interval (CI): 1.2 – 4.4) was observed between 1 and 12 hours after the dose (t_{max}). The geometric mean area under the plasma concentration versus time curve ($AUC_{0\text{-}24}$) was 19 ng*h/mL (95% CI: 13–28), the geometric mean amount of DA excreted unchanged in urine ($A_{e,\ 0\text{-}24}$) was 5.2 µg (95% CI: 3.6–7.4), and the geometric mean renal clearance (CL_r) was 4.5 mL/min (95% CI: 2.5–8.2). The potential presence of DA or any

potential interference in the assay was also measured in plasma samples collected over a 24 h period from control healthy female cynomolgus monkeys (n = 10) following a single dose of 5% sucrose vehicle solution. A total of 20 plasma samples were analyzed and none of the samples contained detectable DA.

2.5 DISCUSSION

Recent reports of DA consumption exceeding the proposed TDIs in recreational shellfish harvesters[133] and the health risks associated with chronic exposure to subacute levels of DA[134] highlight the need to investigate the exposure-effect relationship of DA. A sensitive method to detect low DA concentrations in plasma and urine, such as the one described here, would provide quantitative biomarker data to define this exposure-effect relationship. On the basis of DA pharmacokinetics observed in monkeys and PBPK modeling, a C_{max} of 2 ng/mL (6.5 nM) was predicted in humans following a single oral DA consumption at the TDI (0.075 mg/kg).[103] This prediction set the required sensitivity threshold of analytical methods for DA quantification at about 5-10-fold below the predicted C_{max} (i.e. 0.2-0.4 ng/mL) to detect and quantify DA in samples from people with DA exposure near the proposed TDIs.

Despite many analytical methods having been developed for DA, only a few of them have been developed to determine DA in biological fluids such as plasma and urine.[122,123,140–143] Current published LC-MS/MS methods have largely been used to confirm the presence of DA in samples that were positive by ELISA detection,[123,135] although the analytical sensitivity of most reported LC-MS/MS methods is lower than ELISA (**Table 2.1**). ELISA methods have been validated for DA quantification in serum and urine,[122,142] whereas no validation data exist for LC-MS/MS methods used for DA quantification in plasma and only a single LC-MS/MS assay has been validated for measuring DA in urine samples.[143] The method reported here is the first

LC-MS/MS method for DA analysis that has been validated for measurement of DA in plasma samples. Importantly, the assay was validated to detect concentrations at 0.16 ng/mL (0.5 nM, LOD) and to reproducibly quantify concentrations at or above 0.3 ng/mL (1 nM, LLOQ) of DA in plasma, demonstrating sufficient sensitivity to assess subchronic exposures to DA. As shown by our study in cynomolgus monkeys, the sensitivity of this validated method was sufficient to quantify DA in plasma following a single oral dose at the proposed TDI. Similarly, our method was validated to detect and quantify DA at or above 7.8 ng/mL (25 nM, LLOQ) in urine. All urine samples collected from the monkeys dosed with DA contained quantifiable DA concentrations. Yet, the LLOQ for urine samples can be further reduced with less dilution to increase the sensitivity of the assay if needed.

One of the major challenges when developing analytical methods to detect DA in biological samples is variable recovery following complex extraction or variable MS response due to matrix effects. The recovery of DA from different marine animal samples following SPE ranged between 20 and 100% resulting in challenging quantitation of DA.[123] A few published methods used KA and ENK as internal standards in seawater and mussel analysis to control for assay variability,[124,126,145] but the distinct chromatographic and mass spectrometric properties of KA and ENK may decrease their usefulness as internal standards for DA. Another recently published method introduced the use of the labelled dansyl chloride derivative of DA as an internal standard,[144] but the sample and internal standard are derivatized separately. To address these issue with selection of an internal standard, we synthesized and validated THDA as an internal standard. THDA is structurally similar to DA and shares similar chromatographic and mass spectrometric properties. We demonstrated the appropriate chromatographic and mass spectrometric performance of THDA to control for assay variability. The use of THDA improved

the reproducibility of the method as demonstrated by acceptable accuracy and precision when the internal standard was used, but inadequate accuracy and precision in the absence of an internal standard during long LC-MS/MS runs. Importantly, although this method uses a simple single methanol extraction step, THDA can easily be applied to other LC-MS/MS and sample preparation methods that quantify DA in more complex matrices.

ELISA-based methods to determine DA concentrations in samples from marine mammals are convenient to use with minimal lab equipment requirements. However, discrepancies between results from ELISA and LC-MS/MS methods have been reported.[142] One of the possible reasons for these discrepancies is that marine mammals chronically exposed to DA may produce antibodies against DA which may interfere with the ELISA assays, and hence ELISA assays would underestimate the DA content. Another possible reason is that complex biological matrices, like plasma or serum, may contain interfering components that bind to the anti-DA antibody used in the ELISA assay which would overestimate the DA content. The validated HPLC-MS/MS method described here provides a key advantage over the ELISA by obviating the above issues and allowing direct detection of DA concentrations and exposure in chronically exposed marine animals. However, the assay described will require the investment or access to a state-of-the-art LC-MS/MS instrumentation.

In summary, the developed HPLC-MS/MS method described here has sufficient sensitivity to determine DA concentrations in monkeys following low level (~TDI) exposures. It also meets the reproducibility criteria for method validation providing improved quality of DA quantification in biological matrices. This validated HPLC-MS/MS method and the new internal standard THDA can be widely applicable to research studies and sentinel programs related to the health risks and exposure levels of DA.

Table 2.1. Summary of published bioanalytical methods and the available validation data for measurement of DA in serum or urine.

Bioanalytical method	Matrix	Species	Extraction	Sample required	LOD (ng/mL)	LLOQ (ng/mL)	Recovery (%)	Intra-day variability (%)	Inter-day variability (%)	Reference
LC-MS	Serum	Bovine	SPE-HLB	1 g	5 ng/g		92-95			[140]
LC-MS	Serum	Rat	SPE-C18	200 µL	3		95			[141]
LC-MS	Serum	Marine mammals	SPE-C18	500 µL			89-93			[123]
LC-MS	Serum	CSL	MeOH + Filtration	1 – 4 g		>20				[122]
LC-MS	Serum	CSL[b]	SPE-C18		0.48					[142]
ELISA[b]	Serum	Rat	MeOH				>100	11.50	7.80	[141]
ELISA[b]	Serum	CSL[b]	MeOH + Filtration	1 – 4 g		0.4				[122]
ELISA[b]	Serum	CSL[b]	n/a		0.25			18		[142]
ELISA[c]	Serum	CSL[b]	SPE-C18		2.5			4		[142]
LC-MS	Urine	Bovine	SPE-HLB	1 g	5 ng/g		90-98			[140]
LC-MS	Urine	Marine mammals	SPE-C18	1000 µL			79-104			[123]
LC-MS	Urine	CSL[b]	MeOH + Filtration	1 – 4 g		>20				[122]
LC-MS	Urine	CSL[b]	SPE-C18		0.48					[142]
LC-MS	Urine	Human	SPE-PAX	100 µL	0.12	0.37	88-103	2.1-7.6	2.6-12.7	[143]
ELISA[b]	Urine	CSL[b]	MeOH + Filtration	1 – 4 g		0.4				[122]
ELISA[b]	Urine	CSL[b]	n/a		0.25			14		[142]
ELISA[c]	Urine	CSL	SPE-C18		2.5			4		[142]

[a]Empty spaces indicate lack of available data. CSL, California sea lion. [b]Using polyclonal antibody (Biosense). [c]Using monoclonal antibody (MeS).

Table 2.2. Accuracy and precision data for monkey and human plasma and urine[a]

	LLOQ		LQC		MQC		HQC	
	Plasma							
	0.31 ng/mL		**0.93 ng/mL**		**7.8 ng/mL**		**12 ng/mL**	
	% error	**% CV**	**% error**	**% CV**	**% error**	**% CV**	**% error**	**% CV**
Monkey intraday	-2.3	5.6	4.4	2.6	2.4	3.7	-2.9	3.1
Monkey interday	-5.6	6.9	-1.2	5.9	0.6	4.7	-2.3	4.7
Human intraday	7.3	11	-6.2	6.9	-7.0	3.5	0.0	3.8
	Urine							
	7.8 ng/mL		**23 ng/mL**		**500 ng/mL**		**780 ng/mL**	
	% error	**% CV**	**% error**	**% CV**	**% error**	**% CV**	**% error**	**% CV**
Monkey intraday	1.8	13	-2.3	4.2	-3.4	3.2	0.0	1.9
Monkey interday	-2.9	10	2.8	7.7	-2.4	4.7	-0.5	2.1
Human intraday	4.4	7.3	8.4	1.8	11.3	3.7	11.4	0.8

[a] Intraday and interday accuracy (% error) and precision (% CV) of plasma and urine quality control (QC) samples. LQC, low QC; MQC, middle QC; HQC, high QC

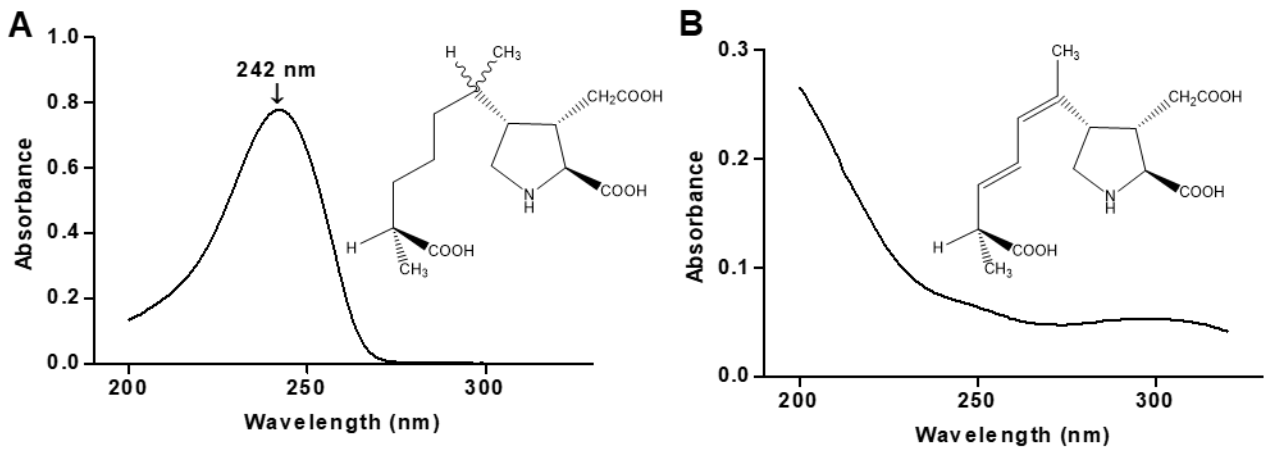

Figure 2.1. UV spectra of (A) 30 µM DA in water and (B) 20 µM tetrahydrodomoic acid (THDA) in 10% aqueous methanol.

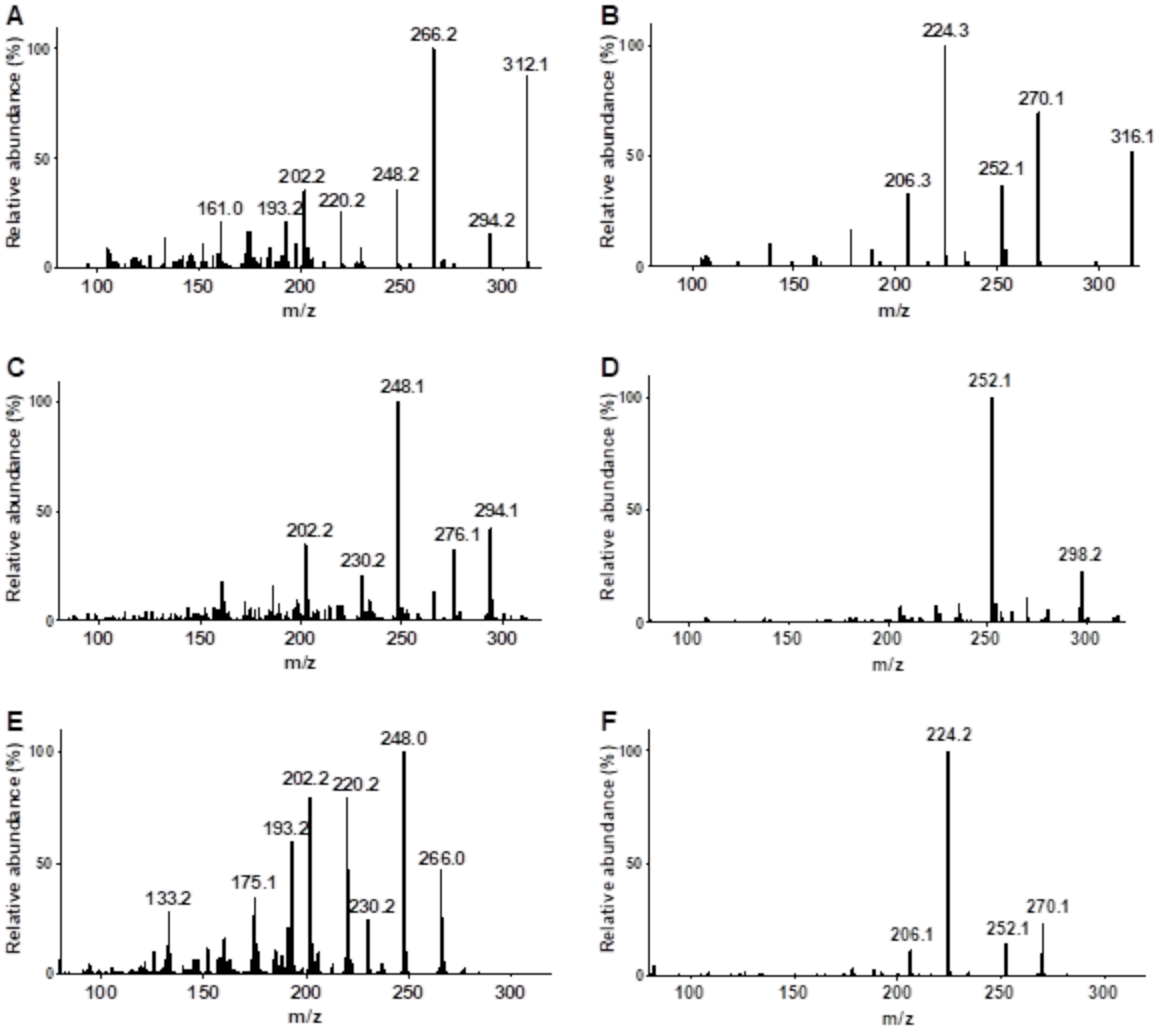

Figure 2.2. Mass spectral analysis of DA and THDA. MS^2 EPI scans of (A) 3.1 ng/mL (10 nM) DA and (B) 0.63 ng/mL (2 nM) THDA. MS^3 EPI scans of DA product ions (C) m/z 312 > 294 and (E) m/z 312 > 266. MS^3 EPI scans of THDA product ions (D) m/z 316 > 298 and (F) m/z 316 > 270.

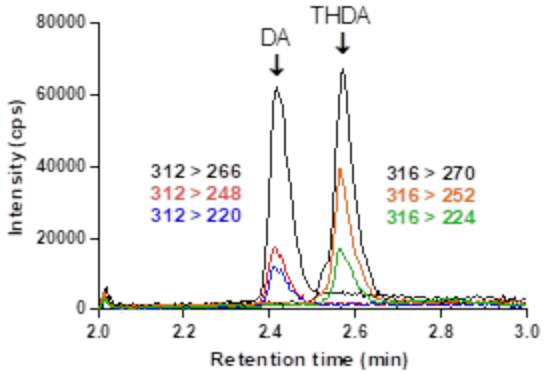

Figure 2.3. MRM chromatogram of 3.1 ng/mL (10 nM) DA and 0.63 ng/mL (2 nM) of THDA. DA elutes at 2.4 minute while THDA elutes at 2.6 minute.

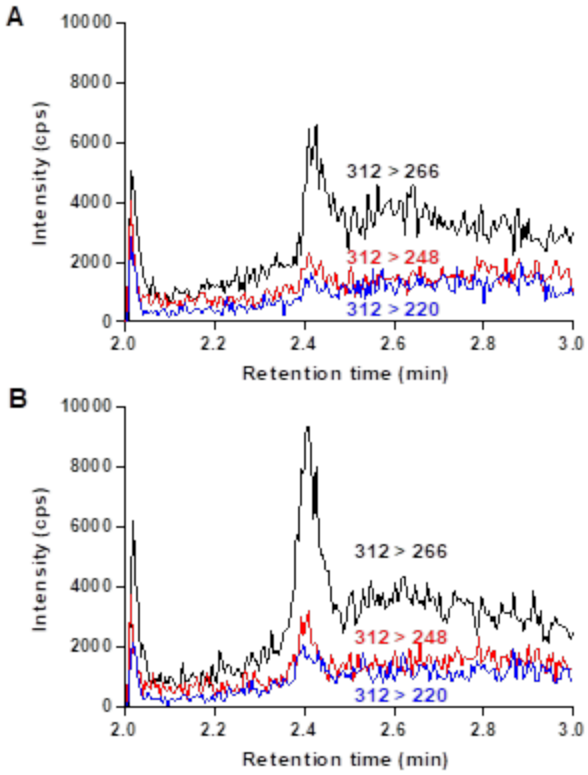

Figure 2.4. MRM chromatograms of DA at (A) on-column LOD at 0.52 pg (1.7 fmol) and (B) on-column LLOQ at 1.0 pg (3.3 fmol).

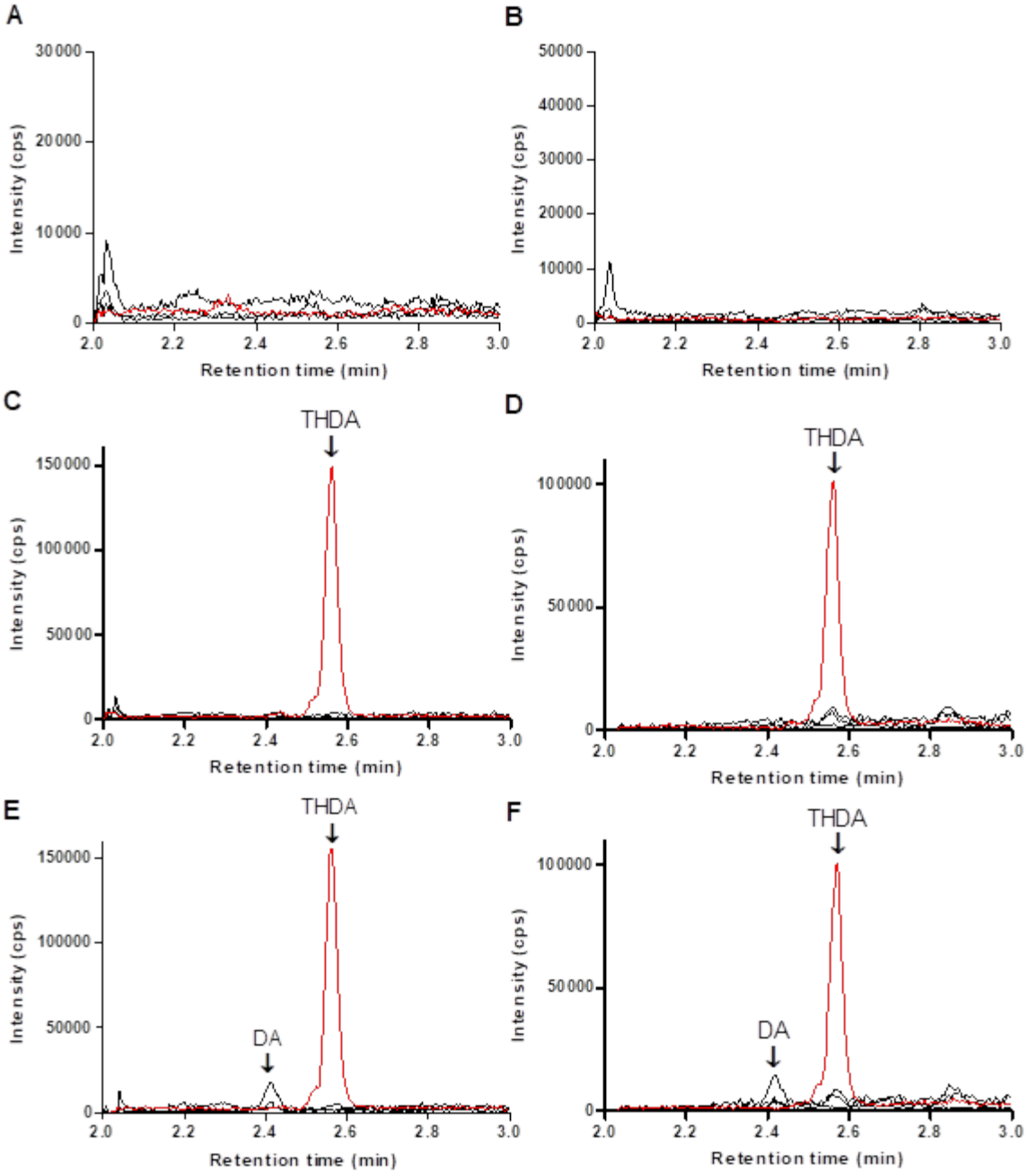

Figure 2.5. MRM chromatograms monitored for DA transitions in plasma and urine. The transitions monitored were m/z 312 > 266, 248, 220 for DA and m/z 316 > 252 for THDA. (A) blank plasma, (B) blank urine, (C) plasma with IS, (D) urine with IS, (E) plasma spiked with 0.31 ng/mL (1 nM) DA (LLOQ), and (F) urine spiked with 7.8 ng/mL (25 nM) DA (LLOQ).

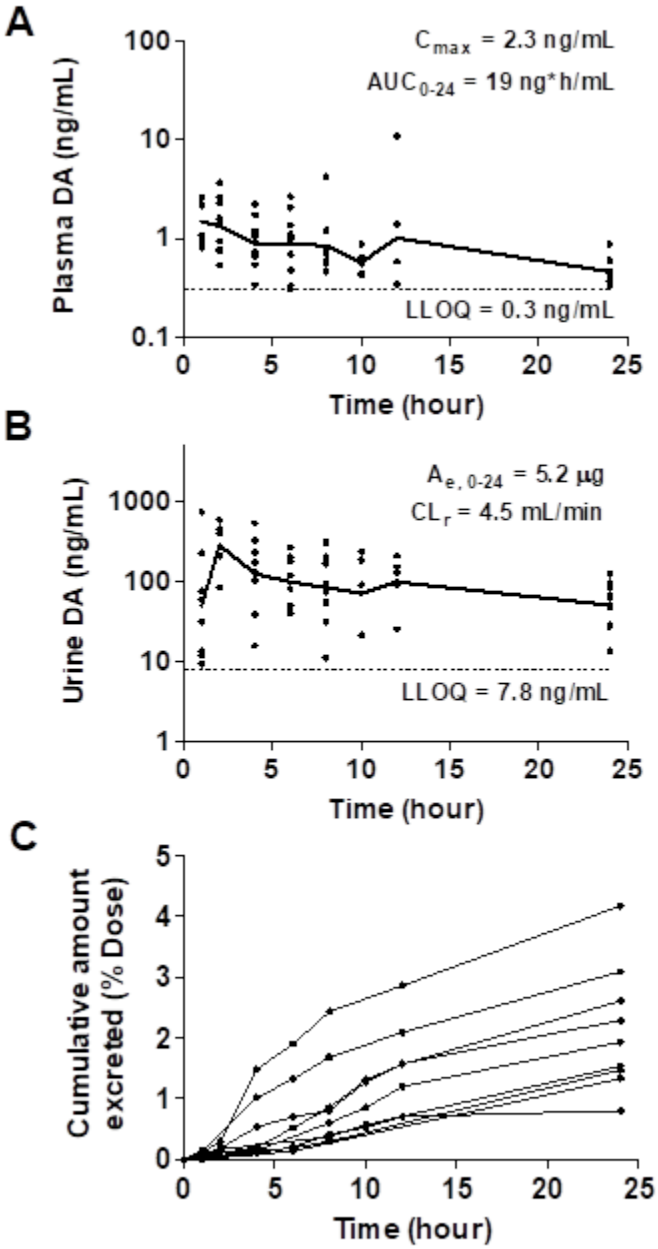

Figure 2.6. DA pharmacokinetics following a single 0.075 mg/kg dose of DA to a group of 10 healthy adult female cynomolgus monkeys. (A) Geometric mean plasma concentration-time curve (black line) with individual data above the LLOQ (82%, n=63) shown as symbols. Mean maximum plasma concentration (C_{max}) and area under the plasma concentration versus curve (AUC) from 0 to 24 h are reported on the graph; (B) Individual urine concentration data measured above the LLOQ (100%, n=60); and (C) individual cumulative % dose excreted unchanged in urine. Geometric mean amount of unchanged DA excreted (A_e) from 0 to 24 h and renal clearance (CL_r) are reported as inset in the graph.

Chapter 3.

Maternal-fetal disposition of domoic acid following repeated oral dosing during pregnancy in nonhuman primate

A version of this chapter was published as a research article: Toxicology and Applied Pharmacology (2020) Jul 1;398:115027

Authors: Sara Shum, Jing Jing, Rebekah Petroff, Brenda Crouthamel, Kimberly S. Grant, Thomas M. Burbacher, and Nina Isoherranen

3.1 ABSTRACT

Domoic acid (DA) is a marine algal toxin that causes acute and chronic neurotoxicity in animals and humans. Prenatal exposure to DA has been associated with neuronal damage and cognitive and behavioral deficits in juvenile California sea lions, cynomolgus monkeys, and rodents. Yet, the toxicokinetics (TK) of DA during pregnancy and the maternal-fetal disposition of DA have not been fully elucidated. In this study, we investigated the TK before, during and after pregnancy and the maternal-fetal disposition of DA in 22 cynomolgus monkeys following daily oral doses of 0.075 or 0.15 mg/kg/day of DA. The $AUC_{0-\tau}$ of DA was not changed while the renal clearance of DA was increased by 30-90% during and after pregnancy when compared to the pre-pregnancy values. DA was detected in the infant plasma and in the amniotic fluid at delivery. The infant plasma concentrations correlated positively with both the maternal plasma and the amniotic fluid concentrations. The paired infant-to-maternal plasma DA concentration ratios ranged from 0.3 to 0.6 and increased as a function of time which suggests placental efflux and longer apparent fetal half-life than the maternal half-life. The paired amniotic fluid-to-infant plasma DA concentration ratios ranged from 4.5 to 7.5 which indicates significant accumulation of DA in the amniotic fluid. A maternal-fetal TK model was developed to explore the processes that give the observed maternal-fetal disposition of DA. The final model suggests that placental transport and recirculation of DA between the fetus and amniotic fluid are major determining factors of the maternal-fetal TK of DA.

3.2 INTRODUCTION

Domoic acid (DA) is a naturally occurring neurotoxin produced by species of the marine phytoplankton, *Pseudo-nitzschia*.[87] It is a potent non-NMDA glutamate receptor agonist[88] which

potentiates the NMDA receptor[89,152] to cause severe excitotoxicity in humans and animals.[90,91,120,135] Over the past decade, an increasing number of DA-producing species of *Pseudo-nitzschia* have been identified around the globe; making this a prominent global problem.[153] To protect humans from DA toxicity, regulatory agencies have established regulatory limit of 20 µg of DA per gram of shellfish[154] and proposed a tolerable daily intake (acute TDI) level of 0.075 – 0.1 mg/kg/day.[136,139] While this limit has successfully protected humans from acute DA toxicity, emerging evidence shows that chronic asymptomatic exposure to DA may cause detrimental health effects in humans and animals.[92,93,159,94,95,134,135,155–158] Chronic low-level DA exposure from the consumption of contaminated shellfish in humans has recently been associated with adverse changes in memory that impacts daily living skills.[95,134] DA caused memory impairments in adults have also been documented in preclinical rodent models and wild populations of California sea lions.[93,159] In animals, the effect of DA on the mammalian brain includes neuronal death, increased oxidative stress, alter glutamatergic transmission and neuronal connectivity in the hippocampus, and altered gene transcription in the central nervous system.[92–94,157,159]

There are compelling data from animal studies that the fetus may be particularly sensitive to the effects of DA.[87,160] Laboratory studies in rodents have shown that DA causes neuronal damage in fetuses and impairments in the behavioral development of young animals following single or repeated dosing.[96–99,161] In California sea lions, DA exposure during pregnancy has been linked to reproductive failure, fetal death, and significant neurological injuries in exposed offspring.[135,162,163] These observations have raised a concern that low-level maternal DA exposure in humans could have significant consequences on fetal brain development[160] similar to other environmental chemicals such as methylmercury, polychlorinated biphenyls (PCBs) or

lead.[85,164] To address the concern of reproductive and fetal toxicity following chronic oral DA exposure, our group initiated a long-term neurotoxicity study in cynomolgus monkeys (*Macaca fascicularis*),[165] in which adult female monkeys received daily DA doses of the proposed TDI (0.075 mg/kg/day), two-times the proposed TDI (0.15 mg/kg/day) or vehicle control before and throughout pregnancy. While DA did not cause reproductive toxicity, our studies demonstrated that chronic subacute DA exposure in adult female monkeys resulted in a significant increase in observations of intentional-tremor and altered brain morphometry.[165,166] Infants born to the female monkeys in the 0.15 mg/kg/day DA group scored poorly on some aspects of a standardized memory test, suggesting that chronic fetal exposure to DA may impact developing cognitive processes.[167]

Our group has previously reported the toxicokinetics (TK) of DA following single intravenous and oral doses in non-pregnant female cynomolgus monkeys[103] but the TK of DA following repeated oral doses and TK changes during pregnancy have not been reported. We have shown that in monkeys, DA follows flip-flop kinetics after a single oral dose and consequently has a terminal half-life of about 10 hours[103]. Based on this half-life, little accumulation (<1.2-fold) of DA is expected following repeated daily oral doses, and plasma concentrations of DA after chronic dosing were predicted to be similar to those after a single dose. DA is mainly eliminated by the kidney with about 40 - 70% of intravenously dosed DA excreted unchanged in the urine in cynomolgus monkeys[102,103]. It is well recognized that the renal clearance of exogenous and endogenous compounds increases during pregnancy in humans due to increased renal blood flow and glomerular filtration[14]. Hence, renal clearance of DA may increase during pregnancy which may lead to an increase in the systemic clearance and a decrease in the area under the plasma concentration-time curve (AUC). Despite the polarity,

ionization at physiological pH, and poor permeability of DA, it has been shown to cross the placenta and distribute to the fetus in California sea lions and rodents.[104,162,168,169] The cognitive effects we observed in this study also support these findings. One study in rats showed that the apparent half-life of DA in fetal rats was twice of the dams' and the fetal-to-maternal plasma AUC ratio was 0.3 following a single intravenous dose to pregnant rats.[169] The residence time of DA in amniotic fluid was longer than in fetal plasma[169] and re-exposure through fetus ingestion of amniotic fluid has been attributed to the long apparent fetal half-life of DA.[104,169]

The goal of this study was to describe the maternal-fetal TK of DA following repeated oral doses of DA around the TDI during pregnancy in a nonhuman primate model. We herein report the maternal TK of DA before, during, and after pregnancy and the fetal disposition of DA at delivery, and provide a kinetic model to explore the mechanisms of maternal-fetal distribution kinetics of DA. Based on the known TK of DA and physiological changes during pregnancy in the nonhuman primate, we hypothesized that the renal clearance of DA would increase and the AUC of DA would decrease during pregnancy and that DA would accumulate in the fetus following repeated DA doses. This is the first report to describe maternal-fetal disposition of DA following chronic oral exposure, a relevant route of exposure in humans. The findings provide new insights into the health risks associated with exposure to this increasingly prevalent neurotoxin, particularly in the sensitive pregnant population.

3.3 Materials and Methods

3.3.1 *Chemicals and reagents*

DA powder purified from biological sources was purchased from BioVectra (Charlottetown, PE, Canada) to prepare dosing solutions. Purity of this DA powder was measured by HPLC-MS/MS as described below and the powder was found to be 94% pure. A

certified calibration standard solution of DA (332 µM) in acetonitrile/water (v/v 1:19) was purchased from National Research Council Canada (Halifax, NS, Canada). HPLC solvents including Optima LC/MS grade water, methanol, acetonitrile, and formic acid were purchased from Fisher Scientific (Pittsburgh, PA). The analytical internal standard, tetrahydrodomoic acid (THDA), was synthesized as previously described [170]. Frozen treatment-naïve monkey plasma and urine were obtained from the Washington National Primate Research Center (WaNPRC) at the University of Washington (Seattle, WA).

3.3.2 *Animal study protocol*

All the monkeys in this toxicokinetic (TK) study were part of a double-blinded randomized vehicle controlled long-term toxicology study of the effects of DA on reproduction and fetal neurodevelopment[165–167]. The animal procedures followed the Animal Welfare Act and the Guide for Care and Use of Laboratory Animals of the National Research Council. All protocols were previously described and approved by the University of Washington Institutional Animal Care and Use Committee to meet the highest standards of ethical conduct and compassionate use of animals in research. Briefly, thirty-two DA-naïve adult female cynomolgus macaques (*Macaca fascicularis*) were randomized to either the vehicle-dosed control group (n=10), or two groups receiving daily oral doses of 0.075 mg/kg/day (TDI) (n=11) or 0.15 mg/kg/day (2-times TDI) (n=11) (**Figure 3.1**). The average age and weight of the monkeys at randomization were 7 years (range: 5.5 – 11 years) and 3.5 kg (range: 2.8 – 4.2 kg), respectively. The monkeys were monitored daily to assess their health and behavior throughout the study. The health and behavior assessments were initiated immediately after randomization and dosing was initiated two months after randomization to allow for time to capture baseline values. Individual dosing solutions were prepared weekly according to the weight of each animal. Powder of DA

was dissolved in tap water with 5% (w/v) sucrose, sonicated for 10 min, and the individual dosing solution was filter-sterilized into a glass vial and stored at 4°C until dosing. All dosing solutions were analyzed by LC-MS/MS to confirm DA concentration. After two months of dosing, the female monkeys were paired with DA-naïve male monkeys for breeding. All monkeys, except for two in the 0.075 mg/kg/day group, conceived between one to seven months after initiation of breeding. After confirmation of pregnancy, the dosing solutions were prepared according to the last recorded pre-pregnancy weight[165]. The pregnant monkeys delivered either naturally or through caesarean sections after 21 to 25 weeks of gestation. Health and behavior monitoring of the infants was initiated after birth. DA dosing continued for the adult female monkeys according to their pre-pregnancy weight until necropsy.

Five TK studies were performed over the course of the study (**Figure 3.1**): on the first day of dosing (Day1), on the 56th day of dosing (Day56), on a day during gestational week eight to ten (GW8-10), on a day during gestational week 16 to 18 (GW16-18), and on a day during two to four weeks post-partum (PP2-4) for each animal. Only Day1 and Day56 TK studies were performed for monkeys who did not get pregnant. The PP2-4 TK study was not performed in three monkeys, two in the 0.075 mg/kg/day group and one in the 0.15 mg/kg/day group. On each TK study day, blood samples were collected from the saphenous vein into sodium heparin tubes at pre-dose and 1, 2, 4, 6, 8, 10, 12, and 24 h post-dose. Extensive behavioral training with positive reinforcement allowed the blood samples to be collected without anesthesia. Collected blood samples were centrifuged at 3,000 g for 15 minutes to isolate plasma within an hour of collection. Plasma samples were aliquoted and stored at -20°C until analysis. At each TK day, all the urine was collected at designated time points over a dosing interval (24 h) from a metabolic pan placed at the bottom of the cage. Volume of the urine collected was recorded and urine

samples were aliquoted and stored at -20°C until analysis. At delivery, maternal blood and infant blood were sampled and processed as described above and amniotic fluid was sampled and stored at -20°C until analysis. Maternal blood was not sampled in one monkey in the 0.15 mg/kg/day group and infant blood was not sampled in one infant in the 0.075 mg/kg/day group and two infants in the 0.15 mg/kg/day group. Amniotic fluid was sampled following c-section delivery in two monkeys in the 0.075 mg/kg/day and five monkeys in the 0.15 mg/k/day group.

3.3.3 *HPLC-MS/MS analysis*

DA concentrations in plasma, urine, and amniotic fluid were measured using a published validated HPLC-MS/MS method[170]. Briefly, plasma, urine, and amniotic fluid samples were thawed at room temperature on the day of analysis. For each plasma and amniotic fluid sample, 120 µL of methanol containing 5 nM THDA (internal standard) was added to 60 µL of sample. The samples were vortexed briefly, centrifuged at 16,100 g for an hour at room temperature, and supernatant was collected. For each urine sample, 490 µL of water containing 10 nM THDA (internal standard) was added to 10 µL of sample. The samples were vortexed briefly, centrifuged at 16,100 g for 15 minutes at room temperature, and supernatant was collected. Calibration standards were prepared in DA-naïve plasma and urine with concentrations ranging between 0.16 and 15.6 ng/mL for plasma and 7.8 and 1000 ng/mL for urine. Amniotic fluid concentrations were measured using the plasma calibration curve. For each urine sample with preliminary measured concentration >1000 ng/mL, 10 µL of sample was first diluted with 90 µL of water before processing as above. Supernatants were analyzed using a Shimadzu UFLC XR DGU-20A5 (Kyoto, Japan) equipped with a Phenomenex Synergi Hydro-RP 100 Å (2.5 µm, 50 x 2 mm^2) LC column and a guard cartridge (2 x 2.1 mm^2, sub 2 µm) (Torrange, CA) linked to a Sciex 6500 QTRAP system (Foster City, CA). The limit of detection (LOD) and the lower limit

of quantitation (LLOQ) in plasma were 0.16 ng/mL and 0.31 ng/mL, respectively[170]. Plasma concentrations below LLOQ but above LOD were assigned a value of 0.23 ng/mL (mid-point between LOD and LLOQ) and plasma concentrations below LOD were assigned as 0 ng/mL. The LLOQ in urine was 7.8 ng/mL[170]. All urine concentrations were above the LLOQ.

3.3.4 *Creatinine analysis*

One plasma and one urine sample from each animal on each TK study were analyzed for creatinine concentrations. The measurement was done by clinical laboratory tests at the Department of Laboratory Medicine at the University of Washington Medical Center. Creatinine concentrations were measured in all but two monkeys at GW8-10 and PP2-4 in the 0.075 mg/kg/day group, one monkey at GW16-18 in the 0.075 mg/kg/day group, and one monkey at PP2-4 in the 0.15 mg/kg/day group.

3.3.5 *Toxicokinetic analysis*

TK parameters including steady-state area under the plasma concentration time curve over a dosing interval ($AUC_{0\text{-}\tau}$) and oral clearance (CL/F) at each TK study for each monkey were calculated by noncompartmental analysis (NCA) using Phoenix WinNonlin (St Louis, MO). $AUC_{0\text{-}\tau}$ was calculated by the linear up log down method and CL/F was calculated using the following equation:

$$CL/F = \frac{D_\tau}{AUC_{0-\tau}}$$

where τ is a dosing interval (24 h) and D_τ is the amount of daily dose received. The rest of the TK parameters including renal clearance (CL_R), creatinine clearance ($CL_{creatinine}$), ratio between CL_R and $CL_{creatinine}$, and fraction of the dose excreted in urine unchanged (f_e) at each TK study

for each animal were calculated using Microsoft Excel 2013 (Redmond, WA). Renal clearance (CL_R) was calculated using the following equation:

$$CL_R = \frac{A_{e,0-\tau}}{AUC_{0-\tau}}$$

where $A_{e,0-\tau}$ is the total amount of DA excreted in urine unchanged over a dosing interval and was calculated by summation of urine DA concentrations multiplied by urine volumes for cumulative urine samples collected. Fraction of the oral dose excreted unchanged in urine (f_e) was calculated using the following equation:

$$f_e(\%) = \frac{A_{e,0-\tau}}{D_\tau} \times 100\%$$

Creatinine clearance ($CL_{creatinine}$) was calculated using the following equation:

$$CL_{creatinine} = \frac{\frac{A_{e,creatinine}}{\Delta t}}{C_{creatinine}}$$

where $A_{e,creatinine}$ is the amount of creatinine excreted in urine over a collection period calculated by multiplying the urine creatinine concentration by the urine volume, Δt is the duration of the urine collection period, and $C_{creatinine}$ is the plasma creatinine concentration. Renal clearance to creatinine clearance ($CL_R/CL_{creatinine}$) ratio was calculated by dividing CL_R by $CL_{creatinine}$. Infant-to-maternal plasma concentration ratio was calculated by dividing the infant plasma concentration by the maternal plasma concentration at the time of delivery when both concentrations were above the LLOQ. The geometric mean and the 95% confidence interval for each TK parameter were calculated using GraphPad Prism version 5 (San Diego, CA).

3.3.6 *Power analysis*

Intra-individual variability of the plasma AUC before and during pregnancy was assessed using the biweekly 5-h-post-dose plasma concentrations sampled prior to and during pregnancy,

respectively, from each monkey[165]. A power analysis using the averaged intra-individual variability before and during pregnancy showed that 11 animals per group would allow detection of 70% increase or 40% decrease in $AUC_{0-\tau}$ of DA during pregnancy with 80% power ($\beta = 0.2$) and significance level of $\alpha = 0.017$.

3.3.7 *Statistical analysis*

Statistical analysis was performed using GraphPad Prism version 5 (San Diego, CA). Differences in the natural log-transformed $AUC_{0-\tau}$, CL/F, CL_R, and $CL_{creatinine}$ during pregnancy (GW8-10 and GW16-18), and after pregnancy (PP2-4) in comparison to before pregnancy (Day56) were tested for each dose group by paired t-tests with p-value <0.017 (Bonferroni correction for multiple comparisons, $\alpha = 0.05/3$) considered significant. The correlations between (1) maternal plasma and infant plasma concentration at delivery, (2) infant plasma and amniotic fluid concentration at delivery, (3) maternal plasma concentration at delivery and infant-to-maternal plasma concentration ratio, and (4) infant plasma concentration at delivery and infant-to-maternal plasma concentration ratio, were tested by simple linear regression. The deviation of the slope of the linear regression line from zero was tested using t-test with a p-value ≤ 0.05 considered significant.

3.3.8 *Maternal-fetal toxicokinetic model of DA*

3.3.8.1 Model structure

A maternal-fetal TK model of DA was developed using SimBiology R2018b (Natick, MA) to simulate late pregnancy maternal-fetal DA disposition. This model was structured to include compartments of the maternal whole-body, fetal whole-body, and amniotic fluid. Each compartment has a fixed volume of distribution assigned for a 4 kg cynomolgus monkey. The

maternal volume of distribution was assigned to be 0.6 L according to the observed volume of distribution of DA in cynomolgus monkeys following an IV dose (0.15 L/kg bodyweight).[103] The fetal volume of distribution was assigned to be 0.06 L according to the mean birthweight of the infant monkeys observed in this study (0.4 kg) and the observed volume of distribution of DA in adult cynomolgus monkeys (0.15 L/kg bodyweight) assuming fetal DA distribution is similar to adult monkeys.

3.3.8.2 Absorption

The steady-state maternal and fetal DA disposition following repeated oral DA doses during pregnancy was simulated by applying fifty daily (every 24 h) DA doses of 0.075 or 0.15 mg/kg/day to the maternal compartment. DA absorption was assumed to be first-order defined by an oral absorption rate constant (k_a). The initial k_a was assigned as 0.07 h^{-1} as previously reported in adult non-pregnant monkeys.[103] The bioavailability of DA was set at 7.5% as previously reported in the same study.[103]

3.3.8.3 Distribution

DA distribution from the maternal compartment to the fetal compartment (k_{mf}) and vice versa (k_{fm}) was modeled according to first-order kinetics. The initial distribution rate constant k_{mf} was calculated by dividing the transplacental clearance from mother to fetus (CL_{mf}) with the maternal volume of distribution (0.6 L). The initial CL_{mf} was assigned as 0.1 L/h, a value estimated by multiplying the reported Caco2 permeability[171] with the extrapolated placental microvillus surface area based on human physiology[172,173]. The initial distribution rate k_{fm} was calculated by dividing the transplacental clearance from fetus to mother (CL_{fm}) with the fetal volume of distribution (0.06 L). The initial CL_{fm} was assigned to be the same as $CL_{mf.}$ (0.1 L/h). DA distribution from the fetal compartment to the amniotic fluid compartment (through fetal

urination) with assumed to be according to first order kinetics with a first order rate constant ($k_{e,\ amniotic\ fluid}$). The $k_{e,\ amniotic\ fluid}$ was calculated by dividing fetal renal clearance ($CL_{e,\ fetal}$) by the fetal volume of distribution (0.06 L). The initial $CL_{e,\ fetal}$ was assigned as 0.015 L/h, a value calculated assuming fetal renal clearance is 2.5%[174–176] of the maternal renal clearance observed in this study. DA distribution from the amniotic fluid compartment to the fetal compartment (through fetal swallowing of amniotic fluid) was modeled according to first order kinetics with a first order rate constant ($k_{a,\ amniotic\ fluid}$). The initial $k_{a,\ amniotic\ fluid}$ was assigned to be the same as k_a ($0.07\ h^{-1}$).

3.3.8.4 Elimination

DA elimination from the maternal compartment was assumed to be first order with a first order elimination rate constant (k_e). The initial k_e was calculated by dividing the maternal systemic clearance ($CL_{e,\ maternal}$) by the maternal volume of distribution (0.6 L). The initial $CL_{e,\ maternal}$ was assigned as 1.66 L/h and 0.97 L/h, which was calculated by multiplying the observed oral clearance at GW16-18 in the 0.075 mg/kg/day group and 0.15 mg/kg/day group, respectively, with the 7.5% bioavailability reported previously.[103]

3.3.8.5 Simulations

Steady-state (after the 50^{th} dose) maternal-fetal disposition was first simulated using the initial parameters described above. Local sensitivity analyses were then conducted to explore how specific TK parameters (k_a, $k_{a,\ amniotic\ fluid}$, $CL_{e,\ maternal}$, $CL_{e,\ fetal}$, CL_{mf}, and CL_{fm}) impact simulation results of maternal fetal disposition of DA. Sensitivity analyses were conducted by altering the value of each of the above parameters individually within the range of 10% to 10-fold of the initial values. Based on the sensitivity analyses, specific parameters for maternal-fetal disposition (CL_{mf}, CL_{fm}, and $CL_{e,\ fetal}$) were optimized simultaneously to capture the time course

of the observed infant-to-maternal plasma concentration ratio. All other parameters were kept as described above for the model. The simulated maternal and fetal steady-state $AUC_{0-\tau}$ (after the 50^{th} dose, from 1200 to 1224 h) and terminal half-lives ($t_{1/2,}$ after distribution equilibrium is reached) were analyzed using Phoenix WinNonlin (St Louis, MO). The fetal-to-maternal $AUC_{0-\tau}$ and plasma concentration ratios were calculated using Microsoft Excel 2013 (Redmond, WA). The maternal DA concentrations observed at GW16-18 were compared to the simulated maternal DA concentrations using GraphPad Prism version 8 (San Diego, CA). Similarly, observed maternal and infant concentrations at delivery were compared to the simulated maternal and fetal concentrations at term using GraphPad Prism version 8 (San Diego, CA).

3.4 RESULTS

3.4.1 *Toxicokinetics (TK) of DA following daily oral doses in adult female monkeys before, during, and after pregnancy*

TK of DA following daily oral doses in adult female monkeys before, during, and after pregnancy is reported in **Table 3.1** and **Figure 3.2**. The $AUC_{0-\tau}$ on Day56 following a dose of 0.075 mg/kg/day was 20 h*ng/mL (95% CI: 16 – 25 h*ng/mL), when the dose was increased by 2-fold to 0.15 mg/kg/day, the $AUC_{0-\tau}$ increased by 3.3-fold to 65 h*ng/mL (95% CI: 48 – 87 h*ng/mL). This more than dose-proportional increase was observed throughout the study, with the $AUC_{0-\tau}$ in the 0.15 mg/kg/day group being 2.5 to 3.3-fold greater than that of the 0.075 mg/kg/day group. The weight-normalized CL/F of DA was 22 to 41% lower in the 0.15 mg/kg/day group in comparison to the 0.075 mg/kg/day group throughout the study. The CL_R of DA, $CL_{creatinine}$, and the $CL_R/CL_{creatinine}$ ratio were not different between the two dose groups on any study day. However, the $CL_{creatinine}$ of the control group appeared to be consistently lower than the $CL_{creatinine}$ in the 0.15 mg/kg/day group throughout the study (**Table 3.1**). Both the CL_R

of DA and the $CL_{creatinine}$ showed a trend to increase during and after pregnancy in both dose groups when compared to the pre-pregnancy values (**Figure 3.2e-h**), but these increases did not translate to a change in $AUC_{0-\tau}$ and CL/F of DA during and after pregnancy (**Figure 3.2a-d**). The $CL_R/CL_{creatinine}$ was <1 throughout the study and was not altered by pregnancy.

3.4.2 *Maternal plasma, infant plasma and amniotic fluid DA concentrations at delivery*

The DA concentrations in maternal plasma, infant plasma, and amniotic fluid were measured at delivery to assess maternal-fetal disposition of DA (**Figure 3.3a-b**). The infant plasma concentration correlated positively with both the maternal plasma (**Figure 3.3c**) and the amniotic fluid concentrations (**Figure 3.3d**), and the infant plasma DA concentrations were consistently lower than the maternal plasma and amniotic fluid DA concentrations. The infant-to-maternal plasma concentration ratios were 0.3 (range: 0.2 – 0.5) in the 0.075 mg/kg/day group and 0.6 (range: 0.3 – 1.0) in the 0.15 mg/kg/day group while the amniotic fluid-to-infant plasma concentration ratios were 4.5 (range: 3.9 – 5.1) in the 0.075 mg/kg/day group and 8.9 (range: 2.7 – 13) in the 0.15 mg/kg/day group (**Figure 3.3e,f**). Correlations between the infant-to-maternal plasma concentration ratios and the maternal and infant plasma concentrations were tested to explore whether any potential nonlinearity in the maternal-fetal distribution could be observed but no correlation was detected (**Figure 3.3g,h**). Instead, the infant-to-maternal plasma concentration ratio appeared to vary with time after dosing of DA, with lower ratios observed in monkeys who delivered shortly (<12 h) after dosing and higher ratios observed in monkeys who delivered later (>12 h) after dosing.

3.4.3 *DA maternal-fetal toxicokinetic modeling and simulations*

To explore the potential mechanisms controlling maternal-fetal disposition of DA, a TK model was developed to simulate DA maternal-fetal disposition at the time of delivery (**Figure 3.4**). The initial parameter values were assigned either as values observed in this and previous studies or estimated based on the known physiology of pregnant monkeys at late gestation as described in materials and methods. The steady-state maternal-fetal disposition of DA (after the 50^{th} dose) was first simulated using the initial parameter values. The simulation showed an increase in fetal-to-maternal plasma concentration ratio with time after dosing, but the simulated fetal-to-maternal plasma concentration ratio overpredicted the observed ratios at delivery (**Figure 3.5a**). To address this overprediction, local sensitivity analyses were conducted to define the impact of each individual model parameter on the simulated maternal-fetal disposition of DA (**Table 3.2**).

Local sensitivity analyses were conducted by changing one parameter at a time while keeping the rest of the parameters at their initial values. Decreasing maternal absorption rate (k_a) increased both the fetal and maternal half-lives of DA (**Table 3.2**) due to the flip-flop kinetics ($k_e > k_a$, elimination is absorption rate limited) of DA, but decreasing k_a had a minimal effect on the fetal-to-maternal plasma concentration ratio. Increasing k_a had no impact on the fetal and maternal half-lives of DA once distribution equilibrium was achieved (**Table 3.2**) as under this scenario the reabsorption from the amniotic fluid becomes rate-limiting. Increasing k_a shortened the initial half-life and also increased the fetal-to-maternal plasma concentration ratio.

As expected, fetal and maternal AUCs of DA correlated positively with maternal clearance ($CL_{e,\ maternal}$ and k_e) (**Table 3.2**) but changing $CL_{e,\ maternal}$ had no impact on the fetal-to-maternal plasma concentration ratio. Conversely, decreasing maternal-to-fetal transfer clearance

(CL_{mf}) or increasing fetal-to-maternal transfer clearance (CL_{fm}), as would happen in the presence of active transport in the placenta, decreased fetal AUC but had no effect on maternal AUC (**Table 3.2**) and resulted in a considerable decrease in both the fetal-to-maternal AUC and plasma concentration ratio. Decreasing fetal reabsorption rate of DA from amniotic fluid ($k_{a,\ amniofic\ fluid}$) increased the fetal and maternal half-lives (**Table 3.2**) and increased the fetal-to-maternal plasma concentration ratio (**Figure 3.6b-e**). It is interesting to note that the fetal and maternal half-lives were the shortest in the absence of fetal reabsorption ($k_{a,\ amniofic\ fluid} = 0$) (**Figure 3.6a**) due to the switch of amniotic fluid from a distribution compartment to an elimination compartment under this scenario. Increasing fetal renal clearance of DA into the amniotic fluid ($CL_{e,\ fetal}$ and $k_{e,\ amniotic\ fluid}$) increased the fetal and maternal half-lives (**Table 3.2**) and increased the fetal-to-maternal plasma concentration ratio (**Figure 3.5a, Figure 3.6f-j**). These simulations demonstrated that the CL_{mf}, CL_{fm}, $k_{a,\ amniotic\ fluid}$, and $CL_{e,\ fetal}$ have significant impact on the maternal-fetal distribution kinetics of DA. Moreover, altering each parameter alone did not fully replicate the observed infant-to-maternal plasma concentration ratio over time (**Figure 3.5a**). Therefore, the kinetic model parameters were optimized to define the combination of model parameters that can capture the observed data.

Since the maternal-fetal TK model was developed using observed maternal TK during pregnancy and the sensitivity analysis showed that k_a and k_e has minimal effect on maternal-fetal distribution kinetics of DA, we focused on optimizing CL_{mf}, CL_{fm}, and $CL_{e,\ fetal}$ to capture the maternal-fetal disposition of DA. The optimized physiologically plausible model incorporated a 4-fold higher $CL_{e,\ fetal}$ together with an 82% lower CL_{fm} and a 94% lower CL_{mf} compared to the initial values (**Figure 3.4**). This optimized model captured the observed maternal plasma concentration-time profiles during pregnancy (GW16-18) well (**Figure 3.5b**). However, it

slightly underpredicted the maternal and fetal concentrations at delivery. Hence, a bioavailability of 12% was applied (initial value was 7.5%) in the final model to predict the maternal and fetal plasma concentration-time profiles at delivery. The final model captured the maternal and fetal plasma concentration time profiles at delivery (**Figure 3.5c**) and the time course of the maternal-to-fetal concentration ratios observed in this study (**Figure 3.5d**) with a simulated fetal-to-maternal AUC ratio of 0.35.

3.5 DISCUSSION

Despite the abundance of evidence that DA acts as a developmental neurotoxin,[96–99,135,161,162] only a limited number of studies have reported TK of DA during pregnancy and fetal disposition following *in utero* exposure.[104,162,168,169] A previous study in rats showed that DA crosses the placenta and distributes to the fetus with a fetal-to-maternal plasma AUC ratio of 0.3 following a single intravenous dose.[169] However, since DA follows flip-flop kinetics after oral doses in monkeys and possibly in humans, route of administration could have a profound impact on maternal-fetal TK due to different maximum concentrations (C_{max}) and duration of exposure. As previously demonstrated through physiologically-based pharmacokinetic (PBPK) modeling, the C_{max} and concentration-time profile of DA in the brain varied drastically following intravenous or oral dosing.[103] To date, fetal TK analyses following oral DA exposure have been limited to opportunistic studies in California sea lions.[104,162] Based on these observations, a maternal-fetal TK model of DA was proposed which suggests that the fetus is continuously re-exposed to DA through swallowing of amniotic fluid which increased fetal exposure.[104] However, the extent and duration of DA exposure in the fetus cannot be ascertained in these opportunistic studies and verification of the proposed model is not possible. This study is the first to describe the TK of DA during pregnancy and maternal-fetal disposition following oral doses

in any species. In this study, we show that the renal clearance of DA is increased by 30 – 90% during pregnancy, however, this renal clearance increase did not alter the AUC of DA. The AUC of DA was not significantly different before, during, and after pregnancy. We also show that the fetal plasma DA concentrations were lower than, but positively correlated with, maternal plasma and amniotic fluid concentrations. A maternal-fetal TK model was developed to simulate maternal-fetal distribution kinetics of DA. The kinetic simulations suggested that placental transport and recirculation of DA between the fetus and amniotic fluid are the main determining factors of the maternal-fetal distribution kinetics of DA.

The pre-pregnancy weight-normalized mean oral clearance following 0.075 or 0.15 mg/kg/day of DA observed in this study was 40 – 90% higher than that observed in our previous crossover study where three non-pregnant female monkeys were given a single oral dose of 0.075 or 0.15 mg/kg of DA.[103] This difference can be due to the inter-individual variability of DA disposition. A greater than dose proportional increase of AUC (~ 3-fold) was observed between the groups that received 0.075 or 0.15 mg/kg/day DA throughout the study, consistent with the greater than dose proportional increase observed in our previous crossover study.[103] The fact that the CL_R of DA and the $CL_R/CL_{creatinine}$ were not different between the two dose groups in this study suggests that renal clearance and renal clearance processes (filtration and active reabsorption) of DA are not affected by the dose. Together, the data suggest saturation of either extra-renal elimination or efflux transporters during absorption of DA.

As we hypothesized, the renal clearance of DA was increased during and after pregnancy when compared to the pre-pregnancy values. The increase in DA renal clearance was likely due to the increase in GFR as the $CL_R/CL_{creatinine}$ values were not different throughout pregnancy when compared to pre-pregnancy. Although renal clearance is a major elimination pathway of

DA (f_e = 0.4 – 0.7), the increased renal clearance during and after pregnancy did not alter the AUC of DA during pregnancy likely due to the presence of other elimination pathways and the large intraindividual variability.[103] Hence, the dose-exposure relationship determined in non-pregnant monkeys is likely to predict the relationship in pregnant monkeys. While we cannot rule out the possibility that pregnant women are pharmacologically more susceptible to DA toxicity, our results suggest that pregnant women are exposed to similar concentrations of DA as non-pregnant individuals following the same dose.

Consistent with previous studies in other species,[104,162,168,169] our study shows that DA crosses the placenta and distributes to the fetus. The infant-to-maternal plasma concentration ratio at delivery was between 0.3 and 0.6, which agrees with the fetal-to-maternal AUC ratio of 0.3 observed previously in rats following a single intravenous dose.[169] As demonstrated through the sensitivity analyses, either a decrease in CL_{mf} or an increase in CL_{fm} (both can occur in the presence of placental efflux) lead to a <1 fetal-to-maternal AUC ratio. This <1 fetal-to-maternal AUC ratio suggests that the placenta is partially protecting the fetus from exposing to DA, likely via active transport. DA has been shown to be transported by MRP5,[177] an ABC efflux transporter that is expressed in the syncytiotrophoblasts,[178,179] and other anion transporters[171] which may be present in the placenta and decrease DA distribution to the fetus. Although irreversible fetal elimination may also decrease fetal-to-maternal AUC ratio, such clearance pathway is not likely because there is no evidence of DA metabolism. Hence, our results suggest that the placenta acts as a partial protective barrier that decreases the risk of fetal toxicity. Despite the placenta acting as a partial barrier to protect the fetus from DA, fetal AUC is driven by maternal AUC as shown by the positive correlation between fetal and maternal plasma concentrations at delivery, and by the sensitivity analyses that both maternal and fetal DA AUCs

significantly changed with altered maternal elimination. Therefore, an increase in maternal AUC will increase the risk of DA toxicity in both the mother and the fetus, consistent with the observed dose-dependent increase in tremor rates in the adult female monkeys and dose-dependent impact on the developing cognitive processes in the infants of this study.[165,167]

As observed previously in rats,[169] the apparent fetal half-life was longer than the maternal half-life in this study as evidenced by the infant-to-maternal plasma concentration ratio increase over time after dosing. The longer apparent fetal half-life has been attributed to fetal re-exposure through swallowing of amniotic fluid.[169] We observed a 4.5 – 7.5-fold higher DA concentration in amniotic fluid compared to fetal plasma which, in agreement with the previous studies,[104,169] suggests that DA accumulates and is eliminated slowly from the amniotic fluid. We demonstrated using the maternal-fetal TK modeling and simulations, that placental transport and the recirculation between fetus and amniotic fluid are likely the main determining factors of the maternal-fetal distribution kinetics of DA. We proposed a final model to simulate a kinetic scenario of maternal-fetal disposition of DA that can explain the observed maternal and infant plasma concentrations at delivery. The final model incorporated the presence of placental efflux which resulted in a CL_{mf} to CL_{fm} ratio of 0.3, rapid fetal elimination (fetal renal clearance equals to 10% maternal renal clearance), and fetal reabsorption of DA through swallowing of amniotic fluid. It is important to note that, as shown through simulations, the maternal and fetal terminal half-lives are the same, however, the apparent fetal half-life (0-24 hour) was longer than the apparent maternal half-life due to the delay in reaching distribution equilibrium (**Figure 3.5c**). As we hypothesized, the prolonged apparent half-life may increase the duration of fetal exposure to DA and hence, the risk of fetal toxicity. Nevertheless, the observed <1 infant-to-maternal

plasma concentration ratio suggests that the fetus is exposed to lower plasma concentrations of DA than the mother.

In conclusion, this study shows that the plasma AUC of DA is not significantly changed by pregnancy, the fetal AUC of DA is less than the maternal AUC likely due to placental efflux, and that the maternal fetal distribution kinetics increases the duration of DA exposure in the fetus. Overall, our study suggests that pregnant women and developing fetuses are not subjected to additional exposures in comparison to non-pregnant population based on the maternal-fetal TK. To fully assess the risks of DA toxicity, future studies to elucidate the toxicological response and exposure-toxicity relationships in pregnant women and developing fetuses are warranted.

Table 3.1 Toxicokinetic (TK) parameters of DA measured following daily oral doses of 0.075 mg/kg/day and 0.15 mg/kg/day before, during, and after pregnancy in adult female monkeys. The creatinine clearance values measured in vehicle control animals are also reported for the study days. TK parameters are reported as geometric means (95% confidence interval). Pregnancy (GW8-10 and GW16-18) and post-partum (PP2-4) parameters were compared to pre-pregnancy (Day56) parameters and a p-value of 0.017 was considered significant (Significance level adjusted for multiple comparisons). Values that are significantly different from values on Day56 are **bolded**.

		n=	[a] $AUC_{0-\tau}$ (ng/mL*h)	[a] CL/F (mL/min/kg)	[a] CL_R (mL/min)	[b] $CL_{creatinine}$ (mL/min)	[c] $\frac{CL_R}{CL_{creatinine}}$	f_e (%)
0.075 mg/kg/day	Day1	11	19 (14 – 27)	--	5.2 (2.8 – 9.9)	5.9 (4.0 – 8.7)	0.8 (0.4 – 1.7)	--
	Day56	11	20 (16 – 25)	61 (49 – 76)	6.2 (5.3 – 7.4)	8.1 (4.9 – 13)	0.8 (0.4 – 1.5)	2.7 (2.1 – 3.4)
	GW8-10	9	19 (13 – 28) *p = 0.54*	67 (44 – 100) *p = 0.54*	7.7 (4.6 – 13) *p = 0.34*	15 (11 – 19) *p = 0.06*	0.7 (0.4 – 1.1) *p = 0.93*	3.3 (1.9 – 5.9) *p = 0.40*
	GW16-18	9	14 (8.5 – 22) *p = 0.04*	92 (58 – 146) *p = 0.04*	**11 (7.3 – 17) *p = 0.014***	16 (12 – 22) *p = 0.07*	0.6 (0.5 – 0.8) *p = 0.94*	3.2 (2.5 – 4.1) *p = 0.19*
	PP2-4	7	17 (8.8 – 34) *p = 0.41*	72 (37 – 142) *p = 0.41*	10 (5.1 - 20) *p = 0.11*	12 (10 – 14) *p = 0.15*	0.9 (0.4 – 1.9) *p = 0.60*	3.5 (1.8 – 6.9) *p = 0.20*
0.15 mg/kg/day	Day1	11	44 (34 – 57)	--	6.4 (4.9 – 8.2)	12 (7.5 – 20)	0.5 (0.3 – 0.9)	--
	Day56	11	65 (48 – 87)	39 (29 – 52)	6.2 (4.7 – 8.2)	11 (7.9 – 14)	0.6 (0.5 – 0.8)	4.2 (3.0 – 5.9)
	GW8-10	11	48 (38 – 62) *p = 0.06*	52 (40 – 67) *p = 0.06*	**10 (8.2 - 13) *p <0.001***	**17 (14 – 20) *p = 0.003***	0.6 (0.5 – 0.8) *p = 0.73*	5.1 (3.9 – 6.8) *p = 0.30*
	GW16-18	11	46 (33 – 65) *p = 0.04*	54 (38 – 76) *p = 0.04*	9.4 (6.6 - 13) *p = 0.018*	**17 (15 – 20) *p = 0.006***	0.5 (0.4 – 0.8) *p = 0.54*	4.5 (3.2 – 6.3) *p = 0.75*
	PP2-4	10	51 (39 – 68) *p = 0.13*	49 (37 – 65) *p = 0.13*	**9.1 (6.9 - 12) *p = 0.002***	**17 (14 – 21) *p = 0.002***	0.5 (0.4 – 0.6) *p = 0.56*	4.9 (3.8 – 6.2) *p = 0.13*
Control	Day1	10	--	--	--	5.7 (4.0 – 8.0)	--	--
	Day56	10	--	--	--	6.5 (5.3 – 8.0)	--	--
	GW8-10	8	--	--	--	**12 (8.7 – 16) *p = 0.005***	--	--
	GW16-18	8	--	--	--	**11 (8.2 – 16) *p = 0.002***	--	--
	PP2-4	7	--	--	--	**11 (7.8 – 14) *p = 0.006***	--	--

a. More than 50% of plasma samples collected from one monkey in the 0.075 mg/kg/day group were below BLQ (0.3 ng/mL), hence, $AUC_{0-\tau}$, CL/F, and CL_R were not calculated for that monkey for the whole study (i.e. Day1, n=10; Day56, n=10; GW8-10, n=8; GW16-18, n=8; PP2-4, n=6)

b. For the 0.075 mg/kg/day group, $CL_{creatinine}$ was measured in n=7 monkeys at GW8-10 and n=8 monkeys at GW16-18

c. For the 0.075 mg/kg/day group $CL_R/CL_{creatinine}$ ratio was calculated only when both values were availbale (i.e. Day1, n=10; Day56, n=10; GW8-10, n=6; GW16-18, n=7; PP2-4, n=6)

Table 3.2. Sensitivity analyses to illustrate the effect of altering individual TK parameters on steady state (after the 50th dose) maternal-fetal DA disposition. Simulations were performed by changing only one parameter as listed in the first column within the range described for New k and New CL, while keeping the other parameters at their initial values. Initial values were as described in materials and methods: k_a = 0.07 h^{-1}, k_e = 2.76 h^{-1} *($CL_{e,maternal}$ = 1.66 L/h)*, k_{mf} = 0.17 h^{-1} *(CL_{mf} = 0.1 L/h)*, k_{fm} = 1.7 h^{-1} *(CL_{fm} = 0.1 L/h)*, $k_{e,\ amniotic\ fluid}$ = 0.25 h^{-1} *($CL_{e,\ fetal}$ = 0.015 L/h)* and $k_{a,\ amniotic\ fluid}$ = 0.07 h^{-1}. Greater than 30% changes in the simulated $AUC_{0-\tau}$, terminal half-life ($t_{1/2}$), and fetal-to-maternal (F/M) $AUC_{0-\tau}$ ratio with altered individual TK parameters compared to initial condition are **bolded**.

Altered TK parameter	New k (h^{-1})	*New CL (L/h)*	Maternal		Fetal		F/M $AUC_{0-\tau}$ ratio
			$t_{1/2}$ (h)	$AUC_{0-\tau}$ (h*ng/mL)	$t_{1/2}$ (h)	$AUC_{0-\tau}$ (h*ng/mL)	
None (Initial parameters)	--	--	11	14	12	14	1.0
k_a	0.007	--	**99**	14	**99**	14	1.0
	0.02	--	**35**	14	**35**	14	1.0
	0.2	--	11	14	11	14	1.0
	0.7	--	11	14	11	14	1.0
k_e	0.3	*0.18*	13	**130**	13	**130**	1.0
	1.0	*0.6*	12	**37**	12	**37**	1.0
	8.0	*4.8*	11	**4.7**	11	**4.7**	1.0
	25	*15*	10	**1.5**	11	**1.5**	1.0
k_{mf}	0.017	*0.01*	10	14	11	**1.4**	**0.1**
	0.051	*0.03*	11	14	11	**4.1**	**0.3**
	0.51	*0.3*	12	14	12	**41**	**3.0**
	1.7	*1.0*	12	14	12	**140**	**10**
k_{fm}	0.17	*0.01*	**28**	14	**28**	**140**	**10**
	0.51	*0.03*	**16**	14	**16**	**45**	**3.3**
	5.1	*0.3*	10	14	10	**4.5**	**0.3**
	17	*1.0*	10	14	10	**1.4**	**0.1**
$k_{e,\ amniotic\ fluid}$	0.025	*0.0015*	10	14	10	14	1.0
	0.08	*0.0048*	10	14	10	14	1.0
	0.8	*0.048*	**15**	14	**15**	14	1.0
	2.5	*0.15*	**26**	14	**26**	14	1.0
$k_{a,\ amniotic\ fluid}$	0.0	--	10	13	10	12	0.9
	0.007	--	**115**	14	**115**	14	1.0
	0.02	--	**40**	14	**40**	14	1.0
	0.2	--	10	14	10	14	1.0
	0.7	--	10	14	10	14	1.0

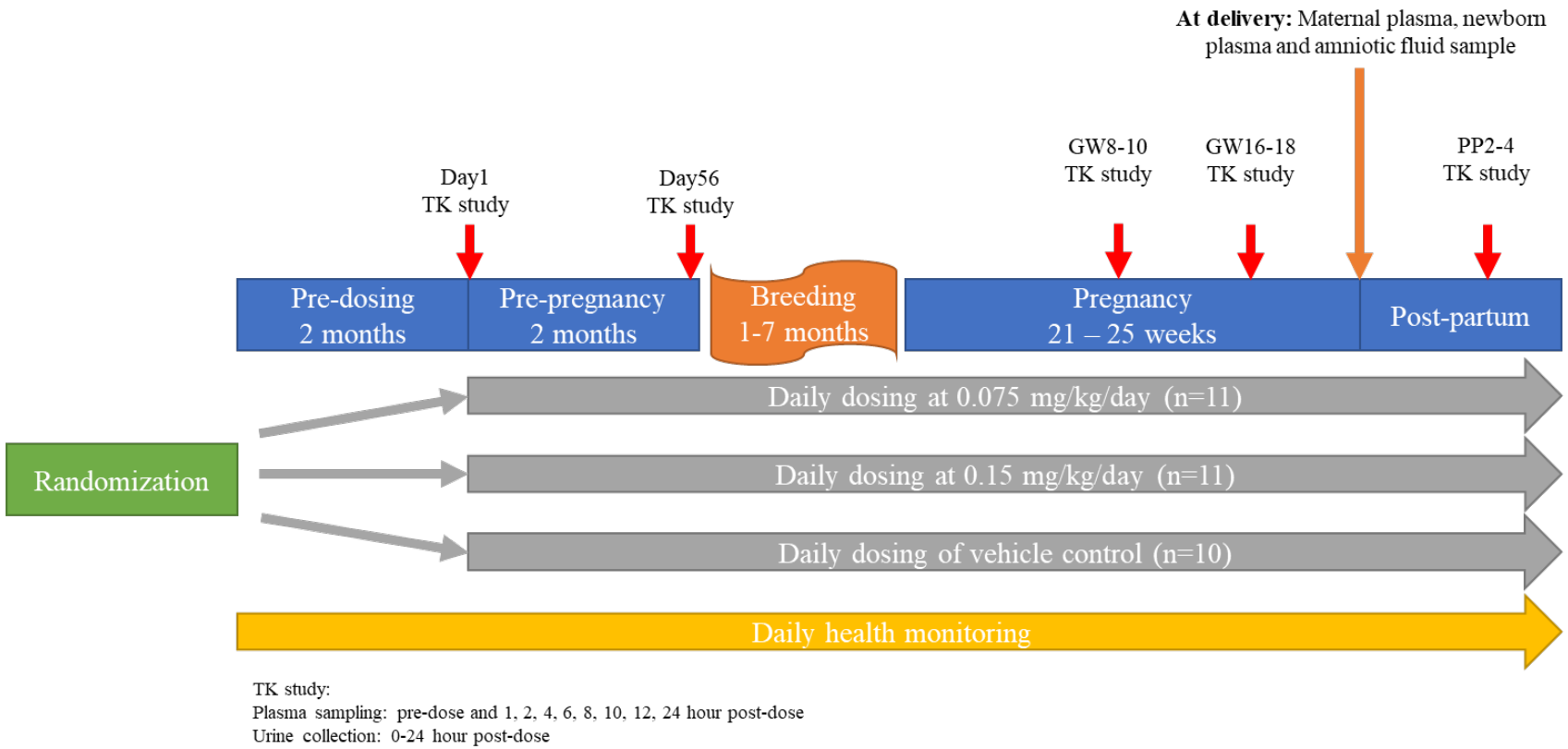

Figure 3.1. Toxicokinetic study design

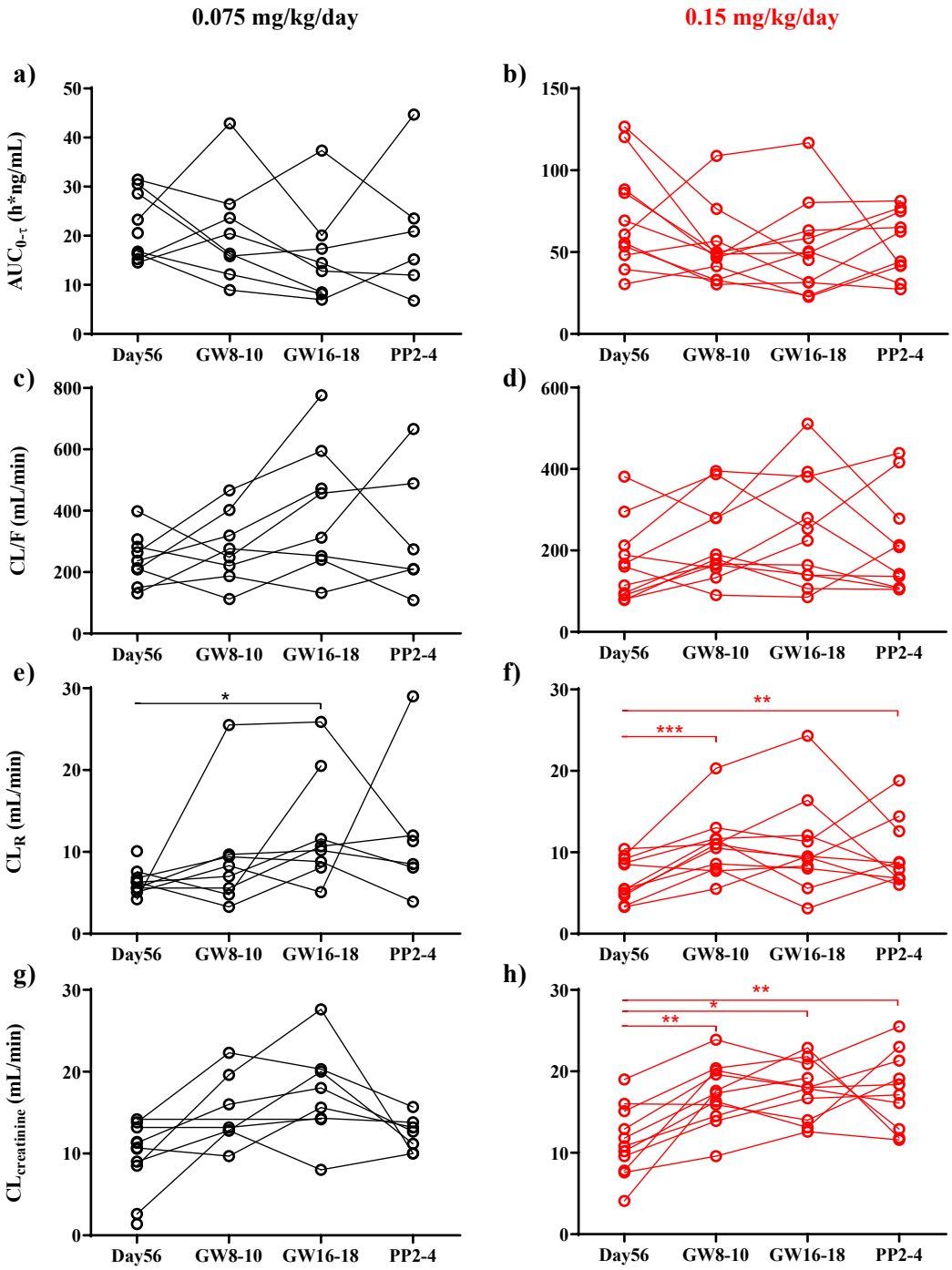

Figure 3.2. Toxicokinetic parameters of DA measured in individual animals before (Day 56), during (GW8-10 and GW16-18) and after (PP2-4) pregnancy. Panel (a, b) $AUC_{0-\tau}$, panel (c, d) oral clearance (CL/F), panel (e, f) renal clearance (CL_R), and panel (g, h) creatinine clearance ($CL_{creatinine}$). Each open circle represents the observed value in an individual monkey and the values observed in each monkey over the course of the study are linked with lines. (* p <0.017, ** p <0.003, *** p <0.001). Black symbols are for the 0.075 mg/kg group and red symbols are for the 0.15 mg/kg group.

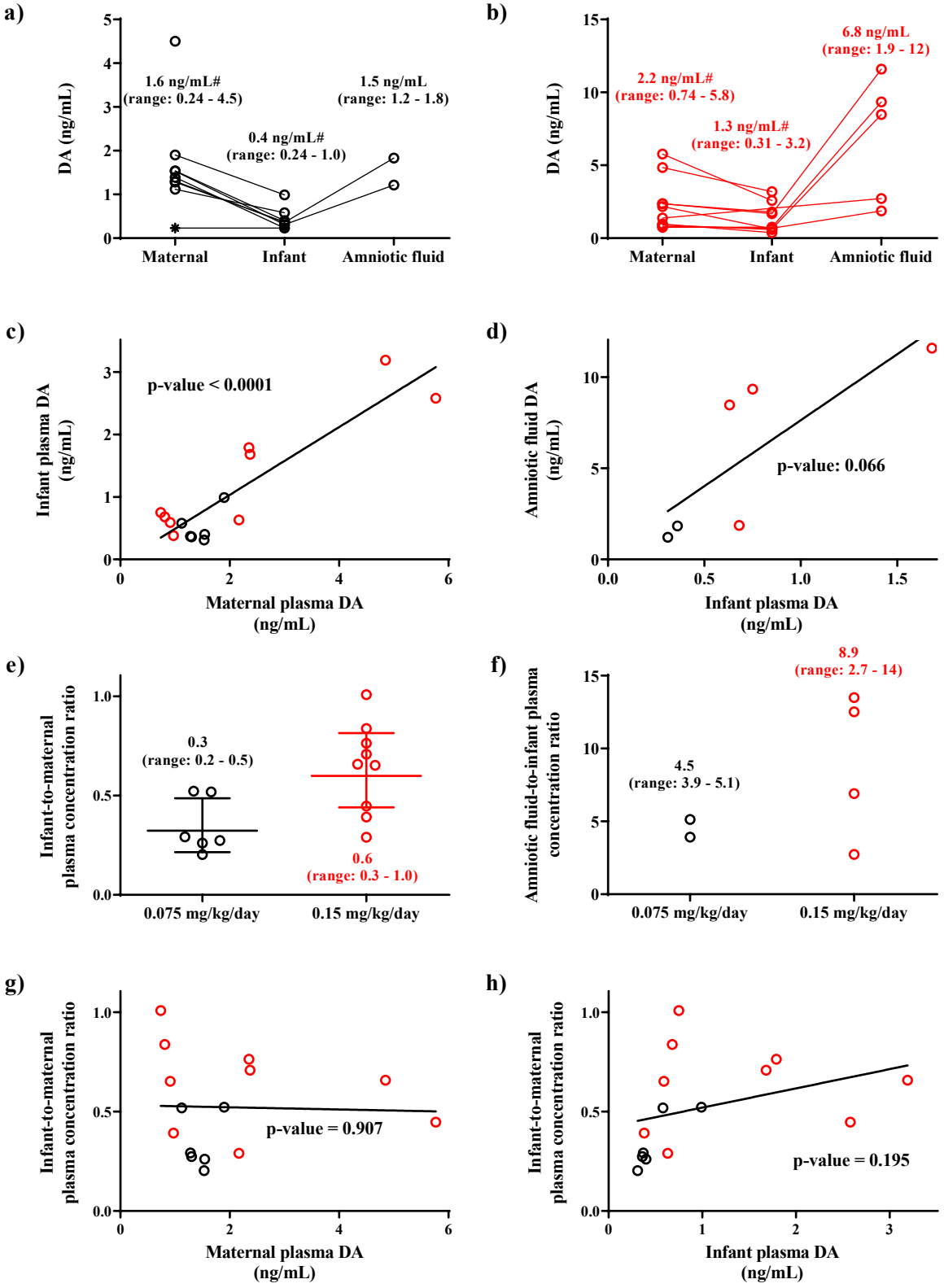
a)
DA (ng/mL)
1.6 ng/mL#
(range: 0.24 - 4.5)
1.5 ng/mL
(range: 1.2 - 1.8)
0.4 ng/mL#
(range: 0.24 - 1.0)
Maternal
Infant
Amniotic fluid
b)
DA (ng/mL)
6.8 ng/mL
(range: 1.9 - 12)
2.2 ng/mL#
(range: 0.74 - 5.8)
1.3 ng/mL#
(range: 0.31 - 3.2)
Maternal
Infant
Amniotic fluid
c)
Infant plasma DA
(ng/mL)
p-value < 0.0001
Maternal plasma DA
(ng/mL)
d)
Amniotic fluid DA
(ng/mL)
p-value: 0.066
Infant plasma DA
(ng/mL)
e)
Infant-to-maternal
plasma concentration ratio
0.3
(range: 0.2 - 0.5)
0.6
(range: 0.3 - 1.0)
0.075 mg/kg/day
0.15 mg/kg/day
f)
Amniotic fluid-to-infant plasma
concentration ratio
8.9
(range: 2.7 - 14)
4.5
(range: 3.9 - 5.1)
0.075 mg/kg/day
0.15 mg/kg/day
g)
Infant-to-maternal
plasma concentration ratio
p-value = 0.907
Maternal plasma DA
(ng/mL)
h)
Infant-to-maternal
plasma concentration ratio
p-value = 0.195
Infant plasma DA
(ng/mL)

Figure 3.3. Maternal-fetal disposition of DA at delivery. Paired maternal plasma, infant plasma, and amniotic fluid DA concentrations of (a) 0.075 mg/kg/day group and (b) 0.15 mg/kg/day group. Open circles represent concentrations measured in each individual animal, and data for each maternal-infant pair are linked with lines. Data presented as (*) represents samples where DA was detected but concentrations were less than LOQ. Mean and range of concentrations in the maternal, infant and amniotic fluid samples are listed on the graph above corresponding datapoints. Panel (c) shows the correlation between maternal and infant plasma DA concentrations and panel (d) shows the correlation between amniotic fluid and infant plasma DA concentrations. Open black circles and red circles represent data from the 0.075 mg/kg/day and 0.15 mg/kg/day groups, respectively. Panel (e) shows the infant-to-maternal plasma DA concentration ratios and panel (f) shows the amniotic fluid-to-infant plasma DA concentration ratios with the mean values and range of ratios listed next to each dataset. The correlation between infant-to-maternal plasma concentration ratio and maternal plasma DA concentration is shown in panel (g) while panel (h) shows the correlation between the infant-to-maternal plasma concentration ratio and infant plasma DA concentration at delivery. Open black circles and red circles represent data from the 0.075 mg/kg/day and 0.15 mg/kg/day groups, respectively. The mean values and ranges of maternal and fetal DA concentrations at delivery indicated with # were reported previously[165]

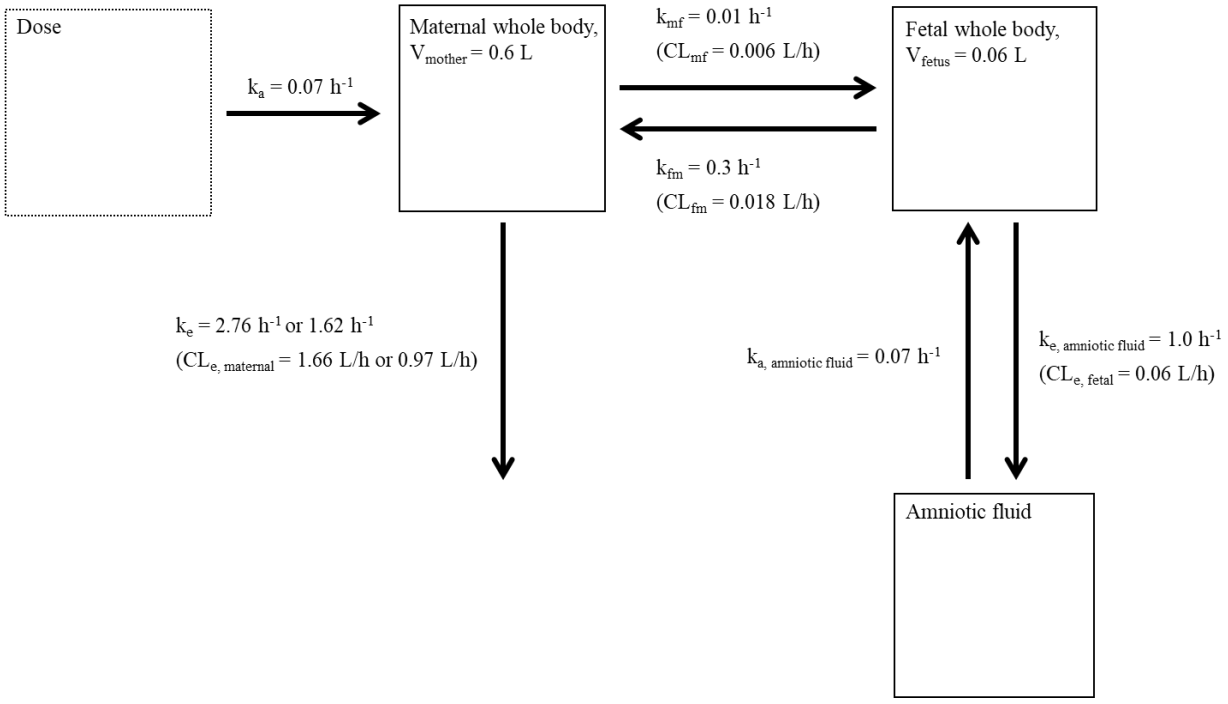

Figure 3.4. Structure and parameters of the final DA maternal-fetal TK model. The two $CL_{e, maternal}$ values used in the model were assigned based on the observed oral clearance values in the two different DA dose groups at GW16-18.

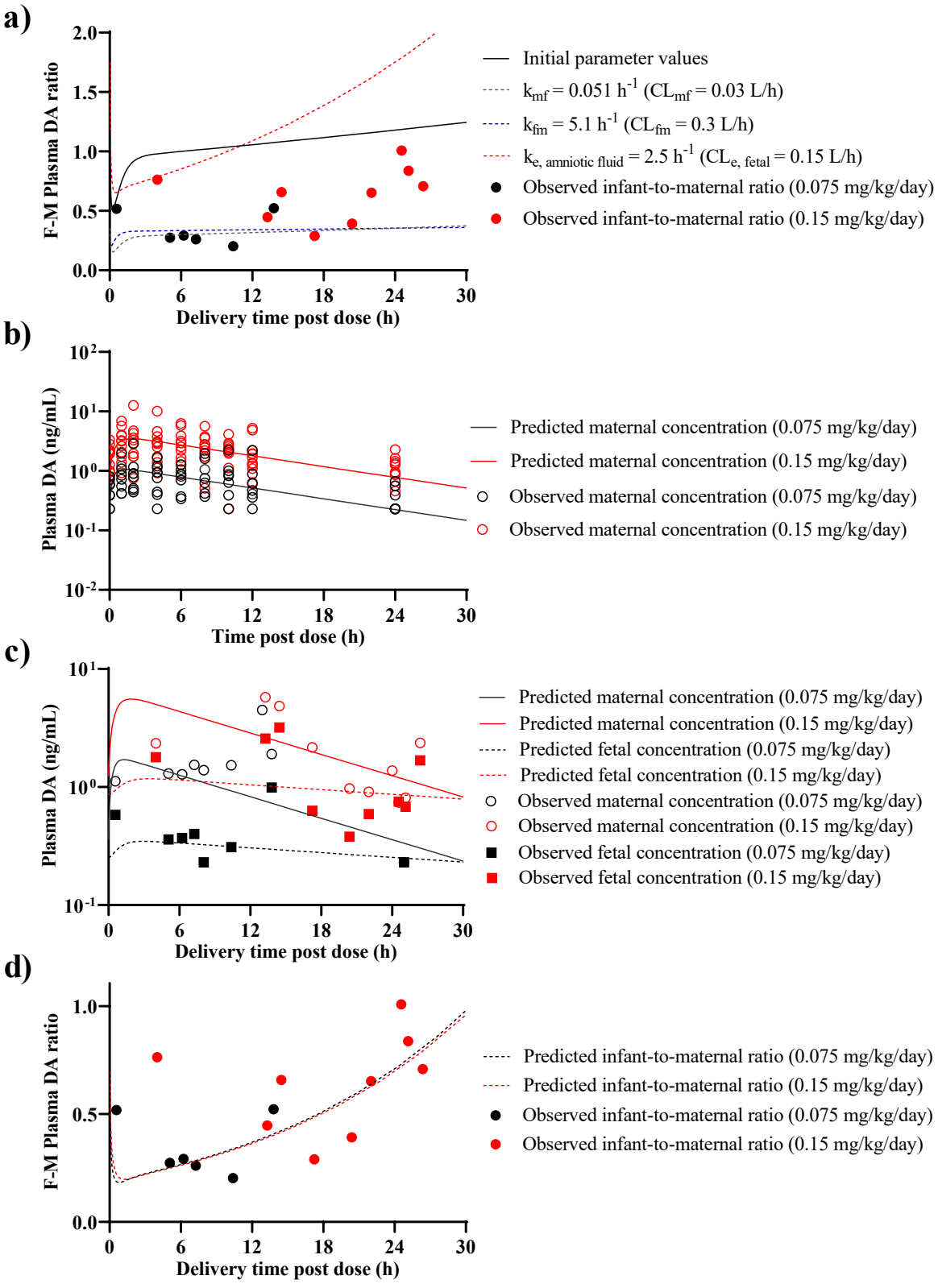
a)
F-M Plasma DA ratio
2.0
1.5
1.0
0.5
0.0
0
6
12
18
24
30
Delivery time post dose (h)
Initial parameter values
k_{mf} = 0.051 h^{-1} (CL_{mf} = 0.03 L/h)
k_{fm} = 5.1 h^{-1} (CL_{fm} = 0.3 L/h)
$k_{e,\ amniotic\ fluid}$ = 2.5 h^{-1} ($CL_{e,\ fetal}$ = 0.15 L/h)
Observed infant-to-maternal ratio (0.075 mg/kg/day)
Observed infant-to-maternal ratio (0.15 mg/kg/day)
b)
Plasma DA (ng/mL)
10^2
10^1
10^0
10^{-1}
10^{-2}
0
6
12
18
24
30
Time post dose (h)
Predicted maternal concentration (0.075 mg/kg/day)
Predicted maternal concentration (0.15 mg/kg/day)
Observed maternal concentration (0.075 mg/kg/day)
Observed maternal concentration (0.15 mg/kg/day)
c)
Plasma DA (ng/mL)
10^1
10^0
10^{-1}
0
6
12
18
24
30
Delivery time post dose (h)
Predicted maternal concentration (0.075 mg/kg/day)
Predicted maternal concentration (0.15 mg/kg/day)
Predicted fetal concentration (0.075 mg/kg/day)
Predicted fetal concentration (0.15 mg/kg/day)
Observed maternal concentration (0.075 mg/kg/day)
Observed maternal concentration (0.15 mg/kg/day)
Observed fetal concentration (0.075 mg/kg/day)
Observed fetal concentration (0.15 mg/kg/day)
d)
F-M Plasma DA ratio
1.0
0.5
0.0
0
6
12
18
24
30
Delivery time post dose (h)
Predicted infant-to-maternal ratio (0.075 mg/kg/day)
Predicted infant-to-maternal ratio (0.15 mg/kg/day)
Observed infant-to-maternal ratio (0.075 mg/kg/day)
Observed infant-to-maternal ratio (0.15 mg/kg/day)

Figure 3.5. Simulated steady-state (after the 50th dose) maternal-fetal disposition of DA overlaid with observed maternal and infant plasma concentrations at delivery. (a) Simulated fetal-to-maternal plasma concentration ratio over time under the initial parameter values (k_a = 0.07 h^{-1}, k_e = 2.76 h^{-1} *($CL_{e,maternal}$ = 1.66 L/h)*, k_{mf} = 0.17 h^{-1} *(CL_{mf} = 0.1 L/h)*, k_{fm} = 1.7 h^{-1} *(CL_{fm} = 0.1 L/h)*, $k_{e,\ amniotic\ fluid}$ = 0.25 h^{-1} *($CL_{e,\ fetal}$ = 0.015 L/h)* and $k_{a,\ amniotic\ fluid}$ = 0.07 h^{-1}), and with decreased k_{mf}, increase k_{fm}, or increased $k_{e,amniotic\ fluid}$ as described for the sensitivity analyses. The simulated fetal-to-maternal ratios are overlaid with observed infant-to-maternal ratios from individual monkeys at delivery. (b) Simulated (using the final model) maternal plasma concentration-time profiles overlaid with observed maternal concentration-time profiles from individual monkeys at GW16-18. (c) Simulated maternal and fetal plasma concentration profiles overlaid with observed maternal and infant concentrations at delivery. (d) Simulated fetal-to-maternal plasma concentration ratio using the final kinetic model (k_{mf} = 0.01 h^{-1} *(CL_{mf} = 0.006 L/h)*, k_{fm} = 0.3 h^{-1} *(CL_{fm} = 0.018 L/h)*, $k_{e,\ amniotic\ fluid}$ = 1 h^{-1} *($CL_{e,\ fetal}$ = 0.06 L/h)*, and initial values for k_a, k_e, and $k_{e,\ amniotic\ fluid}$) overlaid with observed infant-to-maternal ratios from individual monkeys at delivery**.**

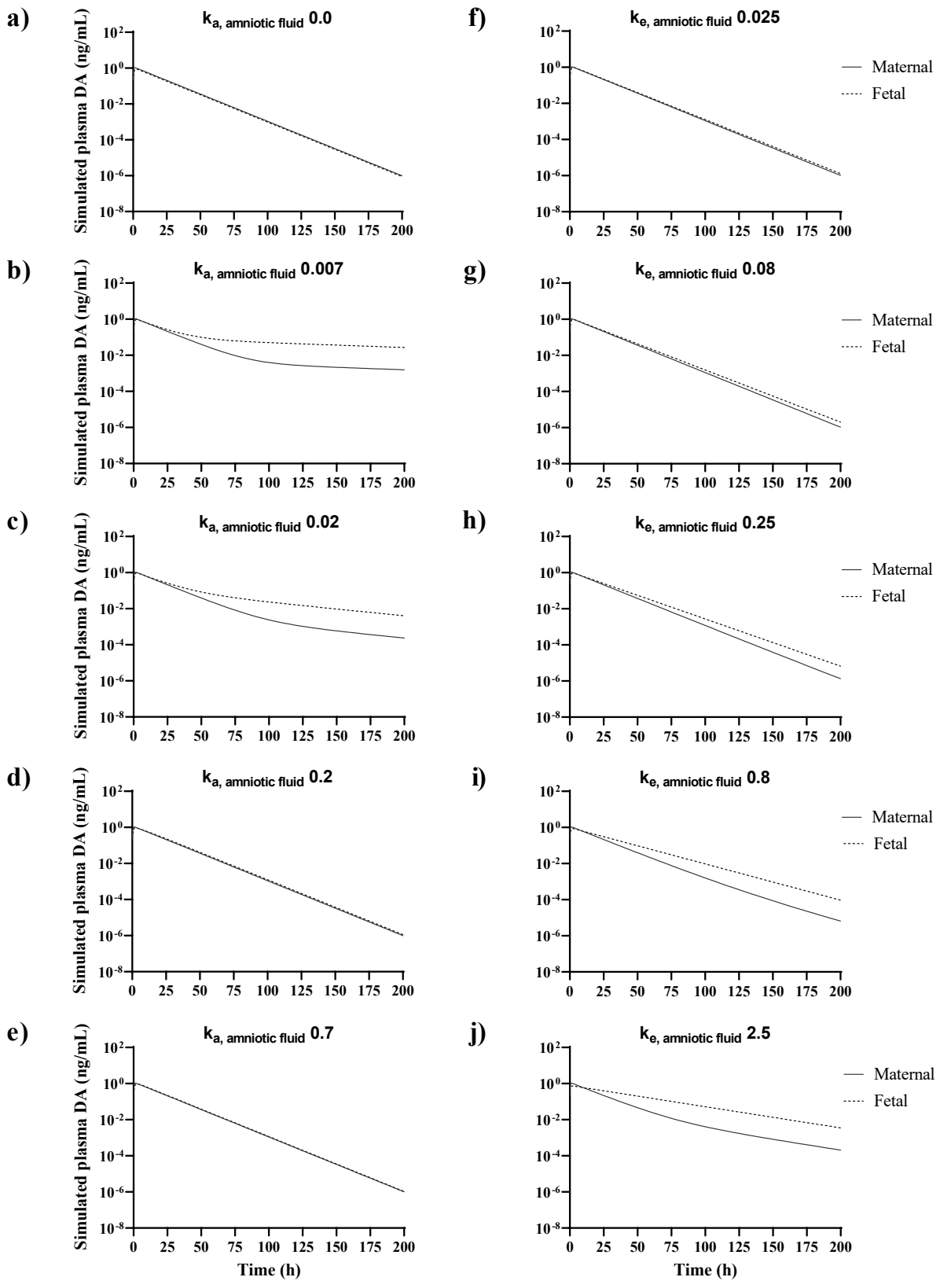
a)
$k_{a,\ amniotic\ fluid}$ 0.0
b)
$k_{a,\ amniotic\ fluid}$ 0.007
c)
$k_{a,\ amniotic\ fluid}$ 0.02
d)
$k_{a,\ amniotic\ fluid}$ 0.2
e)
$k_{a,\ amniotic\ fluid}$ 0.7
f)
$k_{e,\ amniotic\ fluid}$ 0.025
g)
$k_{e,\ amniotic\ fluid}$ 0.08
h)
$k_{e,\ amniotic\ fluid}$ 0.25
i)
$k_{e,\ amniotic\ fluid}$ 0.8
j)
$k_{e,\ amniotic\ fluid}$ 2.5
Simulated plasma DA (ng/mL)
Time (h)
Maternal
Fetal

Figure 3.6. Sensitivity analyses to illustrate the effect of altering $k_{a,\ amniotic\ fluid}$ and $k_{e,\ amniotic\ fluid}$ on steady-state maternal and fetal plasma concentration time profiles up to 200 h post last (the 50th) dose. Simulated maternal and fetal plasma concentration time profiles with (a) in the absence of $k_{a,\ amniotic\ fluid}$, (b-e) altering $k_{a,\ amniotic\ fluid}$ values ranging from 0.007 to 0.7 h^{-1}, (f-j) altering $k_{e,\ amniotic\ fluid}$ values ranging from 0.007 to 0.7 h^{-1}. Simulations were performed by changing either $k_{a,\ amniotic\ fluid}$ or $k_{e,\ amniotic\ fluid}$ while keeping the other parameters at their initial values (k_a = 0.07 h^{-1}, k_e = 2.76 h^{-1} *($CL_{e,maternal}$ = 1.66 L/h)*, k_{mf} = 0.17 h^{-1} *(CL_{mf} = 0.1 L/h)*, k_{fm} = 1.7 h^{-1} *(CL_{fm} = 0.1 L/h)*, $k_{e,\ amniotic\ fluid}$ = 0.25 h^{-1} *($CL_{e,\ fetal}$ = 0.015 L/h)* and $k_{a,\ amniotic\ fluid}$ = 0.07 h^{-1}).

Chapter 4.

Human fetal liver metabolism of oxycodone is mediated by CYP3A7

A version of this chapter is in press for publication as a research article in the AAPS journal

Authors: Sara Shum and Nina Isoherranen

4.1 ABSTRACT

Oxycodone is an opioid analgesic that is commonly prescribed to pregnant women to treat moderate to severe pain. It has been shown to cross the placenta and distribute to the fetus. Oxycodone is mainly metabolized by CYP3A4 in adult liver. Since CYP3A7 is abundantly expressed in the fetal liver and has overlapping substrate specificity with CYP3A4, we hypothesized that the fetal liver may significantly limit fetal exposure to oxycodone. This study showed that oxycodone is metabolized by CYP3A7 to noroxycodone in fetal liver microsomes (FLMs). The measured CYP3A7 expression was 191 – 409 pmol/mg protein in 14 FLMs and an intersystem extrapolation factor (ISEF) for CYP3A7 was 0.016-0.066 in the panel of fetal livers using 6β-OH-testosterone formation as the probe reaction. Noroxycodone formation in the fetal liver was predicted from formation rate by recombinant CYP3A7, CYP3A7 expression level and the established ISEF value with average fold error of 1.25. Based on the intrinsic clearance of oxycodone measured in FLM, the fetal hepatic clearance (CL_h) at term was predicted to be 495 (range: 66.4 – 936) μL/min, a value that is > 99% lower than the predicted adult liver CL_h. The predicted fetal hepatic extraction ratio was 0.0019 (range: 0.00003 – 0.0036). These results suggest that fetal liver metabolism does not quantitatively contribute to the total systemic clearance of oxycodone in pregnant women nor does it provide a barrier for limiting fetal exposure to oxycodone. Additionally, since CYP3A7 forms noroxycodone, an inactive metabolite, the metabolism in the fetal liver is unlikely to affect fetal opioid activity.

4.2 INTRODUCTION

The use of opioid analgesics close to term is associated with neonatal opioid withdrawal syndrome (NOWS)[180–182] and developmental delay in children exposed prenatally.[84,183] In the

United States, there has been a significant increase in the rate of opioid use during pregnancy,[184] and the incidence of NOWS increased from 1.2 per 1000 births in year 2000 to 5.8 per 1000 births in 2012.[185] Yet, large scale epidemiological studies have not established a relationship between maternal opioid dose during pregnancy and associated fetal outcomes.[186,187] While many reasons contribute to the lack of correlation, poor knowledge of the maternal-fetal disposition of opioid analgesics likely impacts the analysis. For example, it has been shown that norbuprenorphine interacts with P-glycoprotein,[188] an efflux transporter that is expressed in the placenta potentially limiting fetal norbuprenorphine exposure. Similarly, fetal metabolism has been observed for morphine,[55] codeine,[52] and dextromethorphan,[52,53] potentially decreasing fetal exposure to these drugs. Fetal metabolism can also result in formation of active metabolites. For example, in nonhuman primates, morphine-6-glucuronide, an active metabolite of morphine, is formed in the fetus.[49] The increased fetal exposure to an active metabolite formed locally in the fetus adds complexity to the maternal-fetal disposition and fetal pharmacological responses to opioids.

Oxycodone is an opioid commonly prescribed during pregnancy to treat moderate to severe pain.[106,182] Oxycodone concentrations in the umbilical cord are similar to those in maternal plasma following intravenous or subcutaneous doses of oxycodone given during early stages of labor,[108,109] demonstrating that oxycodone crosses the placenta and distributes to the fetus. Despite the common usage of oxycodone during pregnancy, knowledge of the mechanisms of maternal-fetal disposition of oxycodone is limited, and whether the fetal liver or the placenta limits exposure of the fetus to oxycodone or its metabolites is not known. In adults, oxycodone is extensively metabolized by CYP3A4 to form noroxycodone (fraction metabolized (f_m): 0.4 – 0.5), an inactive metabolite, and by CYP2D6 to form oxymorphone (f_m: 0.1 – 0.2), an active

metabolite.[110,111] Although CYP3A4 and CYP2D6 expression in the fetal liver is very low,[38,61] CYP3A7 is abundantly expressed in the fetal liver[38,61,189] and has been shown to metabolize many CYP3A4 substrates including midazolam, clarithromycin, carbamazepine, and alfentanil.[59,112,190] In addition, the CYP3A4-mediated metabolic reactions of norcodeine formation from codeine[52] and 3-methoxymorphinan formation from dextromethorphan[52,53] in the adult liver were also observed in fetal liver microsomes (FLM) presumably mediated by CYP3A7. Based on these data of significant xenobiotic metabolic activities of CYP3A7 and FLM in metabolizing opioids that are CYP3A4 substrates, we hypothesized that CYP3A7 metabolizes oxycodone and that the fetal liver metabolism decreases the fetal exposure to oxycodone. The goal of this study was to define the fetal liver metabolism of oxycodone and predict the quantitative importance of fetal liver metabolism of oxycodone.

4.3 Materials and Methods

4.3.1 *Fetal liver microsomes (FLM), adult human liver microsomes (HLM), and recombinant cytochrome P450 enzymes (CYPs)*

Previously collected[57] banked fetal livers from 18 individuals (9 males, 7 females and 2 unidentified sex) were used. All tissues were from healthy pregnancies with no known maternal drug use and with previously published donor characteristics.[57] Tissue collection was approved by the Institutional Review Board (IRB) of the University of Washington and was conducted according to the guidance of the Office of Human Research Protections (OHRP). The estimated gestational age at the time of fetal liver collection ranged from 85 to 137 days.[57] To prepare FLM, approximately 100 mg of fetal liver was homogenized in 0.5 mL 10 mM phosphate buffer (pH 7.4) with 250 mM sucrose and 0.2 mM phenylmethylsulfonyl fluoride (PMSF) using an Omni Bead Ruptor 24 (Kennesaw, GA) at <4°C. The homogenates were centrifuged at 10,000g

for 20 min at 4°C and the supernatants were centrifuged at 100,000g on the Sorvall Discovery M150SE ultracentrifuge (Waltham, MA) for 1 h at 4°C to collect microsomes. The microsomal pellets were reconstituted and stored at -80°C until experiments. Pooled FLM were prepared by pooling 14 individual FLMs. Human liver microsomes pooled from 50 donors were purchased from Sekisui Xenotech, LLC (Kansas City, KS). Membrane preparations of recombinant CYP2D6, CYP3A4, CYP3A5, and CYP3A7 coexpressed with P450 reductase and cytochrome b5 were purchased from Corning Life Sciences (Corning, NY). Recombinant, purified CYP3A7 expressed in *E. coli* and used as a calibration standard for CYP3A7 quantification in FLM was a gift from Emily E. Scott, University of Michigan.

4.3.2 *Quantification of CYP3A7 protein in FLM by HPLC-MS/MS*

The CYP3A7 protein contents of the pooled FLM and 14 individual FLMs were quantified using a previously published HPLC-MS/MS method.[56] Briefly, FLMs were diluted to 1 mg/mL using 100 mM ammonium bicarbonate buffer, 20 µg of protein (20 µL) was denatured and reduced with the addition of 4 µL of 100 mM dithiothreitol, 10 µL of 2.6% w/v sodium deoxycholate, and 10 µL of 100 mM ammonium bicarbonate buffer, and the mixture was incubated at 95°C for 5 min. The denatured protein was alkylated under yellow light using 4 µL of 200 mM iodoacetamide at room temperature for 20 min. Thereafter, 0.4 µg of trypsin (1:50) was added to digest microsomal protein at 37°C for 20 h. The digestion time was adapted from a previously published method[56] and confirmed to result in stable digestion from pooled FLM with no change in signal intensity between 20 and 24 h in a digestion time-course from 4 to 24 h. The digestion was stopped by the addition of 30 µL 50% aqueous acetonitrile containing 0.1% formic acid and 15 nM [$^{13}C_6$ $^{15}N_2$]-lysine labelled peptide as an internal standard. The samples were centrifuged at 20,000g for 45 min. Calibration standards were prepared by spiking a known

amount of purified soluble CYP3A7 protein (expressed in *E. coli*) to pooled HLM (confirmed to lack detectable CYP3A7 expression). Seven calibration concentrations at 40 – 800 pmol/mg protein and three quality control samples (QCs) along with blank controls were included in each assay. The experiment was performed in singlet on three different days, and the protein concentration of each FLM is reported as the arithmetic mean and the standard deviation of the data from three different days.

Target peptide (FNPLDPFVLSIK) concentrations were measured using an AB Sciex Triple Quad™ 5500+ QTRAP mass spectrometer (Foster City, CA) equipped with an Agilent 1290 UHPLC (Santa Clara, CA) and a Phenomenex Aeris™ PEPTIDE XB-C18 LC column (1.7 µm, 50 x 2.1 mm) with a Phenomenex SecurityGuard™ C18-Peptide cartridge (sub-2 µm, 2.1 mm) (Torrance, CA). A 16-min gradient was employed using (A) water containing 0.1% formic acid and (B) acetonitrile containing 0.1% formic acid at a flow rate of 0.4 mL/min. The target peptide and its labelled internal standard were detected by electrospray ionization operated in positive ion mode and two product ions were monitored (m/z 695>918 and 695>565; and m/z 699>927 and 699>569 for target and heavy labeled peptide, respectively) to confirm the analytes and the most sensitive product ion was used for quantification (m/z 695 > 565 and m/z 699 > 569 for target and heavy labeled peptide, respectively). The lower limit of quantification (LLOQ) for CYP3A7 was 20 pmol/mg protein.

4.3.3 *In vitro incubations*

All incubation experiments were done in potassium phosphate buffer (pH 7.4) at 37°C and were initiated by addition of NADPH and included no NADPH controls. Incubations were conducted in duplicates on three different days except for four individual FLMs for which the oxycodone incubations were done in duplicates on two different days due to limited availability

of the fetal liver. Incubations were quenched by addition of two parts of ice-cold methanol containing noroxycodone-d_3 and oxymorphone-d_3 as internal standards, vortexed and centrifuged at 16,100g, and supernatants were stored at -20°C until HPLC-MS/MS analysis. Oxycodone, noroxycodone, oxymorphone, noroxycodone-d_3 and oxymorphone-d_3 were purchased from Millipore Sigma (St Louis, MO).

Noroxycodone and oxymorphone formation kinetics was characterized in recombinant CYP microsomes, pooled HLM, and pooled FLM. Under conditions of protein and time linearity, oxycodone (1, 2, 5, 15, 30 µM) was incubated with recombinant CYP2D6 (5 pmol/mL), CYP3A4 (1 pmol/mL), CYP3A5 (5 pmol/mL), CYP3A7 (5 pmol/mL), pooled HLM (0.05 mg/mL), or pooled FLM (0.1 mg/mL) for 15 min. Additionally, 6β-OH-testosterone formation kinetics was characterized in recombinant CYP3A7 and pooled FLM. Testosterone (5, 10, 15 µM) was incubated with recombinant CYP3A7 (10 pmol/mL) and pooled FLM (0.2 mg/mL) for 15 min. To further evaluate the intrinsic capacity and interindividual variability of the fetal liver metabolism of oxycodone, noroxycodone and oxymorphone formation was measured in FLM from 18 individual fetal livers. Oxycodone (5 µM) was incubated in FLM (0.2 mg/mL) for 30 min. The percent contribution of CYP3A to metabolite formation in FLMs and HLM was determined in incubations with 1 µM of ketoconazole to inhibit CYP3A activity. To measure CYP3A activity in each FLMs (n=18), 6β-OH-testosterone formation from 35 µM testosterone was measured.

4.3.4 *HPLC-MS/MS analysis*

Metabolite concentrations were measured using an AB Sciex 6500 qTrap Q-LIT mass spectrometer (Foster City, CA) equipped with a Shimadzu UPLC XR DGU-20A5 (Columbia, MD) and a Kinetex® EVO C18 LC column (2.6 µm, 100 x 2.1 mm) with a Phenomenex

SecurityGuard™ EVO-C18 cartridge (sub-2 μm, 2.1 mm) (Torrance, CA). For noroxycodone and oxymorphone analysis, a 10-min gradient elution (0.35 mL/min) with (A) 20 mM ammonium formate and (B) 50:50 v/v acetonitrile and methanol starting at 0% (B) for 1 min, increased to 25% (B) over 2 min, kept at 25% (B) for 1.5 min, increased to 100% (B) over 0.5 min and kept at 100% (B) for 0.5 min before returning to initial conditions over 0.5 min was used. An 8-min gradient using the same mobile phases (flow 0.3 mL/min) was used for 6β-OH-testosterone analysis. The gradient was from 5% (B) for 1 min, increased to 100% (B) over 3 min and kept at 100% (B) for 0.5 min, returning to initial conditions over 0.1 min. The analytes were detected by positive ion electrospray ionization. Three product ions were monitored to confirm the identity of analytes, and the most sensitive product ion was used to quantify each analyte (noroxycodone m/z 302 > 187, oxymorphone m/z 302 > 227, 6β-OH-testosterone m/z 305 > 269). Calibration standards were prepared in phosphate buffer. For oxycodone and oxymorphone (calibration range 1 – 300nM), the LLOQ were 1 nM. QCs (3, 30, 150 and 240 nM) were included in every run and the intraday and interday precision and accuracy were within 10% for both analytes throughout. For 6β-OH-testosterone (calibration range 1 – 300 nM), LLOQ was 10 nM. QCs (16, 130 and 230 nM) included in every LC-MS/MS run and the intraday and interday precision were within 15% and accuracy within 10% throughout.

4.3.5 *Data analysis*

The metabolite formation rates were normalized to either pmol CYP or mg microsomal protein. Straight lines were fitted to the noroxycodone formation rate over oxycodone concentration to estimate the intrinsic clearances (CL_{int})[191] of noroxycodone formation by CYP3A4, CYP3A7, pooled HLM, and pooled FLM. Similarly, straight lines were fitted to the 6β-OH-testosterone formation rate over testosterone concentration to estimate the CL_{int} of 6β-

OH-testosterone formation by CYP3A7 and pooled FLM ($CL_{int,FLM}$). The Michaelis-Menten equation was fitted to the oxymorphone formation rate over oxycodone concentration data to estimate the k_{cat}, K_m, and CL_{int} of oxymorphone formation by CYP2D6. All results are reported as the arithmetic means and standard deviations of data from three different days. The intersystem extrapolation factor (ISEF) for CYP3A7 for 6β-OH-testosterone formation was calculated using equation 1:

$$ISEF = \frac{CL_{int,FLM}}{CL_{int,CYP3A7} \times CYP3A7\ abundance} \quad (1)$$

where CYP3A7 abundance is the measured CYP3A7 expression in the pooled FLM. The calculated ISEF was applied to predict the CL_{int} of noroxycodone formation in pooled FLM from the CL_{int} of noroxycodone formation in recombinant CYP3A7 by multiplying the CL_{int} of CYP3A7 with the CYP3A7 expression (pmol CYP/mg protein) and the calculated ISEF. The $CL_{int,FLM}$ of noroxycodone formation were predicted similarly for each individual FLM using the ISEF value calculated from the 6β-OH-testosterone formation in each respective FLM.

The $CL_{int,FLM}$ in 16 livers (two FLMs showed no noroxycodone formation) was calculated as the noroxycodone formation rate divided by the oxycodone concentration. The $CL_{int,FLM}$ of 6β-OH-testosterone formation was calculated as the formation rate divided by the testosterone concentration. The formation rate, intrinsic clearance, and ketoconazole % inhibition were reported as the arithmetic means of data from three different days or as the average of two days when limited data was available. The differences between the mean noroxycodone formation rate in the presence and absence of ketoconazole for individual FLMs were tested using the paired t-test. Correlation between the mean $CL_{int,FLM}$ of noroxycodone formation and the mean $CL_{int,FLM}$ of 6β-OH-testosterone formation or the mean CYP3A7 expression in each FLM were tested by linear regression.

All calculations were performed using Microsoft Excel for Microsoft 365 (Redmond, WA). Graphical presentation of results and statistical analysis were done using GraphPad Prism version 8 (San Diego, CA).

4.3.6 *In vitro-to-in vivo extrapolation (IVIVE)*

Fetal hepatic clearance (CL_h) and extraction ratio (ER) of oxycodone were first predicted for each of the 16 donor livers that showed noroxycodone formation. To do this, the unbound intrinsic clearance for the fetal liver ($CL_{int,u}$) was calculated from $CL_{int,FLM,}$ the microsomal protein per gram of liver (MPPGL) yield, and the estimated fetal liver weight using equation 2:

$$CL_{int,u} = CL_{int,FLM} \times MPPGL \times liver\ weight \quad (2)$$

The measured MPPGL was 8 – 33 mg/g. The liver weight was calculated using the reported [192] equation $16.6-2.9*GA+0.143GA^2$ for fetal liver volume (mL) assuming fetal liver density of 1g/mL and based on the reported[57] gestational age in weeks (GA) in each donor resulting in liver weight 2.2-14.2g. The fetal liver blood flow (Q_h) was calculated as $Q_{UV} + Q_{fetal\_portal\_vein} - Q_{ductus\_venosus}$ (resulting range 1.8-4.4 L/h) using the published [192] equations for $Q_{UV} = 0.647–0.227*GA+0.0179*GA^2$ (resulting range 0.5-3.1 L/h), $Q_{ductus\_venosus} = 2.05–0.297*GA + 0.0116*GA^2$ (resulting range 0.2-0.7 L/h), and $Q_{fetal\_portal\_vein} = 0.714+0.0489*GA+0.0008*GA^2$ (resulting range 1.4-2.0 L/h).

Fetal CL_h was then calculated using equation 3 (the well-stirred model[60]):

$$CL_h = \frac{\frac{f_u}{BP\ ratio} \times CL_{int,u} \times Q_h}{\frac{f_u}{BP\ ratio} \times CL_{int,u} + Q_h} \quad (3)$$

where f_u is the unbound fraction in fetal plasma (same as in adult, f_u=0.55) and BP ratio is the blood to plasma concentration ratio (same as adult, BP ratio=1.3[193]). The extraction ratio (ER) by the fetal liver was calculated as CL_h/Q_h.

To extrapolate the findings from early gestation to later gestational ages, fetal CL_h and ER from gestational weeks 12 to 40 were predicted using equations 2 and 3 with the average $CL_{int,FLM}$*MPPGL measured in the 16 individual fetal livers used in equation 2 together with the calculated fetal liver weight and blood flows for each GA incorporated into equations 2 and 3. The CYP3A7 expression and hence $CL_{int,FLM}$ was assumed to be independent of gestational age as CYP3A7 expression has been shown to be relatively constant from early to late gestation based on mRNA expression, protein expression, and enzymatic activity data.[61,189] The upper and lower limits of the CL_h and ER from gestational weeks 12 to 40 were predicted using the maximum and minimum values obtained for $CL_{int,FLM}$*MPPGL of the 16 fetal livers.

Adult hepatic clearance (CL_h) and extraction ratio (ER) of oxycodone were also predicted using the well stirred model with Q_h = 1.5 L/min and incorporating the sum of the pooled HLM measured noroyxoconde and oxymorphone CL_{int}'s multiplied by MPPGL of 39.8 mg/g and liver weight of 1,648 g.

4.4 RESULTS

Recombinant CYP3A7 metabolized oxycodone to noroxycodone similar to recombinant CYP3A4, while no quantifiable noroxycodone formation was observed by CYP3A5 (**Figure 4.1a**). With CYP3A4 and CYP3A7, noroxycodone formation was linear from 1 to 30 µM oxycodone suggesting that the K_m's of oxycodone with CYP3A4 and CYP3A7 are much greater than 30 µM (**Figure 4.1b,c**). The intrinsic clearance (CL_{int}) of noroxycodone formation by CYP3A7 (0.042 ± 0.007 µL/min/pmol CYP) was 89% lower than that by CYP3A4 (0.38 ± 0.07 µL/min/pmol CYP). No oxymorphone formation was observed with any of the recombinant CYP3A enzymes, but recombinant CYP2D6 formed oxymorphone and not noroxycodone (**Figure 4.1a**). The K_m of oxycodone with CYP2D6 was estimated to be 14 ± 1.8 µM. The CL_{int}

of oxymorphone formation by recombinant CYP2D6 (0.27 ± 0.05 μL/min/pmol CYP) was 29% lower than that of noroxycodone formation by recombinant CYP3A4 (**Figure 4.1d**). Based on the recombinant enzyme kinetics, a reported ISEF value for CYP3A4 (ISEF: 0.15),[194] and reported CYP3A4 expression data in HLM (78 pmol/mg protein),[62] noroxycodone formation CL_{int} in HLM ($CL_{int,HLM}$) was predicted to be 4.4 μL/min/mg protein. Since no published ISEF value has been reported for CYP3A7, the ISEF value for CYP3A7 was estimated in this study. To determine the CYP3A7 ISEF value for FLMs, CYP3A7 protein expression was measured in pooled FLM and in 14 individual FLMs. The measured CYP3A7 expression was 359 ± 41 pmol/mg protein in pooled FLM (**Figure 4.2**) and ranged from 191 to 409 pmol/mg protein in the individual FLMs (mean 326 ± 74). The 6β-OH-testosterone formation CL_{int} was used for ISEF value estimation and measured in recombinant CYP3A7 to be 0.072 ± 0.002 μL/min/pmol CYP, in pooled FLM to be 1.13 ± 0.21 μL/min/mg protein, and in 14 individual FLMs to be between 0.035 and 1.95 (mean 0.77 ± 0.51) μL/min/mg protein. The ISEF value of CYP3A7 was calculated to be 0.044 based on the pooled FLM and to range from 0.016 to 0.066 (mean 0.036 ± 0.016) in the individual FLMs. The calculated ISEF of CYP3A7 was then applied to the mean noroxycodone formation CL_{int} by recombinant CYP3A7 multiplied by the CYP3A7 expression in pooled FLM, and the $CL_{int,FLM}$ of noroxycodone formation in pooled FLM was predicted to be 0.66 μL/min/mg protein, 85% lower than the predicted $CL_{int,HLM}$. The corresponding individual FLM ISEF and CYP3A7 expression values were used to predict the $CL_{int,FLM}$ of each individual FLM and $CL_{int,FLM}$ were predicted to range from 0.15 to 1.13 (mean 0.50 ± 0.27) μL/min/mg protein. Similarly, the oxymorphone formation $CL_{int,HLM}$ was predicted to be 0.44 μL/min/mg protein using the reported ISEF of 0.18 for CYP2D6[194] and the reported CYP2D6 expression

data in HLM (9.1 pmol/mg protein).[62] No oxymorphone was predicted to form in FLM based on the minimal CYP2D6 expression reported in FLM.[36,53,56]

Both noroxycodone and oxymorphone formation were observed in pooled HLM (**Figure 4.1e**). The noroxycodone formation was linear from 1 to 30 μM oxycodone while the oxymorphone formation was saturated at high oxycodone concentrations consistent with observations with recombinant CYP3A4 and CYP2D6 (**Figure 4.1f**). The $CL_{int,HLM}$ for noroxycodone formation in pooled HLM was 5.8 ± 0.4 μL/min/mg protein and the $CL_{int,HLM}$ for oxymorphone formation in pooled HLM was 0.47 ± 0.06 μL/min/mg protein (**Figure 4.1h**) which were 1.32-fold and 1.07-fold of the respective $CL_{int,HLM}$ values predicted from recombinant CYP3A4 and CYP2D6. In contrast, only noroxycodone and no oxymorphone formation was observed in pooled FLM (**Figure 4.1g**). The $CL_{int,FLM}$ for noroxycodone formation in pooled FLM was 0.60 ± 0.07 μL/min/mg protein which was only 9% lower than that predicted from recombinant CYP3A7.

Noroxycodone formation was characterized in 16 individual FLMs. The mean noroxycodone formation $CL_{int,FLM}$ in the individual FLMs was 0.53 ± 0.30 (range: 0.064 – 1.0) μL/min/mg protein (**Figure 4.3a**). When FLMs were incubated with ketoconazole, a CYP3A inhibitor, noroxycodone formation was decreased by 87 ± 9%, supporting the notion that noroxycodone formation in FLMs is primarily, and nearly entirely, mediated by CYP3A. The noroxycodone formation $CL_{int,FLM}$ correlated significantly with CYP3A7 expression ($p=0.0078$) and 6β-OH-testosterone formation $CL_{int,FLM}$ ($p < 0.0001$), a CYP3A probe reaction,[195] in the individual FLMs (**Figure 4.3b,c**), demonstrating that oxycodone metabolism in fetal liver is predominantly mediated by CYP3A7. The observed $CL_{int.FLM}$ for noroxycodone formation correlated significantly with that predicted from recombinant CYP3A7 in the individual FLMs (p

< 0.0001) (**Figure 4.3d**) and the observed CL_{int} were within 83 – 177% (mean 127 ± 24%) of the predicted $CL_{int,FLM}$.

The fetal hepatic clearance (CL_h) and extraction ratio (ER) for oxycodone were predicted based on the noroxycodone formation data obtained for each fetal liver tested and the known fetal liver size and hepatic blood flow at different gestational stages. The predicted values for fetal CL_h and ER were 0.020 ± 0.012 (range: 0.002 – 0.044) mL/min and 0.00042 ± 0.00021 (range: 0.00005 – 0.00081), respectively for the fetal livers from early gestation (85 – 137 days) (**Figure 4.4a**). The predicted fetal liver CL_h and ER at term (GA 40 weeks) were 0.496 (range: 0.066 – 0.936) mL/min and 0.0019 (range: 0.00003 – 0.0036), respectively (**Figure 4.4b**). In comparison, the predicted adult CL_h was 154 mL/min, more than 300-fold greater than that of the fetus at term, reflecting the substantial difference in the size of adult and fetal livers and the higher catalytic activity of CYP3A4 in comparison to CYP3A7. The predicted adult hepatic ER was 0.10, more than 50-fold greater than that of the fetal liver.

4.5 DISCUSSION

Fetal metabolism of drugs has been extensively studied for more than 60 years,[196,197] and the anatomical and biochemical functions of the fetal liver have been shown to be different from those of the adult liver.[196,198] For example, the fetal liver receives a significant fraction of its blood supply from the placenta in addition to the portal vein and hepatic artery,[33] the morphology of the endoplasmic reticulum changes over gestation,[196] and the zonation of drug metabolizing enzyme expression along the acinus is less apparent than in the adult liver.[198] Drug metabolizing enzyme expression in the fetal liver is also substantially different from that in the adult liver. It has been shown through gene expression analysis,[36,53,61] protein quantification,[38,56] and measurements of enzyme activities[38,52,53] that CYP3A7 is the most abundant CYP expressed in

the fetal liver while the expression of other CYPs including CYP3A4 and CYP2D6 in the fetal liver is minimal.[36,38,56,61,189] Additionally, FMO1 and GSTP proteins have been shown to be abundantly expressed in the fetal liver at levels comparable to FMO3 and GSTM in adult liver.[37] Of the conjugation enzymes, SULTs and UGTs have been detected in the fetal liver.[37] For example, UGT2B7, UGT2B15, and UGT2B17 are expressed in the fetal liver but at levels of about 10% of the adult liver.[37,199] Taken together these findings show that the fetal liver possesses its own unique complement of drug metabolizing enzymes and may have different metabolic capacity and specificity than the adult liver.

This study clearly shows that CYP3A7, the most abundantly expressed CYP enzyme in the fetal liver,[38,61] metabolizes oxycodone. Oxycodone is N-demethylated by CYP3A4 to noroxycodone, a major metabolite, and O-demethylated by CYP2D6 to oxymorphone, an active metabolite.[111] These metabolic pathways of oxycodone by CYP3A4 and CYP2D6 were confirmed in this study and CYP3A7 was found to N-demethylate oxycodone similar to CYP3A4. This finding is in agreement with the shared substrate specificity between CYP3A4 and CYP3A7.[112] However, in contrast to a previous report,[111] no noroxycodone formation by CYP3A5 was observed in this study despite the fact that a positive control (testosterone) was metabolized by the recombinant CYP3A5 at a rate similar to what has been previously observed[195] (data not shown). The difference between the studies could be due to different expression systems used (i.e. baculovirus-infected insect cells in this study compared to human lymphoblastoid cells in the previous study) or the coexpression of reductase with the CYPs used in this study. The observation that oxycodone is metabolized by both CYP3A4 and CYP3A7 but not by CYP3A5 is somewhat surprising, since CYP3A5 has overlapping substrate specificity

with CYP3A4 and CYP3A7,[112,200] and the CL_{int} of CYP3A5 is often higher than that of CYP3A7.[112]

The CYP3A7 protein expression in FLM quantified in this study (191 – 409 pmol/mg protein) is consistent with that observed before based on CYP3A7 activity towards metabolizing DHEA (201 – 311 pmol/mg protein)[38] while higher than that quantified by LC-MS/MS (10 – 160 pmol/mg protein).[56] This discrepancy is likely due to the difference in calibration standards. In this study, purified CYP3A7 protein spiked into HLMs was used as a calibration standard while surrogate peptide was used in the previous study. To our knowledge, this is the first study to use purified CYP3A7 protein to quantify CYP3A7 expression in microsomes. The use of whole protein as a standard digested in the HLM matrix will correct for digestion efficacy and variability and is less likely to underpredict true protein expression as shown before.[201] Although CYP2D6 expression was not measured in this study, multiple studies have reported that CYP2D6 is minimally expressed in the fetal liver.[36,53,56] As expected from the CYP3A7 and CYP2D6 expression patterns, this study showed that noroxycodone was formed in FLM, but oxymorphone was not. Similarly, CYP3A7 mediated metabolism has been observed for other opioids in FLM. For example, norcodeine formation from codeine, 3-methxymorphinan formation from dextromethorphan, and norethylmorphine formation from ethylmorphine have been observed in FLM.[53,54] On the other hand, CYP2D6 mediated metabolism, such as morphine formation from codeine or dextrorphan formation from dextromethorphan has not been observed in FLM when tested.[52] With the finding of lack of oxymorphone formation by the fetal liver in this study it may be concluded that fetal liver metabolism does not increase the risk of fetal exposure to active opioid metabolites formed by CYP2D6.

All of the data collected in this study support the conclusion that CYP3A7 is the main enzyme catalyzing noroxycodone formation from oxycodone in FLMs. This conclusion is supported by the nearly complete inhibition of noroxycodone formation in the FLM by ketoconazole, a CYP3A7 inhibitor,[202] and tight correlations of noroxycodone formation clearance with 6β-OH-testosterone formation clearance and CYP3A7 expression in each FLM.[195] Although the role of CYP3A4 and CYP3A5 cannot be ruled out in the above experiments, the combination of the observations in this study that show minimal noroxycodone formation activity by CYP3A5 and previous studies that show that expression of CYP3A7 in fetal liver is more than 100-fold greater than CYP3A4[61] suggest that CYP3A7 is the main enzyme responsible for noroxycodone formation in FLM.

It has been shown for several CYPs that the activities measured in recombinant CYPs cannot be directly scaled to the adult or fetal liver without the consideration of the ISEF or a relative activity factor (RAF).[62,194] This study is the first to establish an ISEF value to scale CYP3A7 activity to FLM enabling predictions of FLM metabolism of variety of drugs based on recombinant enzyme data. However, ISEF values can vary between substrates and they are sensitive to the lot of enzyme, cytochrome b5 and reductase expression and expression system [62] and as such may vary between sources or even with gestational age if reductase or b5 expression is gestational age dependent. It should be noted that the fetal liver CL_h for GA 20-40 weeks shown here is based on extrapolation and assuming minimal changes in intrinsic activity of CYP3A7 or changes in f_u or B/P ratio with gestational age. The fact that these parameters may change with gestational age yields some uncertainty to the CLh and ER values predicted beyond 20 weeks. The ISEF value established here based on 6β-OH-testosterone formation was applied to predicting noroxycodone formation $CL_{int,FLM}$ at early gestation fetal liver from activity

measured with recombinant CYP3A7. The observed noroxycodone formation $CL_{int,FLM}$ were 83 – 177% of those predicted suggesting that the CYP3A7 expression is a major contributor to the observed variability in noroxycodone formation CL_{int} in FLM. Notably, there was a 4-fold range of ISEF values (0.016 – 0.066) calculated for the individual FLMs indicating that intrinsic factors such as membrane environment and reductase or b5 expression in the individual livers also contribute to the interindividual variability independent of CYP3A7 expression. Without an ISEF (i.e. ISEF = 1), the scaled noroxycodone formation CL_{int} in FLM overpredicts the observed $CL_{int,FLM}$ of noroxycodone 25-fold. There are examples of drugs commonly used during pregnancy that are metabolized by CYP3A7, including midazolam, clarithromycin, alfentanil, glyburide, and carbamazepine.[56,59,61,112,190] The catalytic activity of CYP3A7 to metabolize these drugs has been shown to be up to 26% of that of CYP3A4. The establishment and further refinement of an ISEF value for CYP3A7 using several substrates together with the robust measurement of CYP3A7 protein expression in FLMs, provides a valuable tool to quantitatively predict fetal liver metabolism for these drugs and other CYP3A substrates administered to pregnant women without the need to acquire fetal liver tissue.

The quantitative *in vitro*-to-*in vivo* extrapolation (IVIVE) of fetal liver clearance of oxycodone suggests that the fetal liver plays a minor role in the maternal-fetal disposition of oxycodone. An obvious factor for the insignificant contribution by the fetal liver is that the fetal liver weight is less than 10% of that of the adult liver,[60] and hence, the fetal liver CL_h is predicted to be small when compared to the adult CL_h as demonstrated previously for retinoic acid.[57] Another factor is the low intrinsic capacity of the fetal liver to metabolize oxycodone. The interindividual variability observed in the CL_{int} of noroxycodone formation in individual FLM was considerable (16-fold), consistent with the observed variability in 6β-OH-testosterone

formation and CL_{int} of retinoic acid metabolism reported previously.[57] However, this interindividual variability has a minor impact on the systemic clearance of oxycodone in pregnant women, as shown by the predicted ranges of fetal CL_h in comparison to the adult CL_h. Since the fetal liver is acting as a first-pass organ for the fetus that half of the blood coming from the placenta passes through the fetal liver before entering the fetal circulation, the fetal hepatic ER can be used to predict how well the fetal liver protects the fetus from exposure to xenobiotics. The extremely low predicted fetal hepatic ER of oxycodone suggest that the fetal liver does not act as a barrier to protect the fetus from exposure to oxycodone that passes through the placenta. Similar to the predicted low fetal hepatic ER for oxycodone, the fetal hepatic ERs were predicted to be <0.05 for other drugs with available FLM metabolism information including codeine,[52] dextromethorphan,[53] and glyburide.[56] These predictions further support the results of this study that the fetal liver does not act as a barrier to protect the fetus from exposure to xenobiotics. Based on the data obtained in this study a xenobiotic with no protein binding and B/P ratio = 1 would need to have an $CL_{int,FLM}$ of at least 45 μL/min/mg protein to have an ER > 0.3 by the fetal liver that could provide some protection to the fetus from maternal exposures.

In conclusion, this study demonstrates that CYP3A7 in the fetal liver metabolizes oxycodone but the role of the fetal liver is minimal in the maternal-fetal disposition of oxycodone. These results complement the clinical and preclinical studies performed to study the maternal-fetal disposition of opioids during pregnancy.[108,109,203–207] The findings of this study are in agreement with previous work showing that the quantitative contribution of fetal hepatic clearance to the total body clearance of CYP3A4/7 substrates is predicted to be minimal and the fetal liver does not act as a first-pass barrier to protect the fetus. This study also highlights the need to quantitatively scale CYP3A7 activity to fetal liver to assess significance of fetal liver

metabolism. An ISEF value for CYP3A7 was established together with CYP3A7 expression levels in FLMs to provide tools to predict fetal liver metabolism from recombinant enzyme data. Altogether, this study suggests that fetal liver is unlikely to generally contribute to the maternal-fetal disposition of xenobiotics unless the CYP3A7 catalytic activity is significantly greater than that of CYP3A4.

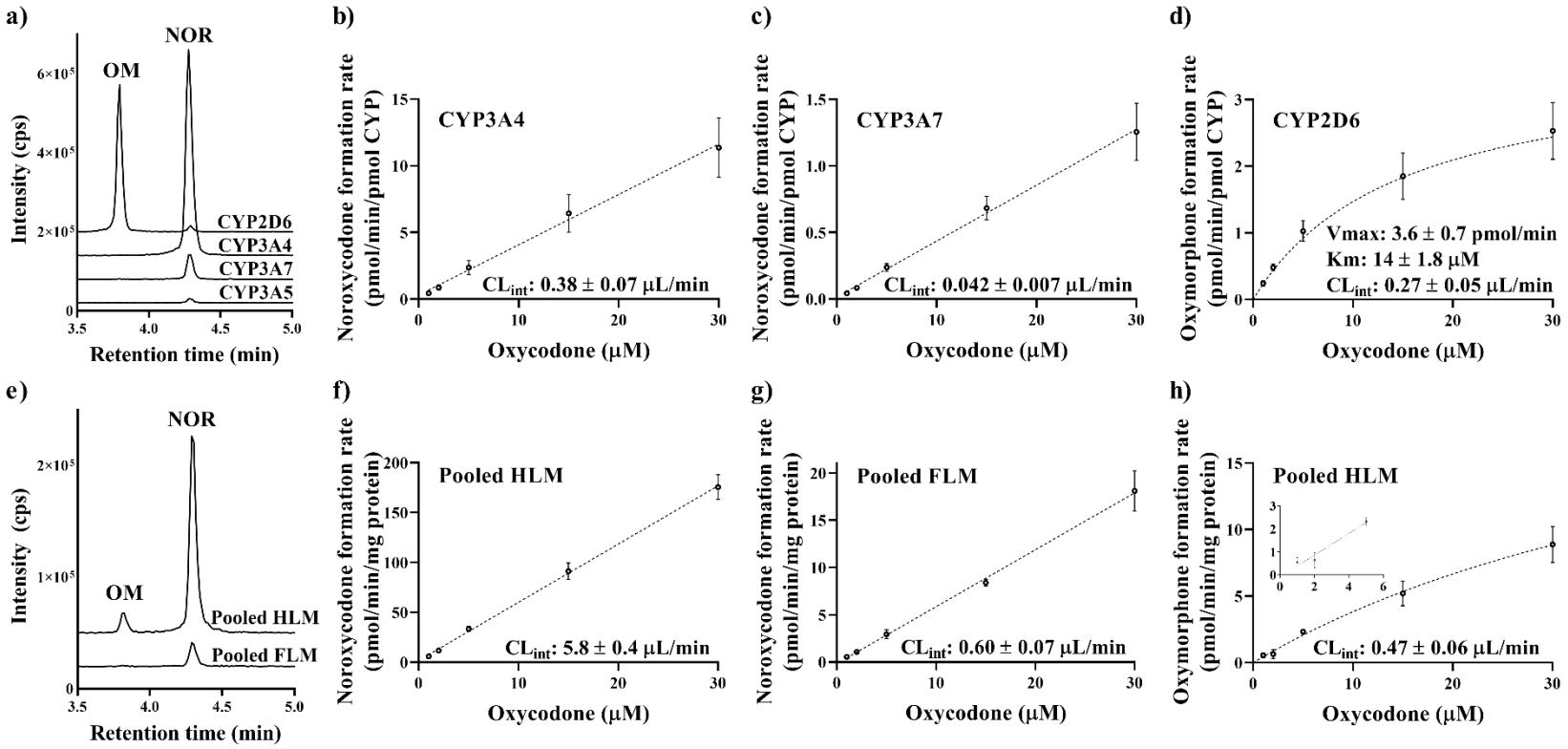

Figure 4.1. Noroxycodone and oxymorphone formation kinetics in recombinant CYPs, pooled HLM (50 donors), and pooled FLM (14 donors). HPLC-MS/MS chromatograms showing noroxycodone (NOR) and oxymorphone (OM) formation from 5 µM oxycodone after 15 min incubation with 5 pmol/mL CYP2D6, CYP3A4, CYP3A5, and CYP3A7 are shown in (a). Metabolite formation rate as a function of oxycodone concentration for noroxycodone formation by recombinant CYP3A4 (b) and CYP3A7 (c), and for oxymorphone formation by recombinant CYP2D6 (d) are shown with CL_{int} or Michaelis-Menten parameters determined for the metabolite formation listed in inset. The CL_{int} values were normalized to per pmol of CYP. HPLC-MS/MS chromatograms showing NOR and OM formation from 5 µM oxycodone after 15 min incubation with 0.1 mg/mL pooled HLM and 0.1 mg/mL pooled FLM are shown in (e). Metabolite formation rate as a function of oxycodone concentration for noroxycodone formation with pooled HLM (f) and pooled FLM (g), and for oxymorphone formation pooled HLM (h) are shown with the estimated CL_{int} values for the metabolite formation listed in inset. The CL_{int} values were normalized to per mg of microsomal protein. Oxymorphone formation in

pooled HLM was not linear but V_{max} and K_m could not be reliably estimated from 1 to 30 μM oxycodone and CL_{int} of oxymorphone formation was estimated using the initial concentration from 1 to 5 μM oxycodone (linear regression shown in inset). Mean and standard deviation of intrinsic clearance (CL_{int}), Vmax, and K_m reported were calculated from three different experiments conducted on separate days.

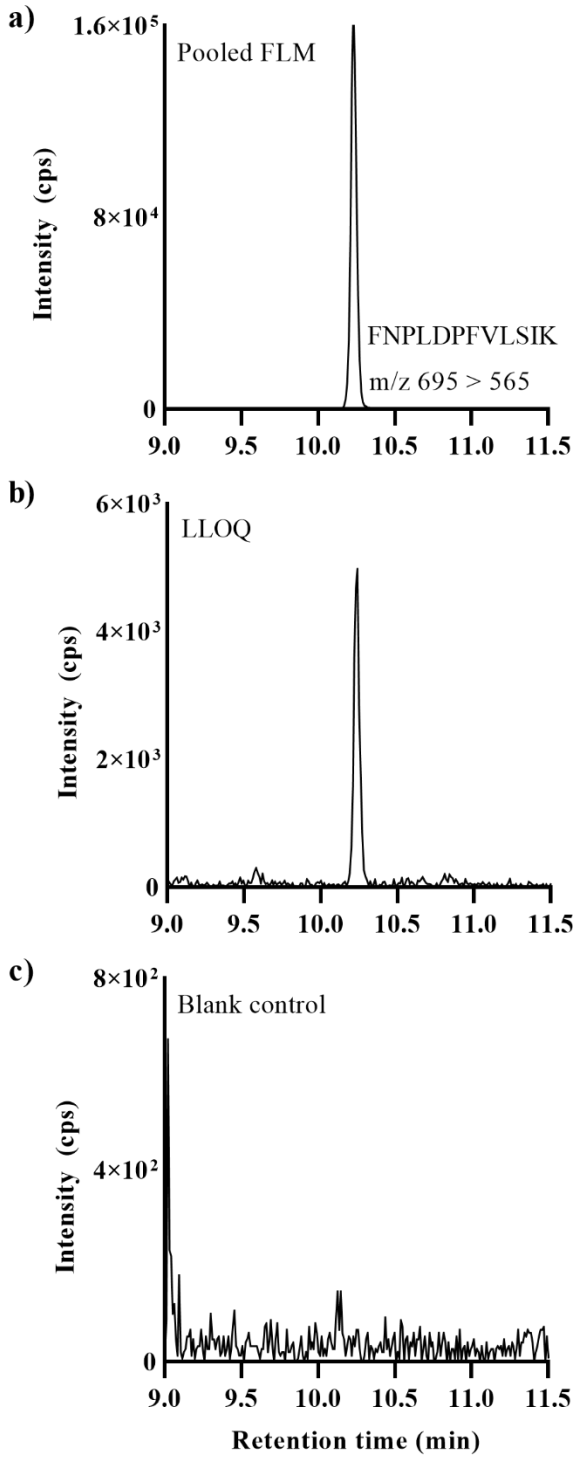

Figure 4.2. HPLC-MS/MS chromatograms of CYP3A7 a) pooled FLM, b) HLM spiked with 20 pmol CYP3A7 per mg microsomal protein (LLOQ), and c) blank HLM matrix control. The targeted peptide sequence and the MRM transitions are listed as insets in panel (a).

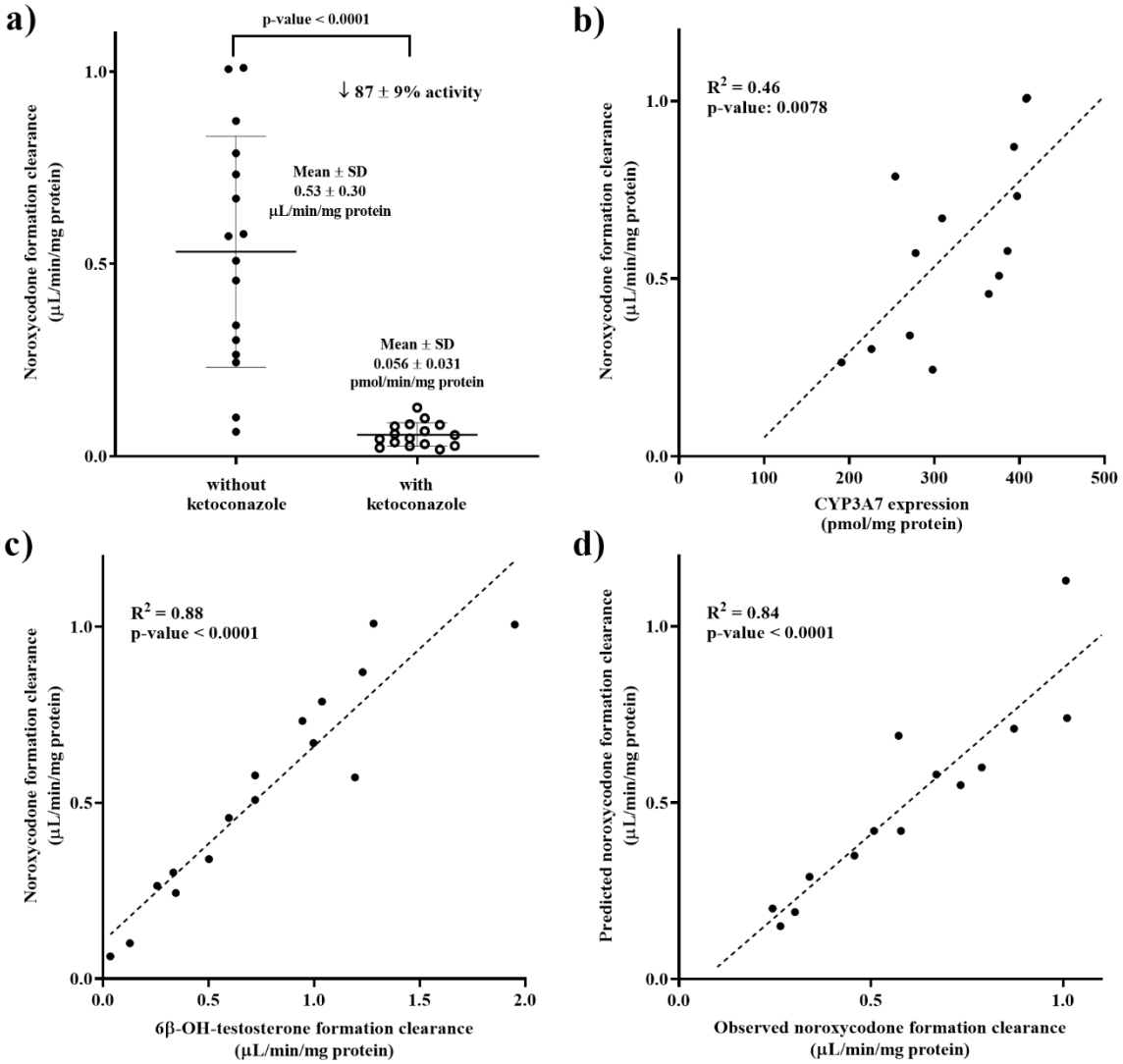

Figure 4.3. Characterization of noroxycodone formation from oxycodone in FLMs. a) Noroxycodone formation rate in the absence (filled circles) and presence (open circles) of 1 µM of ketoconazole in the individual FLMs (n=16). b) Correlation between noroxycodone formation clearance with CYP3A7 protein expression in the individual FLMs (R^2: 0.46) with a slope significantly different from zero (p-value: 0.0078) (n=14). The mean CYP3A7 expression in the FLMs was 326 ± 74 pmol/mg protein. c) Correlation between noroxycodone and 6β-OH-testosterone formation clearances in the individual FLMs. The mean 6β-OH-testosterone $CL_{int,FLM}$ was 0.68 ± 0.54 µL/min/mg protein and the 6β-OH-testosterone $CL_{int,\ FLM}$ correlated with the noroxycodone $CL_{int,\ FLM}$ (R^2: 0.88) with a slope significantly different from zero (p-value <0.0001) (n=16). d) Correlation between the predicted noroxycodone formation clearance using ISEFs calculated for individual FLMs and the measured CYP3A7 expression in individual microsomes with the observed noroxycodone formation clearance in the individual FLMs (R^2: 0.84) with a slope significantly different from zero (p-value <0.0001) (n=14).

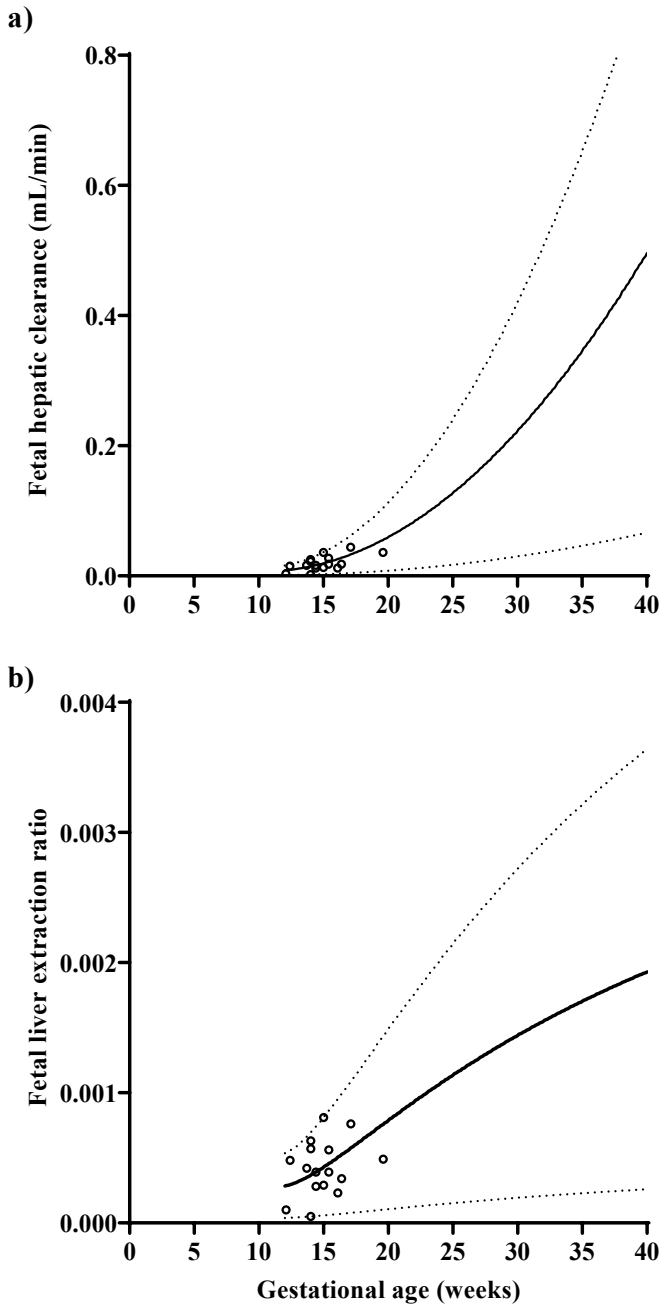

Figure 4.4. Predicted a) fetal hepatic clearance (CL_h) and b) fetal liver extraction ratio (ER) from gestational week 12 to gestational week 40. The open circles represent the predicted fetal CL_h and fetal liver ER for each individual donor liver. The solid lines represent the CL_h and ER extrapolated using the mean estimated fetal liver intrinsic clearance (CL_{int}); the dotted lines represent CL_h and ER extrapolated using the range of the estimated CL_{int}, in the fetal livers tested.

Chapter 5.

Predicting maternal-fetal disposition of fentanyl following intravenous and epidural administration using physiologically-based pharmacokinetic modeling

A version of this chapter was submitted as a research article to the Drug Metabolism and Disposition.

Authors: Sara Shum, Danny D. Shen and Nina Isoherranen

5.1 ABSTRACT

Fentanyl is an opioid analgesic commonly given to parturient women through epidural or intravenous route resulting in fetal exposure to fentanyl. The observed umbilical venous to maternal venous (UV/MV) plasma fentanyl concentration ratio following epidural and IV injections to parturient women varies with time post-dose and route of administration. Hence, single timepoint UV/MV ratio is insufficient to capture the maternal-fetal disposition of fentanyl. We hypothesized that the maternal and fetal plasma concentration-time profiles of fentanyl following various dosing regimens to parturient women can be predicted by PBPK modeling. A maternal-fetal PBPK (mf-PBPK) model with an epidural dosing site was developed for fentanyl. Fetal hepatic clearance of fentanyl was predicted from CYP3A7 mediated norfentanyl formation in fetal liver microsomes (CL_{int} = 0.20 ± 0.05 µL/min/mg protein). Fetal fentanyl metabolism was predicted to have minimal impact on the maternal-fetal disposition of fentanyl. The simulations using the verified mf-PBPK model of fentanyl showed that maternal and fetal C_{max}-values are 3 to 42-fold higher following an IV bolus dose in comparison to an epidural bolus dose, depending on the sampling site, but C_{max}-values following IV and epidural infusion are similar in maternal and fetal compartments. The mf-PBPK model successfully simulated individual subject maternal and umbilical vein concentrations of fentanyl after epidural infusion during delivery with AAFE of 1.45 and 1.68, respectively, demonstrating that mf-PBPK modeling can be used successfully to predict fentanyl disposition in pregnant women, transplacental distribution, and exposures to the fetus.

5.2 INTRODUCTION

Fentanyl and other opioid analgesics are commonly used together with local anesthetics to relieve pain during surgical procedures. Depending on the procedure, fentanyl is typically given epidurally or intrathecally for regional anesthesia. Despite the similar plasma concentrations observed following epidural and IV infusion,[208,209] epidural fentanyl has been considered superior for pain relief based on proposed spinal mechanisms suggesting that less fentanyl is needed via epidural administration to produce the same analgesic effect when compared to IV fentanyl.[210,211] However, others have reported that the pain relief of epidural fentanyl is mainly mediated through systemic action and that the analgesic effect is the same for epidural and IV fentanyl.[212]

Fentanyl is often given regionally through epidural and intrathecal injections to parturient women during labor and delivery.[213] Although undesirable maternal and fetal side effects such as hypotension, nausea, and pruritus in the mom[213–215] and bradycardia and lower neurologic and adaptive capacity score in the newborns[214,216] were observed following the use of fentanyl during labor and delivery, these effects are considered transient, and the use of fentanyl is generally considered safe in parturient women.[115,217] Epidural fentanyl was shown to provide superior pain relief compared to IV fentanyl in post caesarean-section women,[211] and it is commonly believed that epidural fentanyl is safer than IV fentanyl for parturient women because fetal exposure is believed to be lower following epidural dosing. On the other hand, there is an increasing interest in exploring the option to use IV fentanyl during early stages of labor because IV dosing is feasible and less invasive in many settings.[114] Hence, it is important to compare fetal exposure following epidural and IV fentanyl. Fentanyl crosses the placenta and has been detected in the umbilical vein (UV) within 30 min of an epidural dose to parturient women.[116,218–220] However,

the UV to maternal venous (UV/MV) plasma concentration ratios following epidural and IV fentanyl dosing have only been reported from single timepoints during labor. Following a single epidural dose of fentanyl, the UV/MV ratios were 0.3-3.4 within an hour after dosing.[206,218–220] Following epidural infusion, the UV/MV ratios were 0.6-3.1 at 1-15 h after dosing.[116,117,214] Following IV fentanyl, the UV/MV ratios were 0.3-1.9 within an hour after dosing.[221] These data demonstrate the variability of UV/MV ratios observed with time of delivery and route of administration.

Fentanyl is a synthetic opioid more potent than morphine.[222] It is a lipophilic (logP = 4.05) weak base (pKa = 8.99)[118] that is widely distributed in the body with an estimated steady-state volume of distribution (V_{ss}) of 4 L/kg.[223,224] The elimination of fentanyl is mainly through hepatic metabolism mediated by CYP3A4 with less than 5% of IV dose eliminated unchanged in urine.[119] The pharmacokinetics (PK) of fentanyl following epidural injections in parturient women has been reported in multiple studies[116,218–220] and the steady-state concentrations (C_{ss}) following IV and epidural infusion of fentanyl to women after caesarean-section were shown to be similar.[208] Yet comparisons of fentanyl PK after IV and epidural injections during labor have not been reported leaving a gap in the knowledge of maternal-fetal disposition of fentanyl. We hypothesized that the maternal-fetal disposition of fentanyl following an epidural or IV dosing to parturient women can be predicted using physiologically-based pharmacokinetic (PBPK) modeling. To test this hypothesis a maternal-fetal-PBPK (mf-PBPK) model for fentanyl was developed with incorporation of a novel epidural dosing site. The goal of this study was to predict the fetal concentration-time profile of fentanyl following maternal epidural and IV doses and to establish a PK basis to inform future decisions on opioid analgesic dosing during labor and delivery.

5.3 MATERIALS AND METHODS

5.3.1 *Development of a maternal-fetal physiologically based pharmacokinetic (mf-PBPK) model with an epidural dosing site*

A mf-PBPK model was developed in MATLAB and the Simulink platform (R2019b; MathWorks, Natick, MA). The structure of the model was modified from a previously published mf-PBPK model which includes a 14-compartment maternal PBPK model and a 7-compartment fetal PBPK model linked together by a placenta compartment.[192] A similar structural model without the placenta and fetal PBPK model was used for simulations of drug disposition in nonpregnant population (**Figure 5.1**). Drug distribution to all organs was modeled as perfusion-limited process except for the clearances to and from the placenta which incorporated potential permeability-limited kinetics. Simulated concentrations were sampled from the same site as reported in the observed studies. To accomplish this, a previously developed peripheral sampling site (arm vein)[225] was incorporated into the maternal PBPK model. Additionally, to model the maternal-fetal disposition following epidural dosing, an epidural dosing site model was developed and incorporated in parallel to the other organ compartments in the maternal PBPK model.

The structure of the epidural dosing site model was developed based on known physiology of the human epidural space. The epidural space is located between the ligamentum flavum posteriorly and the posterior longitudinal ligament anteriorly surrounding the spinal cord outside of the dura mater which is filled mainly with adipose tissue.[226–228] The epidural space is highly vascularized and receives oxygenated blood from the spinal arteries superiorly from the aorta and drains to the internal vertebral venous plexus that empties into the inferior vena cava.[226,227] An epidural bolus injection is usually given with volume between 4 and 20 mL which

creates a sheath of solution surrounding the epidural space upon injection.[229] The dose will either partition into the epidural adipose tissue or be taken up by the venous system according to the direct connection between the epidural space and the venous system.[230] Based on the physiology, the epidural dosing site was modeled such that the dose is given into the epidural fluid surrounding the epidural space. From there, the dose can either passively diffuse to and partition into the adipose tissue or passively diffuse to and be taken up by the epidural vein (i.e. internal vertebral venous plexus) (**Figure 5.1**). Distribution to CSF (through the dura mater) was not included in the model as most of the volume injected into the epidural space has been shown to stay outside of the dura mater,[229] and the rate of opioid transfer from the epidural space to the CSF has been shown to be significantly slower than that to the epidural adipose tissue and venous plasma.[231] A sensitivity analysis was also performed to assess whether a direct connection between the CSF and the vasculature can be kinetically discerned from plasma kinetics.

The physiological parameters (i.e. organ volumes and blood flows) of the nonpregnant model (including the arm sampling site model) were adopted from a previously published PBPK model.[225] The physiological parameters of the mf-PBPK model to match a pregnant woman at term (gestational week 40) were calculated using previously published equations to describe physiological changes of pregnant women and fetuses during gestation.[73,77] A CYP3A4 induction factor of 1.99 was used in the maternal-fetal model based on previous observation that CYP3A4 expression increased by 1.99-fold during late pregnancy.[16] Parameters without published values in pregnant women were assigned to be the same as those in the nonpregnant model (**Table 5.1**). For the drugs studied, the transplacental clearances were assumed to be mediated by passive processes although active transport could be incorporated in the model if present, and only

unbound fraction of the drug was assumed to passively diffuse across the placenta (i.e. syncytiotrophoblast monolayer).

The physiological parameters for the epidural dosing site were the parameters for the lumbar vertebrae region (L1 to L5) since epidural injection is typically given into the lumbar section. The volume of the epidural adipose tissue ($V_{epidural,adipose}$) in the lumbar region has been reported to be around 3.5 mL[232] and the blood flow to the epidural space ($Q_{epidural}$) was calculated based on the reported velocity of blood flow in spinal arteries into the lumbar region and the diameter of spinal arteries (calculated arterial blood flow = 1.12 L/h).[233,234] Since the spinal blood drains through the internal vertebral venous plexus (inside the epidural space) and the external vertebral venous plexus (outside of epidural space), the $Q_{epidural}$ was assumed to be 50% of the arterial blood flow (i.e. 0.56 L/h). The volume of the epidural vein ($V_{epidural,vein}$) was assumed to be the same as $V_{epidural,adipose}$ (3.5 mL). The volume of the epidural fluid ($V_{epidural,fluid}$) was assumed to be the same as the typical epidural injection volume of 10 mL. The clearances from the epidural fluid to the epidural adipose tissue and the epidural vein were assumed to be mediated by passive processes and only unbound fraction of the drug was assumed to passively diffuse across the adipocyte cell membrane and the venous endothelium lining. The bioavailability following epidural administration was assumed to be 100% based on the previous observations that similar C_{ss} was observed following IV and epidural infusions at the same dose[208,209] (**Table 5.1**).

5.3.2 *Sensitivity analyses of the epidural dosing site model*

The absorption profile of epidurally dosed drugs including the rate of absorption and the fraction of dose sequestered in the epidural adipose tissue have been shown to depend on the physicochemical properties (i.e. molecular weight, logP, pKa, etc) of the dosed drug.[231,235]

Hence, sensitivity analyses were performed for the developed epidural dosing site model to identify the sensitive physicochemical and physiological parameters. To do this, a hypothetical drug X model was developed. Drug X was assumed to be a neutral compound with tissue partitioning coefficients (K_p's), blood-to-plasma (B/P) ratio, and plasma fraction unbound (f_u) assumed to be 1 unless the parameter was assessed in the sensitivity analysis. The hepatic clearance of drug X was assumed to be 45 L/h (ER = 0.5) and the renal clearance of drug X was assumed to equal to the GFR (i.e. 7.2 L/h). The bidirectional unbound permeability clearance from the epidural fluid to the epidural adipose tissue ($CL_{pd,adipose}$) of drug X was calculated to be 0.003 L/h using the estimated surface area of the epidural adipose tissue based on reported anatomical dimensions of the epidural fat in the lumbar region (8.6 cm^2)[236] and an assumed permeability (P_{app}) of 100 × 10^{-6} cm/s. Since the exact surface area for the epidural venous compartment is not well characterized, the bidirectional unbound permeability clearance from the epidural fluid to the epidural vein ($CL_{pd,vein}$) of drug X was assumed to be the same as $CL_{pd,adipose}$ (i.e. 0.003 L/h).

Four sets of three-dimensional local sensitivity analyses were performed by varying two parameters at a time to evaluate the impact of covarying parameters on the simulated C_{max} and t_{max} following a single epidural bolus dose of 100 µg of drug X. The C_{max} and t_{max} were chosen as the measurements of the rate of absorption following epidural administration. The range of values explored for each parameter was divided into 25 equal steps and the possible combinations of the two varying parameters were simulated (i.e. 25x25 = 625 simulations per sensitivity analysis). To identify the sensitive physicochemical parameters that affect drug disposition following epidural dose, sensitivity analyses were performed with **(1)** varying $CL_{pd,adipose}$ and $CL_{pd,vein}$ each from 0.00003 to 0.3 L/h (i.e. P_{app} from 1x10^{-6} to 1x10^{-2} cm/s), **(2)**

varying f_u from 0.1 to 1 (only in the epidural venous plasma to assess the effect of protein binding on the distribution kinetics at the epidural site to avoid the effect on hepatic and renal clearances) and $K_{p,epidural,adipose}$ from 0.01 to 100 (while keeping the K_p of the adipose tissue for the rest of the body constant at 1 to avoid the effect on varying V_{ss}). To evaluate the effect of epidural blood flow on drug disposition following epidural dose, sensitivity analysis was performed with **(3)** $Q_{epidural}$ from 0.056 to 5.6 L/h (10% to 10-fold of the physiological value of 0.56 L/h) and $CL_{pd,vein}$ from 0.00003 to 0.3 L/h (same range as **(1)**). To test whether a direct connection between the CSF and the vasculature (i.e. epidural fluid → CSF → spinal vein) can be kinetically discerned, additional sensitivity analysis was performed with **(4)** asymmetrical $CL_{pd,vein}$, in which the $CL_{pd,vein}$ from epidural vein to epidural fluid ($CL_{pd,veintofluid}$) ranged between 10 and 100% of each test value of $CL_{pd,vein}$ from epidural fluid to epidural vein ($CL_{pd,fluidtovein}$).

5.3.3 *Verification of the epidural dosing site model using alfentanil as a model compound*

Since the exact surface areas for the epidural vein are not well characterized to predict the $CL_{pd,vein}$ by extrapolation, the $CL_{pd,vein}$ was first optimized and verified using a structurally similar compound, alfentanil, as a model compound. Then the $CL_{pd,vein}$ of fentanyl and other epidurally administered compounds can be scaled using the optimized $CL_{pd,vein}$ of alfentanil using a similar approach as previously described to scale placental passive diffusion clearance.[79] To do this, a PBPK model of alfentanil was developed. The B/P ratio, plasma f_u, and K_p's of alfentanil were collected from literature[237–239] and the parameter values are listed in **Table 5.2**. Alfentanil is exclusively eliminated through hepatic metabolism mediated by CYP3A4 with only 1% of the dose excreted unchanged in urine.[240] The unbound hepatic intrinsic clearance of alfentanil ($CL_{int,u}$ = 185 L/h) was calculated using the hepatic well-stirred model from the

averaged total body clearance (average CL = 13.5 L/h) observed following IV dose of alfentanil to healthy subjects reported in five studies.[241–245] The alfentanil model was verified using the plasma concentrations observed in the above five IV studies. Simulations of alfentanil plasma concentration-time profiles following IV dose were performed using the nonpregnant PBPK model and the same dose and sampling site (arm vein) as in the original studies. One of the five studies did not specify the sampling site and comparison was done to the simulated plasma concentrations at the arm vein sampling site.

All observed mean plasma concentrations throughout were digitized using WebPlotDigitizer (version 4.3, https://apps.automeris.io/wpd/). The performance of all simulations was quantitatively evaluated based on the absolute average fold error (AAFE) calculated for each study according to equation 1:

(1) $$AAFE = 10^{\frac{1}{n}\Sigma\left|log_{10}\frac{Simulated\ concentration}{Observed\ concentration}\right|}$$

An AAFE of ≤ 2 was considered acceptable for the alfentanil model based on the interstudy variability of alfentanil CL observed in the above five IV studies (CV = 17.4%). The 99.998% geometric confidence interval of the AUC was calculated as previously described[246] to be 48% to 2.1-fold of the mean.

After verification of the PBPK model of alfentanil, an epidural dosing model was developed for alfentanil. The $CL_{pd,adipose}$ of alfentanil was extrapolated to be 0.01 L/h by multiplying the observed Caco-2 permeability of alfentanil at pH 7.4 ($P_{app} = 300 \times 10^{-6}$ cm/s) and the surface area of the epidural adipose tissue estimated based on the reported anatomical dimension of the epidural fat in the lumbar region (8.6 cm^2).[236] The K_p of the epidural adipose tissue was assumed to be the same as the rest of the adipose tissue in the body ($K_p = 2.1$). The f_u in the epidural fluid was assumed to be 1. The $CL_{pd,vein}$ was optimized from 0.01 L/h (same as

$CL_{pd,adipose}$) to 0.3 L/h and verified using the observed mean plasma concentration-time profiles in healthy subjects from two epidural dosing studies of alfentanil[247,248] (**Table 5.2**). Simulations of alfentanil plasma concentration-time profiles following epidural dose were performed using the nonpregnant PBPK model and the same dose and sampling from the arm vein as in the original studies.

5.3.4 *Verification of the epidural dosing site model of fentanyl*

To develop the epidural dosing PBPK model of fentanyl, a previously reported and verified PBPK model of fentanyl was adopted (**Table 5.2**).[225] This model was previously verified for arterial and venous sampling of fentanyl following IV and buccal administration defining the distribution parameters of fentanyl. The B/P ratio, f_u in plasma, and K_p's for different tissues for fentanyl were adopted as previously reported. The previous model only considered overall plasma CL in each study and it did not define the enzymatic pathways of fentanyl CL. Therefore, a hepatic clearance (CL_h) of fentanyl was calculated from the average observed plasma clearance (CL = 62 L/h) following IV administration of fentanyl to healthy subjects from four studies[119,223,224,249] and the observed renal clearance (CL_r) of 3 L/h.[119] The $CL_{int,u}$ was calculated from the mean CL_h using the hepatic well-stirred model resulting in $CL_{int,u}$ of 1,055 L/h. Of the calculated $CL_{int,u}$, 80% was assumed to be mediated by CYP3A4 based on the result of a drug-drug interaction study[119] ($CL_{int,u,CYP3A4}$ = 844 L/h) and the remaining 20% was assigned to unknown pathways ($CL_{int,u,other}$ = 211 L/h). The modified fentanyl PBPK model was verified using the plasma concentrations observed in the above four IV studies. Simulations of fentanyl plasma concentration-time profiles following IV dose were performed using the nonpregnant PBPK model using the same dose and sampling site as specified in the original studies (three studies reported venous concentrations [119,224,249] and one study reported arterial concentrations

[223]). An AAFE was decided based on the interstudy variability of fentanyl CL observed in the above mentioned four IV studies (CV = 22.0%). The 99.998% geometric confidence interval of the AUC was calculated as previous described[246] to be 40% to 2.5-fold of the mean. Therefore, an AAFE of ≤ 2 was used as an acceptance criterion for verification of the fentanyl model.

After verification of the PBPK model of fentanyl following IV dosing, the epidural dosing model of fentanyl was developed and verified using the observed plasma concentration-time profiles following epidural dosing in healthy subjects from two studies.[250,251] The K_p of the epidural adipose tissue was assumed to be the same as the rest of the adipose tissue in the body. The f_u in the epidural fluid was assumed to be 1. The $CL_{pd,adipose}$ and $CL_{pd,vein}$ of fentanyl were scaled from the observed Caco-2 permeability of fentanyl at pH 7.4 ($P_{app} = 35 \times 10^{-6}$ cm/s)[252] using alfentanil as a scaler, a similar scaling approach as previously described for placental passive diffusion.[79] The $CL_{pd,adipose}$ and $CL_{pd,vein}$ of fentanyl for the epidural site were scaled using equation 2:

(2) $$CL_{pd,fentanyl} = CL_{pd,alfentanil} \times \frac{P_{app,fentanyl}}{P_{app,alfentanil}}$$

The $CL_{pd,adipose}$ and $CL_{pd,vein}$ of fentanyl were scaled to be 0.0012 and 0.023 L/h, respectively. Simulations of fentanyl plasma concentration-time profiles following epidural dose were performed using the nonpregnant PBPK model at the same dose and sampling from the artery as in the original studies. An AAFE of ≤ 2 was considered acceptable as described above.

5.3.5 *Metabolism of fentanyl by fetal liver microsome (FLM) and recombinant CYP3A7 and in vitro-to-in vivo extrapolation (IVIVE)*

Pooled FLM were prepared from 14 individual fetal livers (mixture of males and females) previously collected from healthy pregnancies with no known maternal drug use.[57] The estimated gestational age at the time of tissue collection ranged from 87 to 137 days. Fetal liver

microsomes (FLM) were prepared and pooled as previously described (**chapter 4**) and the microsomal pellets stored at -80°C until experiments. Stock solutions of fentanyl, norfentanyl, and deuterated norfentanyl-d_5 were purchased from Millipore Sigma (St Louis, MO). Norfentanyl formation kinetics was characterized in the pooled FLM and recombinant CYP3A7 supersomes purchased from Corning, Inc. (Corning, NY). All incubations were done in potassium phosphate buffer (pH 7.4) at 37°C in a shaking water bath under conditions of protein and time linearity. Fentanyl (2, 5, 15, 30 μM) was incubated with pooled FLM (0.2 mg/mL) and recombinant CYP3A7 (10 pmol/mL) for 15 minutes after reactions were initiated with 1 mM NADPH (or potassium phosphate buffer for no NADPH controls) and quenched by addition of four parts of ice-cold acetonitrile containing norfentanyl-d_5 as internal standard. Samples were vortexed briefly and centrifuged at 16,100 g for 15 min. The supernatants were stored at -20°C until HPLC-MS/MS analysis.

Norfentanyl formation clearance (CL_{int}) by pooled FLM or CYP3A7 was estimated through linear regression as described previously (**chapter 4**). The CL_{int}'s were reported as the arithmetic means of data generated on three different days. The $CL_{int,FLM}$ was scaled to the whole fetal liver CL_{int} (fCL_{int}) at term through IVIVE by multiplying the $CL_{int,FLM}$ with the measured microsomal protein per gram of liver (MPPGL: 17.8 ± 4.2 mg protein/g liver) and the estimated fetal liver weight at term (i.e. 129 g)[192] to be used in the mf-PBPK model.

5.3.6 *HPLC-MS/MS analysis*

The HPLC-MS/MS method to quantify norfentanyl was modified from a previously reported method.[253] Briefly, norfentanyl concentrations were measured using an AB Sciex 6500 qTrap Q-LIT mass spectrometer (Foster City, CA) equipped with an Agilent 1290 Infinity II UHPLC (Santa Clara, CA) and a Phenomenex Kinetex® EVO C18 LC column (2.6 μm, 100 x

2.1 mm) with a Phenomenex SecurityGuard™ EVO-C18 cartridge (sub-2 µm, 2.1 mm) (Torrance, CA). A 7-min gradient was employed using (A) 0.1% formic acid in water and (B) 0.1% formic acid in acetonitrile at a flow rate of 0.35 mL/min. The analytes were detected by positive ion electrospray ionization. A product ion each was monitored and quantified for norfentanyl (m/z 233 > 84) and norfentanyl-d_5 (m/z 238 > 84). The lower limit of quantitation (LLOQ) of norfentanyl was 1 nM.

5.3.7 *Development of the mf-PBPK model of fentanyl*

After verification of the PBPK model with epidural dosing of fentanyl, the mf-PBPK model was applied to predict fentanyl disposition in pregnant women and the maternal-fetal disposition of fentanyl at term. The K_p's and B/P ratio of fentanyl were assumed to be the same as those verified using the nonpregnant model. The maternal and fetal plasma f_u were set as 0.12 and 0.14, respectively, as reported in a group of 40 parturient women and their newborns.[254] The maternal hepatic $CL_{int,u}$ of fentanyl was predicted to be 1,891 L/h based on the built-in 1.99 induction factor for CYP3A4, and the reported calculated CL_{int} for CYP3A4 described in the above sections. The fetal $CL_{int,u}$ was scaled from the measured $CL_{int,FLM}$ described above. The syncytiotrophoblast metabolism ($CL_{syncytiotrophoblast}$) of fentanyl was assumed to be negligible (**Table 5.2**).

The unbound transplacental clearance ($CL_{pd,placenta}$) of fentanyl ($CL_{pd,placenta,fentanyl}$) was scaled using midazolam as the scaler as previously described[79] using equation 3:

(3) $$CL_{pd,placenta,fentanyl} = CL_{pd,placenta,midazolam} \times \frac{P_{app,fantanyl}}{P_{app,midazolam}}$$

The $CL_{pd,placenta,midazolam}$ was previously estimated to be 500 L/h[79] and the $CL_{pd,placenta,fentanyl}$ was scaled to be 357 L/h using the observed Caco-2 permeability at pH 7.4 of fentanyl (P_{app} = 35 × 10^{-6} cm/s)[252] and midazolam (P_{app} = 49 × 10^{-6} cm/s).[79]

5.3.8 *Verification of the mf-PBPK model of fentanyl and simulation of maternal-fetal disposition of fentanyl*

The mf-PBPK model of fentanyl was verified by comparing the simulated maternal arm venous (MV), umbilical venous (UV) and umbilical arterial (UA) plasma fentanyl concentrations with the same dose and sampling site (**Figure 5.1**) to the respective plasma concentration observed in seven PK studies.[116,117,206,214,218–220] These studies were performed in parturient women at the first two stages of labor administered either a bolus epidural injection or continuous infusion of fentanyl. Four out of the seven studies reported maternal venous plasma concentrations during labor[116,218–220] and all seven studies reported MV, UV and/or UA concentrations at delivery. The reported mean maternal plasma concentrations were digitized except one study that reported individual plasma concentrations for which mean plasma concentrations were calculated from individual data. One of the seven studies reported individual MV and UV concentrations at the time of delivery [117] and the reported concentrations were digitized. The AAFE was calculated by comparing the simulated and individual observed concentrations. For the remaining six studies, the mean delivery time and the mean MV, UV, and UA plasma concentrations were reported as numerical values and used as is. The absolute fold error was calculated by comparing the simulated concentration at the mean time of delivery with the mean observed plasma concentration at delivery. Since the interstudy variability of maternal-fetal disposition of fentanyl cannot be estimated based on the available data, the same AAFE (≤

2-fold) as the nonpregnant model was adopted as an acceptance criterion for verification of the fentanyl mf-PBPK model.

After verification of the mf-PBPK model of fentanyl, the maternal-fetal disposition of fentanyl at term was simulated following a single 100 µg epidural or IV bolus dose and following continuous epidural or IV infusion of 20 µg/h of fentanyl for 48 h using the mf-PBPK model and plasma fentanyl concentrations were sampled from the maternal artery (MA), MV, UV and UA. The absolute concentrations and concentration ratios between epidural and IV dose were compared to define the differences in maternal and fetal exposure to fentanyl.

5.4 RESULTS

5.4.1 *Development of an epidural dosing site model*

A novel epidural dosing site model was developed according to the physiology of the epidural space and incorporated into a full PBPK model to simulate drug disposition following epidural administration (**Figure 5.1**). To evaluate the impact of physicochemical properties on drug disposition following epidural administration, sensitivity analyses were performed using the PBPK model of a hypothetical drug X (**Figure 5.2**). First, the effect of apparent permeability (P_{app}) of drug X was tested by increasing $CL_{pd,adipose}$ and $CL_{pd,vein}$.(**Figure 5.2a**,**b**) The C_{max} of drug X increased by 282-fold while the t_{max} decreased from 10 to 0.2 h when $CL_{pd,vein}$ increased from 0.00003 to 0.3 L/h, suggesting that increasing P_{app} increases the rate of absorption following epidural administration and that $CL_{pd,vein}$ is a sensitive parameter in the model. In contrast, the C_{max} and the t_{max} of drug X were relatively insensitive to changes in $CL_{pd,adipose}$. Second, the effect of increasing adipose tissue partitioning and increasing plasma f_u were tested (**Figure 5.2c,d**). The C_{max} and t_{max} of drug X were insensitive to changes in $K_{p,adipose}$ (increased from 0.01 to 100) and f_u (increased from 0.1 to 1), suggesting that sequestration of drug X in the

adipose tissue and plasma protein binding have minimal effect on the rate of absorption following epidural administration. As such, neither $K_{p,adipose}$ nor f_u are sensitive parameters in the model. Third, the effect of decreasing epidural blood flow ($Q_{epidural}$ decreased from 5.6 to 0.056 L/h) was tested (**Figure 5.2e**,**f**). The C_{max} of drug X was not affected by decreasing $Q_{epidural}$ when $CL_{pd,vein}$ was low (<0.01 L/h, $P_{app} = 3 \times 10^{-4}$ cm/s), but C_{max} was sensitive to $Q_{epidural}$ under high $CL_{pd,vein}$ conditions. This suggests that the rate of absorption becomes limited by blood-flow for drugs with a high P_{app} and hence correct parameterization for blood flow is important for high permeability compounds. Last, sensitivity analysis was performed to evaluate whether uptake through CSF to the venous system is kinetically discernable by introducing asymmetrical $CL_{pd,fluidtovein}$ and $CL_{pd,veintofluid}$ (**Figure 5.2g**,**h**). The simulations showed that the C_{max} and t_{max} of drug X were not affected by the asymmetrical $CL_{pd,vein}$ suggesting that an alternative route of drug absorption through the CSF is not kinetically discernable following epidural dosing.

5.4.2 *Verification of the epidural dosing model using alfentanil as the model compound*

The epidural model was optimized and verified using alfentanil as the model drug. The final parameters of the alfentanil model are listed in **Table 5.2**. First, a PBPK model of alfentanil was developed to simulate the plasma concentration-time profile of alfentanil following IV administration to nonpregnant healthy subjects (**Figure 5.3a-c**). The simulated venous plasma concentration-time profiles captured the observed mean venous alfentanil plasma concentration-time profiles from five IV studies within the acceptance criterion (AAFE) of 1.20 – 1.98, verifying the alfentanil model. Then, the $CL_{pd,vein}$ of alfentanil was optimized to 0.2 L/h based on the observed venous plasma concentration-time profile following epidural administration in nonpregnant healthy subjects reported in two epidural dosing studies (**Figure 5.3d,e**). The simulated plasma concentration-time profiles using the optimized PBPK model of alfentanil

captured the observed mean alfentanil plasma concentration-time profiles following epidural dosing acceptably (AAFE: 1.21 – 1.31) verifying the epidural dosing model.

5.4.3 *Development and verification of an epidural dosing model of fentanyl*

After verification of the epidural dosing model of alfentanil, an epidural dosing model of fentanyl was developed and verified. First, a previously published[225] fentanyl PBPK model was adopted and modified with a refined hepatic clearance parameters reflecting the CYP3A4 intrinsic clearance (**Table 5.2**). The fentanyl model was verified using the mean venous plasma concentrations observed in three studies and the mean arterial plasma concentrations observed in one study following IV dosing of fentanyl (**Figure 5.4a-c**). All simulations met the acceptance criterion of AAFE ≤ 2 (AAFE: 1.25 – 1.84) when compared to the observed data verifying the fentanyl model. Then, the epidural dosing model of fentanyl was developed using alfentanil as a scaler. The simulated plasma concentration-time profiles following epidural administration of fentanyl to healthy nonpregnant subjects captured the observed venous plasma concentration time-profiles (**Figure 5.4d-f)** with all AAFEs within the acceptance criteria of ≤ 2 (AAFE: 1.21 – 1.99) verifying the epidural dosing model of fentanyl in nonpregnant women.

5.4.4 *FLM metabolism of fentanyl and IVIVE to predict fetal hepatic intrinsic clearance (CL_{int})*

Since fentanyl is mainly metabolized by CYP3A4 to norfentanyl in the liver in adults[255] but no fetal hepatic metabolism has been reported for fentanyl, norfentanyl formation was measured in FLM and recombinant CYP3A7 to estimate the fetal hepatic metabolism of fentanyl. The norfentanyl formation CL_{int} was 0.20 ± 0.05 μL/min/mg protein measured in FLM and 0.019 ± 0.001 μL/min/pmol CYP measured with recombinant CYP3A7 (**Figure 5.5**)

suggesting that the fetal liver metabolizes fentanyl. Using the established intersystem extrapolation factor (ISEF) of 0.044 for CYP3A7 previously established (**chapter 4**) and the measured CYP3A7 expression in the pooled FLM (359 pmol/mg protein) (**chapter 4**), the norfentanyl formation CL_{int} was predicted to be 0.3 μL/min/mg protein in FLM, 1.5-fold of the observed CL_{int} suggesting that CYP3A7 is the main enzyme responsible for norfentanyl formation in the fetal liver. The fetal hepatic $CL_{int,u}$ was predicted to be 0.028 L/h through IVIVE using the measured norfentanyl formation CL_{int} in FLM and this $CL_{int,u}$ was incorporated to the mf-PBPK model of fentanyl (**Table 5.2**).

5.4.5 *Verification of the mf-PBPK model of fentanyl and simulations of fentanyl disposition*

The developed mf-PBPK model of fentanyl was verified by comparing the simulations to the observed mean MV fentanyl plasma concentration-time profiles following epidural doses to parturient women in four studies and the observed MV, UV and UA concentrations at delivery following epidural doses observed in seven studies. The AAFE for the simulated MV plasma concentration-time profiles were 1.34 – 1.91 when compared to the mean observed data (**Figure 5.6a-d**). The AAFE for the simulated MV and UV concentrations from a study that reported data from individual subjects were 1.45 and 1.68, respectively, when compared to the observed individual MV and UV concentrations (**Figure 5.6e,f**).). For the remaining six studies, 75% (3/4) of simulated maternal plasma concentrations, 67% (4/6) of simulated UV plasma concentrations, and 100% (4/4) of simulated UA plasma concentrations at the mean time of delivery were within 2-fold of the mean observed concentrations at delivery (**Table 5.3**) verifying the fentanyl mf-PBPK model.

The verified mf-PBPK model of fentanyl was then used to simulate the maternal (MA and MV) and fetal (UV and UA) plasma concentration-time profiles in pregnant women at term

following a single IV or epidural bolus dose of 100 μg fentanyl or continuous IV or epidural infusion of 20 μg/h of fentanyl. The fentanyl C_{max} values in MA, MV, UV, and UA were 42-fold, 3-fold, 7-fold and 4-fold higher, respectively, after an IV bolus dose in comparison to an equal epidural bolus dose (**Figure 5.7a-d**), suggesting that pregnant woman and fetus are exposed to significantly higher maximum fentanyl concentration following an IV bolus dose than after epidural bolus despite the similar AUC following IV and epidural dosing. In contrast, the simulated plasma concentration-time profiles were similar following IV or epidural infusion (**Figure 5.7e-h**) suggesting that pregnant woman and fetus are exposed to similar fentanyl concentrations including similar C_{max} concentrations following IV and epidural infusion.

The time courses of the UV/MA, UV/MV, UA/UV, and UA/MV plasma fentanyl concentration ratios were similar when compared between IV and epidural bolus doses illustrating similar distribution kinetics to the fetus with different dosing routes. However the time courses of the specific concentration ratios were different from one another demonstrating that the fetal/maternal plasma concentration ratio is highly dependent on the sampling time and sampling sites such as maternal vein or artery and umbilical vein or artery (**Figure 5.8**). Notably, the commonly measured UV/MV ratio was as high as 3.5 in the initial 30 minutes following either bolus or epidural dose while the UV/MA ratio was <1 for the same time period illustrating the effect of arteriovenous differences on the fetal/maternal plasma concentration ratio. Also, the fetal/maternal plasma concentration ratios following a bolus dose and continuous infusion were different. The fetal/maternal plasma concentration ratios (i.e. UV/MA, UV/MV, UA/MV) and the UV/UA ratios increased to >1 following a bolus dose while those following continuous infusion were <1, demonstrating the impact of the maternal and fetal distribution kinetics of fentanyl on the fetal/maternal plasma concentration ratios. The UV/MA, UV/MV, and UA/MV

were 0.9 at steady state reflecting the differential maternal and fetal plasma f_u. The UA/UV was 1 at steady-state following continuous IV or epidural infusion consistent with the lack of significant fetal elimination of fentanyl.

5.5 DISCUSSION

In recent years, there has been an increasing interest to use mf-PBPK modeling to study maternal-fetal disposition of xenobiotics because of the ethical concerns and challenges in conducting clinical studies in pregnant women.[256,257] Fentanyl is of particular interest[114] because it is commonly used to manage pain during labor and delivery and it is a drug of abuse sometimes used by pregnant women with opioid addiction. The fetal disposition of fentanyl and alternative opioid analgesics is of interest to better predict, prevent and manage fetal side effects of opioids. However, information on the fetal disposition of fentanyl is limited to measurements of single timepoint UV/MV ratios at delivery. Moreover, the reported UV/MV ratio appears to be dependent on the time post-dose which makes it difficult to assess overall fetal exposure and the C_{max} reached in the fetus from a single timepoint data. Therefore, we used mf-PBPK modeling to simulate the maternal and fetal disposition of fentanyl to inform future clinical decisions and to establish a modeling and simulations workflow that could be used for other drugs administered to pregnant women.

To simulate the maternal-fetal disposition of fentanyl following epidural dose, an epidural PBPK model was first developed. Drug absorption following epidural administration is a complex process because of the unique physiology of the epidural space. Drug absorption following epidural doses has been reported to be biphasic[235,258,259] with a rapid absorption phase attributed to direct uptake by the spinal vein and slow absorption phase attributed to the sequestration of lipophilic drugs by the epidural adipose tissue.[235] The sensitivity analyses using

a hypothetical drug X demonstrated that $CL_{pd,vein}$ is the major rate-determining factor of drug absorption following epidural injection. Since there is currently no information on the surface area of the epidural venous system, the $CL_{pd,vein}$ of fentanyl was defined using a scaler compound alfentanil. The observed Caco-2 permeability for alfentanil and fentanyl together with alfentanil optimized $CL_{pd,vein}$ were used consistent with a method previously established to predict transplacental clearance.[79] The optimized $CL_{pd,vein}$ was 20-fold higher than the estimated $CL_{pd,adipose}$ scaled based on the surface area of the adipose tissue likely due to larger venous surface area and fenestration in the blood vessels[227] increasing drug permeability. The scaling approach yielded a fentanyl model that successfully simulated fentanyl PK after epidural dosing. This suggests that epidural absorption kinetics is directly proportional to drug permeability and that this method and the developed epidural dosing model can be used more broadly for other drugs and for dosing in non-pregnant individuals to aid in the design of dosing strategies. The model can also be coupled with a pharmacodynamic (PD) model to allow PK-PD simulations for pain management.

Fetal liver metabolism of fentanyl has been suggested based on the high CYP3A4 mediated hepatic $CL_{int,u}$ of fentanyl observed in adults[255] and similar substrate specificity of CYP3A4 and CYP3A7.[112] However, no metabolism of fentanyl by CYP3A7 has been reported to support understanding of fetal fentanyl disposition. This study showed that both CYP3A7 and pooled FLM metabolize fentanyl to norfentanyl, the major fentanyl metabolite formed by CYP3A4 in adults. Fentanyl metabolism in FLM is likely mediated by CYP3A7 based on the extrapolation using a measured CYP3A7 expression and established ISEF for CP3A7. However, the extrapolated fetal hepatic $CL_{int,u}$ (0.028 L/h) was significantly less than the observed adult hepatic $CL_{int,u}$ (1,055 L/h) suggesting that fetal liver is unlikely to quantitatively contribute to the

maternal-fetal disposition of fentanyl. Similarly, the fetal hepatic $CL_{int,u}$ is low in comparison to fetal hepatic blood flow and transplacental clearance suggesting that fetal liver metabolism does not affect fetal drug disposition. The minor role of fetal liver metabolism was also confirmed through the simulations using the mf-PBPK model that the UA/UV ratio was unity following epidural infusion to steady-state.

Using the verified mf-PBPK model, this study compared the maternal and fetal disposition of fentanyl following epidural or IV dosing. The significantly higher maternal and fetal C_{max} following an IV bolus in comparison to epidural bolus dose suggests a higher chance of pharmacological effects including the risk of undesirable effects (e.g. respiratory depression) with IV bolus dose compared to epidural bolus dose of fentanyl. On the other hand, use of IV or epidural infusion of fentanyl avoided the high C_{max} possibly resulting in slow onset of analgesic effect.

The maternal-fetal disposition simulations illustrate an important concept that the umbilical venous and arterial concentrations (commonly collected to reflect fetal exposure) and the maternal arterial and venous concentrations following a bolus dose depend on the distribution kinetics in the mom, fetus, and across the placenta. The UV/MV ratio is most commonly reported to reflect the transplacental transfer from the mom to the fetus. However, physiologically the placenta is perfused with maternal arterial blood instead of venous blood and hence, the maternal arterial blood concentration is the main driver of the distribution kinetics across the placenta (i.e. syncytiotrophoblast monolayer). Depending on the PK properties of the drug, the arteriovenous concentration difference in the mom could be large.[225] The arteriovenous concentration difference of fentanyl was captured by these simulations and is also supported by the observed 2-fold higher placental intervillous space plasma fentanyl concentration (maternal

side) (2.02 nM) compared with the MV plasma concentration (0.92 nM) at about 30 min post epidural bolus dose.[206] Hence, the high UV/MV ratio of fentanyl does not reflect a rapid transplacental transfer but rather the arteriovenous distribution kinetics in the mother. Using MV concentrations as a surrogate of exposure of the fetus may be misleading in early timepoints after drug dosing. As illustrated by the UV/MA ratio, the transplacental distribution of fentanyl to the fetus is relatively slow taking several hours to reach distribution equilibrium. Notably the simulated UV/MA ratios were considerably different than the commonly reported UV/MV ratios, in particular during the earlier time points suggesting a systematic error in assessing transplacental permeability from UV/MV ratios.

The UA/UV ratio reflects the distribution (and metabolism) kinetics in the fetus. The UV concentration is the concentration on the fetal side of the placenta after the drug crosses the placenta and before fetal distribution and metabolism. The UA concentration is the fetal arterial concentration after fetal distribution and metabolism. The UA/UV ratio following a bolus dose of fentanyl suggested that the fetal distribution of fentanyl is slow as distribution equilibrium was not reached until 30 h post-dose. The data presented suggests that to best capture maternal-fetal distribution and potential fetal clearance, steady-state concentration ratios should be measured.

In conclusion, our study demonstrates that maternal-fetal disposition of drugs can be predicted using mf-PBPK modeling and this tool can be further explored to study maternal-fetal disposition of other drugs that are difficult to study in the clinic. The simulations using the mf-PBPK model illustrate that the fetal/maternal plasma concentration ratio is significantly impacted by maternal, fetal, and transplacental distribution kinetics after a bolus dose. The fetal distribution of fentanyl is relatively slow and the maternal and fetal exposures are similar following IV or epidural infusion while the C_{max} is significantly higher following an IV bolus

dose compared to an epidural bolus dose. This study provides PK insights to better understand maternal-fetal disposition kinetics of fentanyl and provide a PK basis to make future clinical decisions on fentanyl dosing to parturient women.

Table 5.1 Physiological parameters of the PBPK models with epidural dosing site. (GW = gestational week)

	Nonpregnant Model[a]		Maternal Model[b] (GW 40)		Fetal Model[b] (GW 40)	
	Volume (L)	Blood flow (L/h)	Volume (L)	Blood flow (L/h)	Volume (L)	Blood flow (L/h)
Adipose	15	16.2	22.6	24.4	--	--
Bone	10	13.1	10	13.1	--	--
Brain	1.4	35.6	1.4	35.6	0.375	13.28
Gut	1.2	46.8	1.2	46.8	0.1	3.95
Heart	0.33	12.5	0.33	12.5	--	--
Kidney	0.31	60	0.31	64.7	0.031	4.16
Liver	1.8	90	1.8	90	0.129	16.42
Lung	0.53	308	0.53	391	--	--
Pancreas	0.098	3.1	0.098	3.1	--	--
Skin	2.6	18.1	2.6	18.1	--	--
Muscle	28	57.3	28.17	57.3		
Spleen	0.18	6.2	0.18	6.2	--	--
Blood	5	--	5.64	--	0.42	--
Rest of body	--	--	--	--	2.384	47.41
Arm adipose	0.0338	0.0709	0.0338	0.0709	--	--
Arm muscle	0.268	0.29	0.268	0.29	--	--
Arm skin	0.0363	0.218	0.0363	0.218	--	--
Arm anastomoses	--	0.06432	--	0.06432	--	--
Epidural adipose	0.0035	--	0.0035	--	--	--
Epidural fluid	0.01	--	0.01	--	--	--
Epidural vein	0.0035	0.56	0.0035	0.297	--	--
Placenta	--	--	0.659	49.1	0.151	20.21
Ductus venosus	--	--	--	--	--	8.73
Syncytiotrophoblast	--	--	0.08	--	--	--
Amniotic fluid	--	--	0.758	--	--	--

a. Physiological parameters used in the nonpregnant PBPK model with arm sampling site model for a 66.8 kg nonpregnant individual were adopted from Huang and Isoherranen, 2020.[225]

b. Physiological parameters used in the maternal-fetal PBPK model for a 75.2 kg pregnant woman and a 3.44 kg fetus were calculated from equations published in Abduljalil *et al.*, 2012 and Zhang *et al*, 2017.[73,77]

Table 5.2 Physicochemical and pharmacokinetic parameters of alfentanil and fentanyl used in the PBPK models.

Parameter	Alfentanil	Fentanyl[a]
Physicochemical properties[b]		
MW (g/mol)	416.52	336.47
logP	2.16	4.05
pKa	6.5	8.99
B/P Ratio	0.55	1
$f_{u,plasma}$[c]	0.1	0.16
$f_{u,epiduralfluid}$	1	1
$f_{u,syncytiotrophoblast}$	--	1
$f_{u,amnioticfluid}$	--	1
Tissue partitioning coefficient (K_p)[d]		
Adipose	2.1	26.7
Bone	0.1	1
Brain	0.13	3.5
Gut	2.12	8.4
Heart	0.55	4.5
Kidney	0.82	12.1
Liver	1	3.8
Lung	0.78	13.5
Muscle	0.31	3.1
Skin	0.1	2.1
Spleen	0.73	27.6
Pancreas	0.96	21.3
Metabolism and excretion		
$CL_{int,u}$ (L/h)[e]	185	1055
CL_r (L/h)	0.4	3.3
$CL_{syncytiotrophoblast}$ (L/h)	--	0
Fetal hepatic $CL_{int,u}$ (L/h)[f]	--	0.028
Passive permeability clearance		
$CL_{pd,adipose}$ (L/h)	0.010	0.0012
$CL_{pd,vein}$ (L/h)	0.20	0.023
$CL_{pd,placenta}$ (L/h)	--	357

a. Fentanyl model parameters were adopted from a previously published PBPK model of fentanyl,[225] parameters were assumed to be the same in pregnant women and fetuses unless otherwise stated.
b. Physicochemical properties of alfentanil were collected from Bower and Hull, 1982[239] and Palm *et al.*, 1999.[238]
c. $f_{u,plasma}$ of pregnant women and fetus were measured to be 0.12 and 0.14, respectively in a group of 40 parturient women and their newborns.[254]
d. K_p's of alfentanil were adopted from values measured in rats[237], K_p's of bone and skin were not reported and were assigned as 0.1 based on the observed V_{ss} of alfentanil (0.7 L/kg) in human.
e. $CL_{int,u}$ of fentanyl was predicted to be 1,891 L/h for pregnant women as described in the method.
f. Measured.

Table 5.3 Simulated and observed MV, UV, and UA plasma concentrations at delivery following epidural bolus or infusion dosing to parturient women during labor. Time is the average (range) reported delivery time since first dose of epidural fentanyl, the observed are the reported mean (range) or mean ± SD concentrations at delivery and the simulated are the simulated concentrations at the mean time of delivery (range of concentration at the range of delivery time). The absolute fold error was calculated using the following equation: absolute fold error = $10^{|\log(\text{simulated concentration/observed concentration})|}$

Dosing route	Dose (µg)	Time (h)	MV (ng/mL)		Absolute fold error	UV (ng/mL)		Absolute fold error	UA (ng/mL)		Absolute fold error
			Observed	Simulated		Observed	Simulated		Observed	Simulated	
Epidural bolus[a]	100	0.45 (0.32 – 0.70)	--	--	--	0.13 (0.05 – 0.19)	0.29 (0.23 – 0.32)	**2.36**	0.06 (0.02 – 0.12)	0.11 (0.10 – 0.11)	**1.65**
Epidural bolus[b]	100	0.48 (0.43 – 0.54)[c]	0.31 (0.28 – 0.32)[c]	0.26 (0.25 – 0.27)	**1.19**	0.25 (0.19 – 0.51)[c]	0.29 (0.27 – 0.30)	**1.15**	--	--	--
Epidural bolus[d]	100	0.50[e]	0.31 (0.17 – 0.72)	0.26	**1.18**	0.24 (0.13 – 0.65)	0.28	**1.18**	0.19 (0.14 – 0.75)	0.11	**1.82**
Epidural bolus[f]	100	0.58 (0.42 – 1.00)	--	--	--	0.12 (0.02 – 0.24)	0.26 (0.17 – 0.30)	**2.18**	0.08 (0.01 – 0.22)	0.10 (0.09 – 0.11)	**1.30**
Epidural bolus + infusion[g]	75 µg + 15 µg/h	3.45 (0.33 – 12.7)	0.52 ± 0.03	0.16 (0.16 – 0.21)	**3.31**	0.18 ± 0.03	0.12 (0.12 – 0.24)	**1.51**	0.10 ± 0.07	0.09 (0.08 – 0.13)	**1.07**
Epidural bolus + infusion[h]	10 µg + 10 µg + 10 µg/h	5.80 (4.47 – 8.10)[c]	0.10 (0.07 – 0.17)[c]	0.09 (0.08 – 0.10)	**1.13**	0.05 ± 0.02	0.07 (0.07 – 0.08)	**1.41**	--	--	--

a. Desprats *et al.*, 1991[218], n = 16.
b. Moises *et al.*, 2005[220], n = 8.
c. Data reported as median (25th percentile – 75th percentile).
d. De Barros Duarte *et al.*, 2009[206], n = 10.
e. No range of delivery time reported.
f. Desprats *et al.*, 1995[219], n = 10.
g. Loftus *et al.*, 1995[214], n = 13 (UA, n = 9).
h. Haidl *et al.*, 2018[116], n = 20 (UV, n = 19).

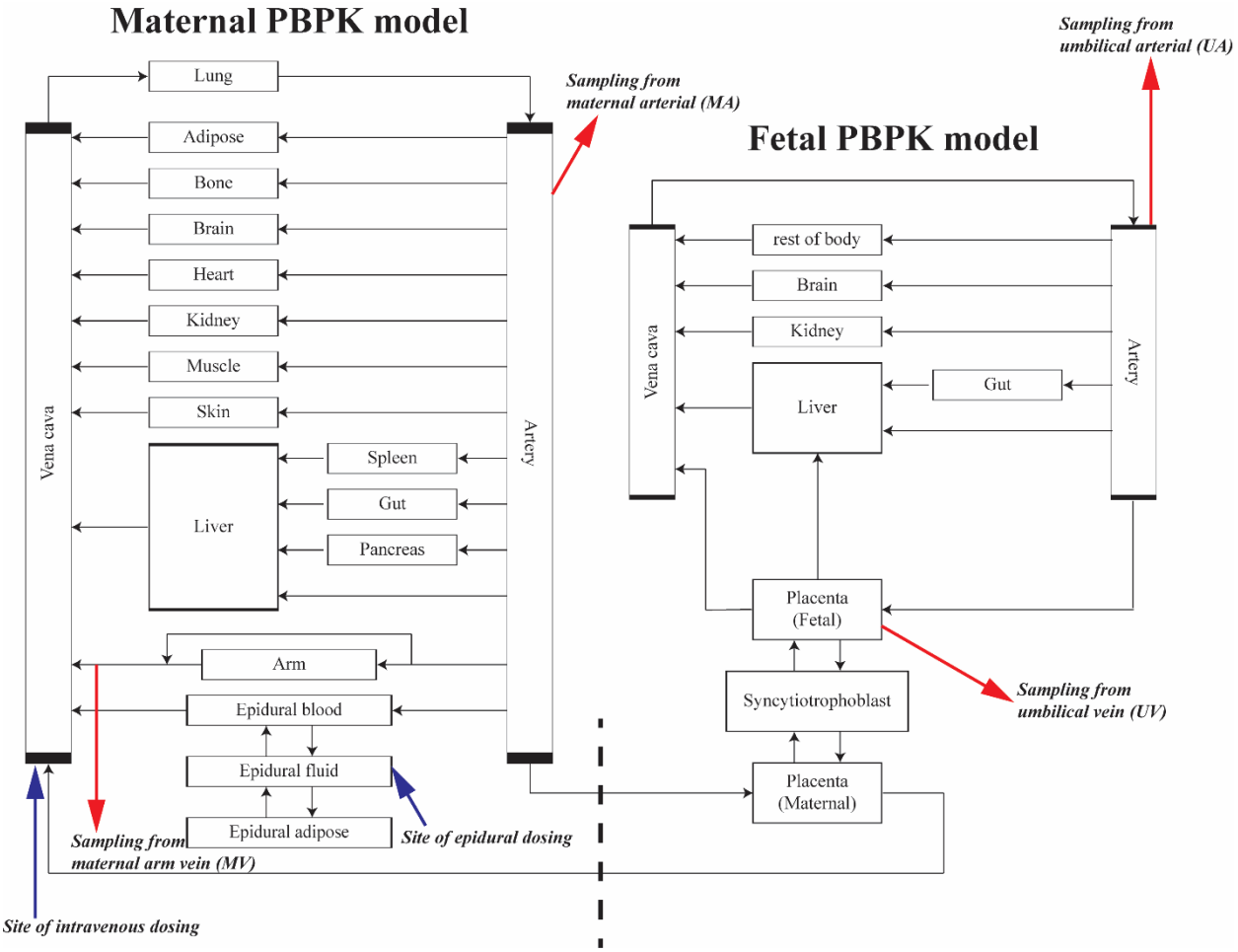

Figure 5.1 Model structure of the maternal-fetal PBPK (mf-PBPK) model with an arm sampling site and an epidural dosing site incorporated. The blue arrows indicate the intravenous and epidural dosing sites to the mother and the red arrows indicate the maternal arterial (MA) and arm venous (MV) plasma sampling locations of the mother and the umbilical arterial (UA) and umbilical venous (UV) plasma sampling site of the fetus. A nonpregnant PBPK model used in this study was structurally identical as the maternal PBPK model but the linkage to the placenta and fetal PBPK model was removed as indicated by the dashed lines.

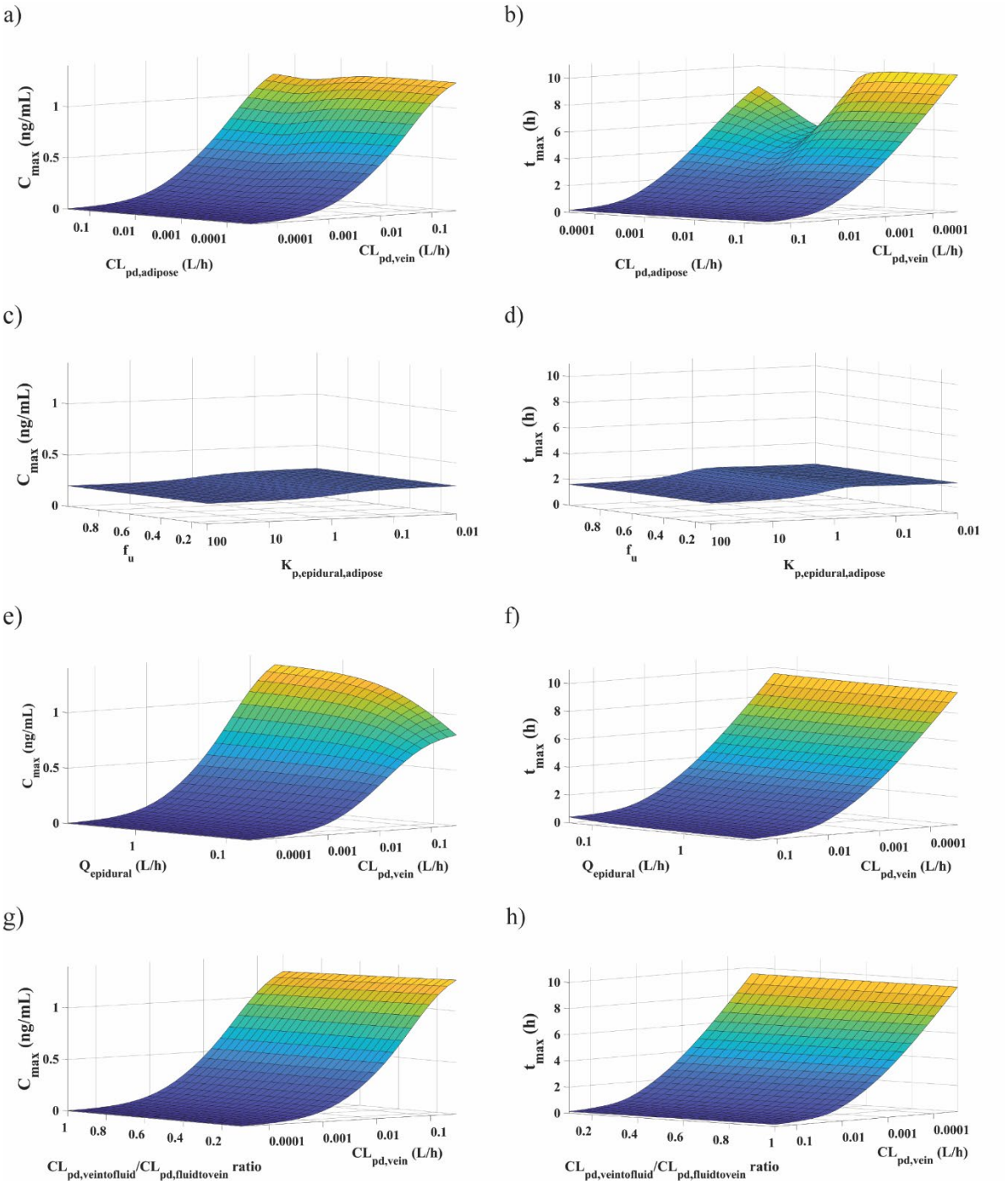

Figure 5.2 Sensitivity analysis for epidural dosing site parameters of drug X. The effect of altered $CL_{pd,adipose}$ and $CL_{pd,vein}$ (ranging from 0.00003 to 0.3 L/h) on C_{max} and t_{max} of drug X is shown in a and b. The impacts of varying K_p (0.01 to 100) and f_u (0.1 to 1) (c,d), and the $Q_{epidural}$ (0.056 to 5.6 L/h) and $CL_{pd,vein}$ (0.00003 to 0.3 L/h) (e,f), and asymmetrical $CL_{pd,vein}$ with $CL_{pd,fluidtovein}$ (10% to 100% of $CL_{pd,veintofluid}$) (g,h) on C_{max} and t_{max} of drug X is shown in c-h. The parameters were kept constant unless stated otherwise ($CL_{pd,adipose}$ = 0.003 L/h, $CL_{pd,vein}$ = 0.003 L/h, K_p = 1, f_u = 1, $Q_{epidural}$ = 0.56 L/h). For comparison, the scales of the heat map for C_{max} and t_{max} were kept unchanged across the sensitivity analyses.

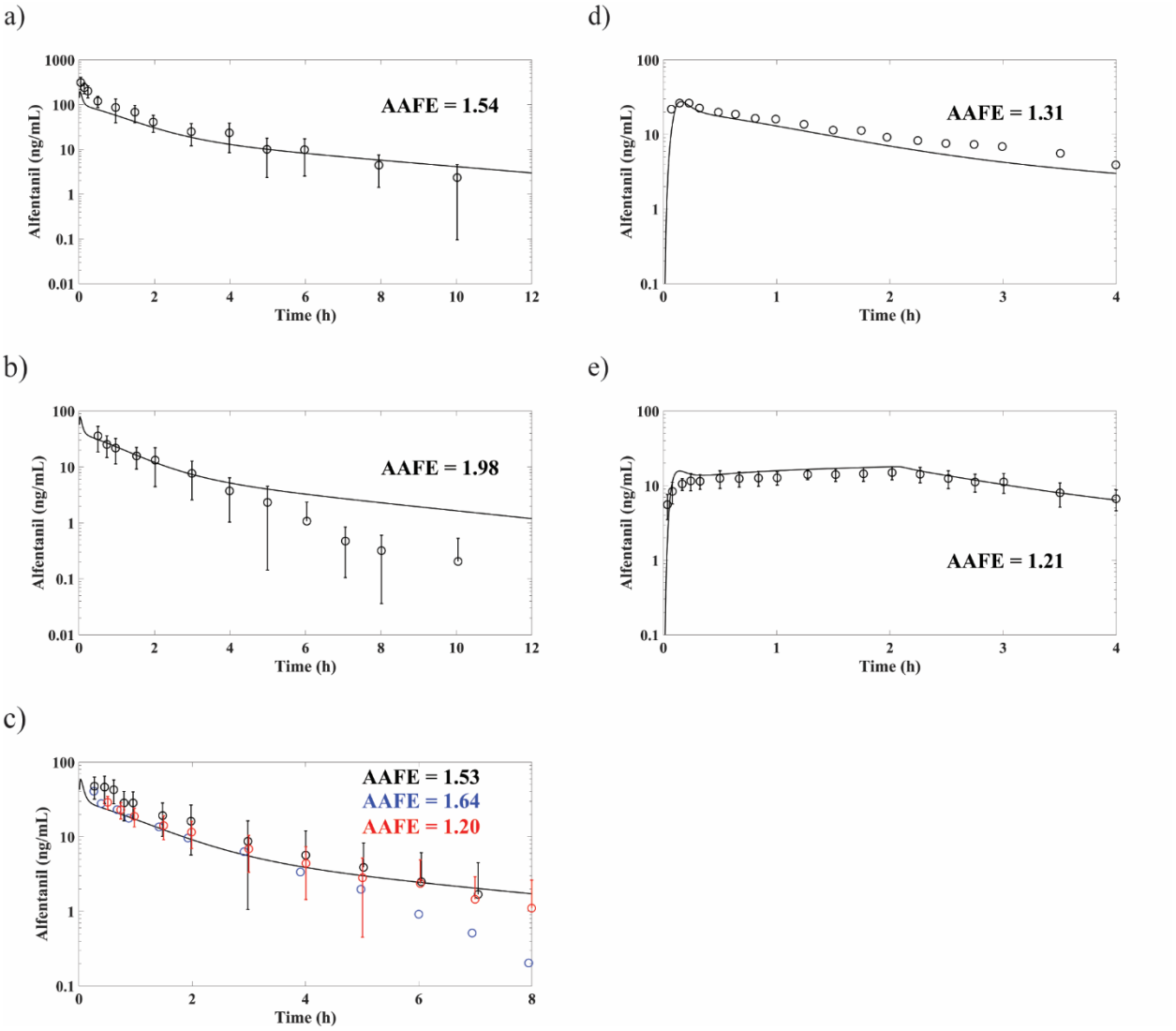

Figure 5.3 Simulated plasma concentration-time profiles following IV and epidural administration of alfentanil using the nonpregnant PBPK model overlaid with mean observed plasma alfentanil concentrations in nonpregnant subjects. Simulated (solid lines) and mean observed (open circles) plasma concentrations from the arm vein following a) a single IV bolus dose of 50 µg/kg (n=10), b) a single IV bolus dose of 20 µg/kg (n=9), c) a single IV bolus dose of 15 µg/kg (n=6), d) a single epidural dose of 750 µg (n=7) and e) a single epidural bolus dose of 400 µg plus an epidural infusion of 400 µg/h for 2 h (n=12). The mean observed fentanyl concentrations are from Ferrier *et al.*, 1985[241] (a), Kharasch *et al.*, 1997[244] (b), black circles: Phimmasone and Kharasch, 2001,[243] blue circles: Kharasch *et al.*, 2004,[244] red circles: Kharasch *et al.*, 2011[245] (c), Coda *et al.*, 1995[247] (d), and Coda *et al.*, 1999[248] (e). The error bars in panels a, b, c, and e represent the SD as reported in the respective study. The AAFE reported in each figure was calculated from the simulated and observed concentrations of each respective study.

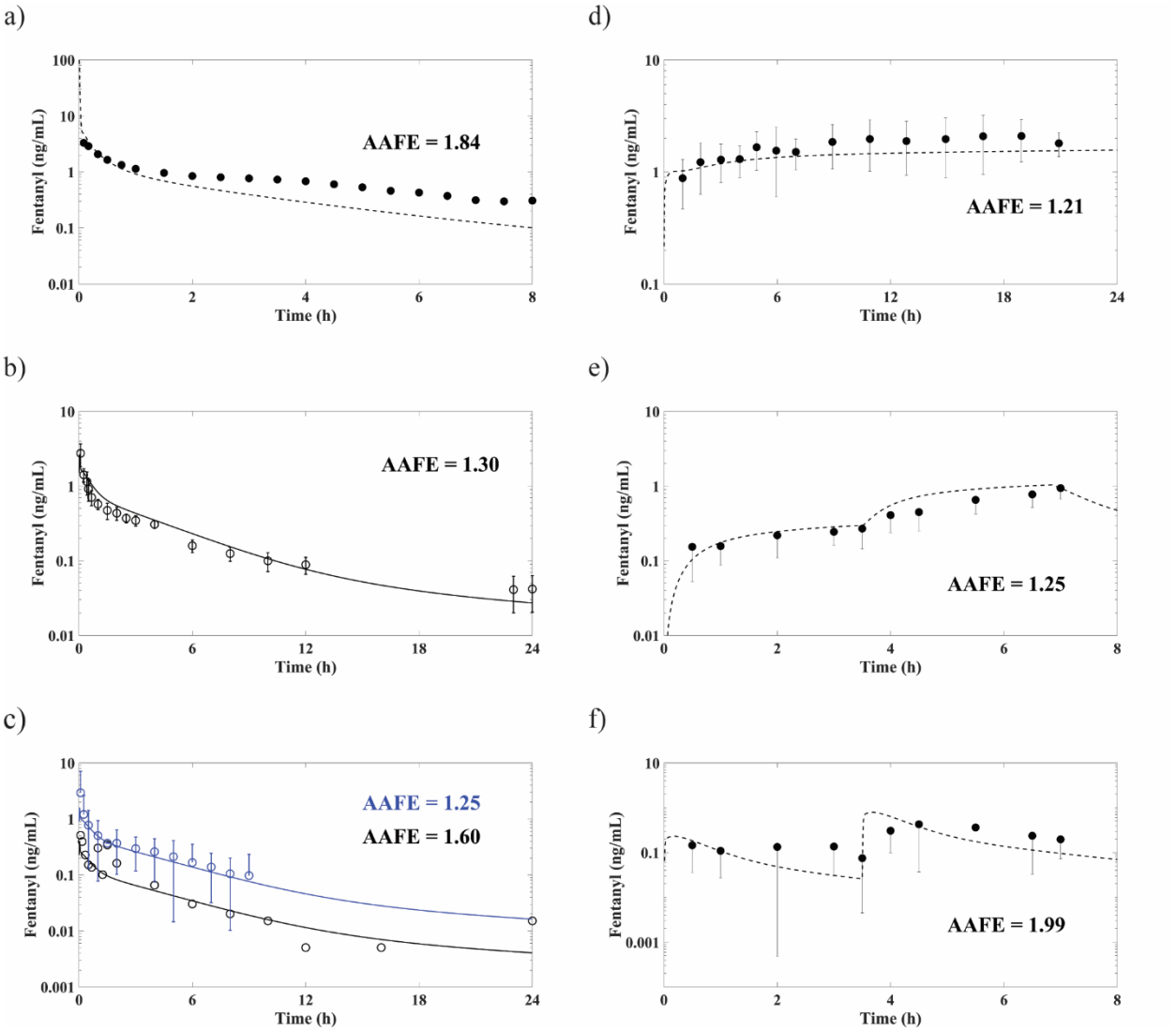

Figure 5.4 Simulated plasma concentration-time profiles following IV and epidural administration of fentanyl using the nonpregnant PBPK model overlaid with mean observed plasma fentanyl concentrations in nonpregnant subjects. Simulated plasma concentrations from the arm vein (solid lines) and the artery (dashed lines), and the mean observed plasma concentrations from the arm vein (open circles) and the artery (closed circles) following a) a single IV bolus dose of 6.4 µg/kg (n=5), b) a single IV bolus dose of 5 µg/kg (n=16), c) a single IV bolus dose of 50 µg (n=10) in black, and a single IV bolus dose of 200 µg (n=8) in blue, d) an epidural bolus dose of 100 µg and continuous epidural infusion of 114.3 µg/h for 24 h (n=10), e) epidural infusion at 30 µg/h for 3.5 h and increased to 100 µg/h for another 3.3 h (n=10), and f) an epidural bolus dose of 30 µg followed by a second epidural bolus dose of 100 µg at 3.5 h (n=10). The mean observed fentanyl concentrations are from McClain and Hug, 1980[223] (a), Ziesenitz *et al.*, 2015[119] (b), Rauck *et al.*, 2017[249] and Nozari *et al.*, 2019[224] (c), Badner *et al.*, 1990[251] (d), and Ginosar *et al.*, 2003[250] (e,f). The error bars in panels b-d represent the SD and in panels e and f represent the 25th quartile as reported in the respective study. The AAFE reported in each figure was calculated from the simulated and mean observed concentrations of each respective study.

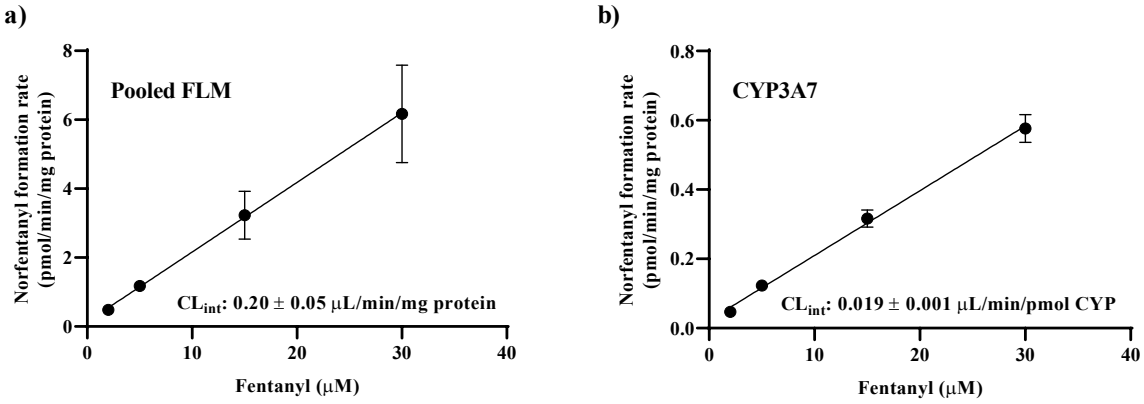

Figure 5.5 Norfentanyl formation kinetics in pooled FLM (14 donors) and recombinant CYP3A7. Metabolite formation rate as a function of fentanyl concentration for norfentanyl formation by a) pooled FLM and b) CYP3A7. The CL_{int} shown were estimated by linear regression. Mean and standard deviation of CL_{int} reported were calculated from three different experiments conducted on separate days.

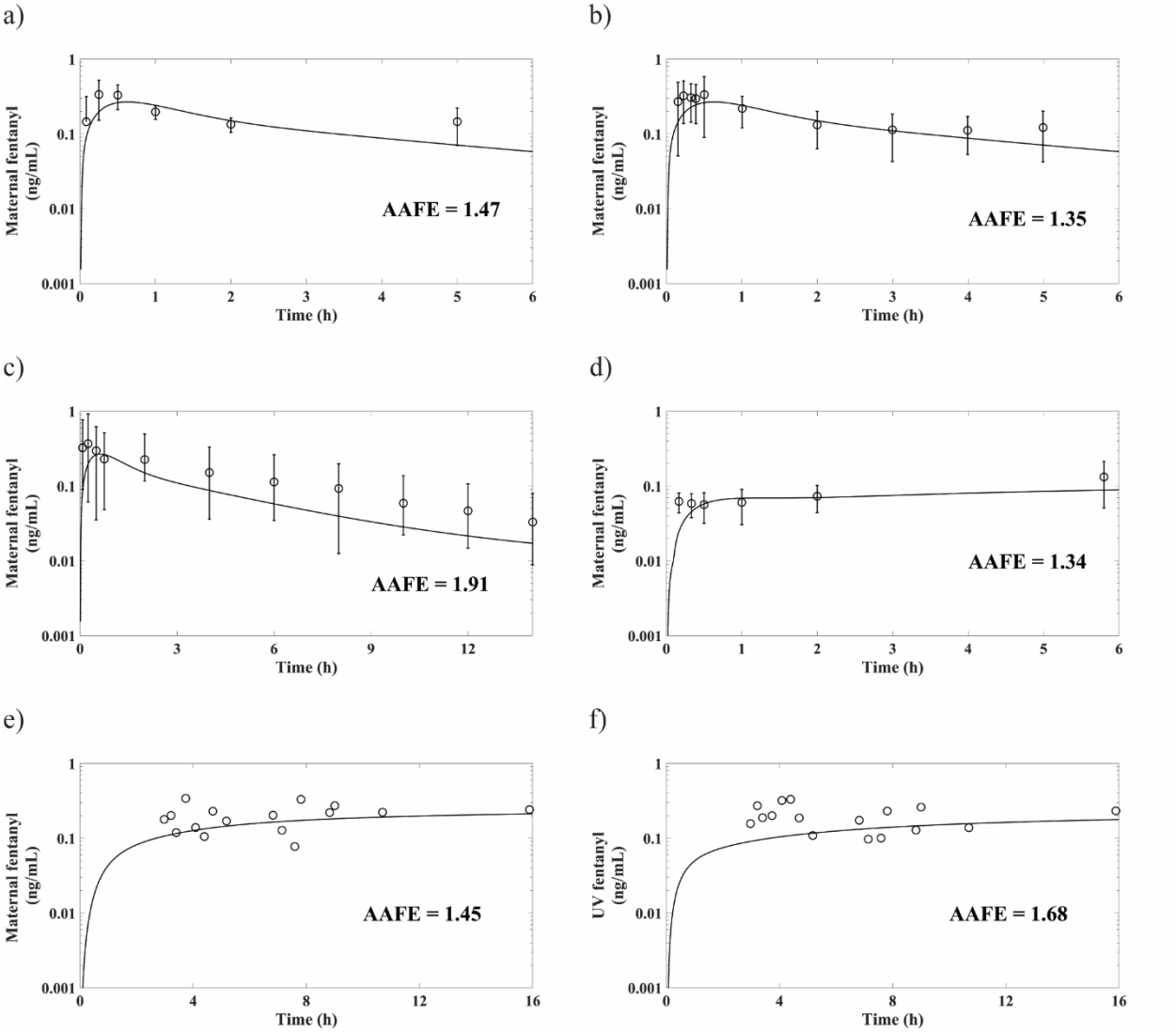

Figure 5.6 Simulated and observed maternal and umbilical venous plasma concentration-time profiles following epidural administration of fentanyl overlaid with observed plasma concentrations. The simulated (solid lines) and observed (open circles) maternal venous concentrations following a) a single epidural bolus dose of 100 µg fentanyl (n=16), b) a single epidural bolus dose of 100 µg fentanyl (n=16), c) a single epidural bolus dose of 100 µg fentanyl (n=10), and d) two bolus doses of 10 µg fentanyl and continuous 10 µg/h infusion of fentanyl (n=19). The AAFE reported in a-d were calculated from the simulated and the mean observed maternal venous concentrations at each timepoint of each respective study. The mean observed fentanyl concentrations are from Desprats *et al.*, 1991[218] (a), Desprats *et al.*, 1995[219] (b), Moises *et al.*, 2005[220] (c), and Haidl *et al.*, 2018[116] (d). Error bars in panels a, b, d represent the SD and in panel c represent the 25th and 75th quartile as reported in the respective study. Panel (e) shows the simulated concentrations in the maternal arm vein (solid line) in comparison to individual subject data at delivery (open circles) (n=16) following epidural infusion of fentanyl at 20 µg/h from Bader *et al.*, 1995[117] and panel (f) shows the corresponding simulated (solid line) and observed individual subject (open circles) concentrations in the umbilical vein at delivery observed in the same study. The AAFE reported in panels e and f were calculated from the simulated and observed concentration of each individual subject.

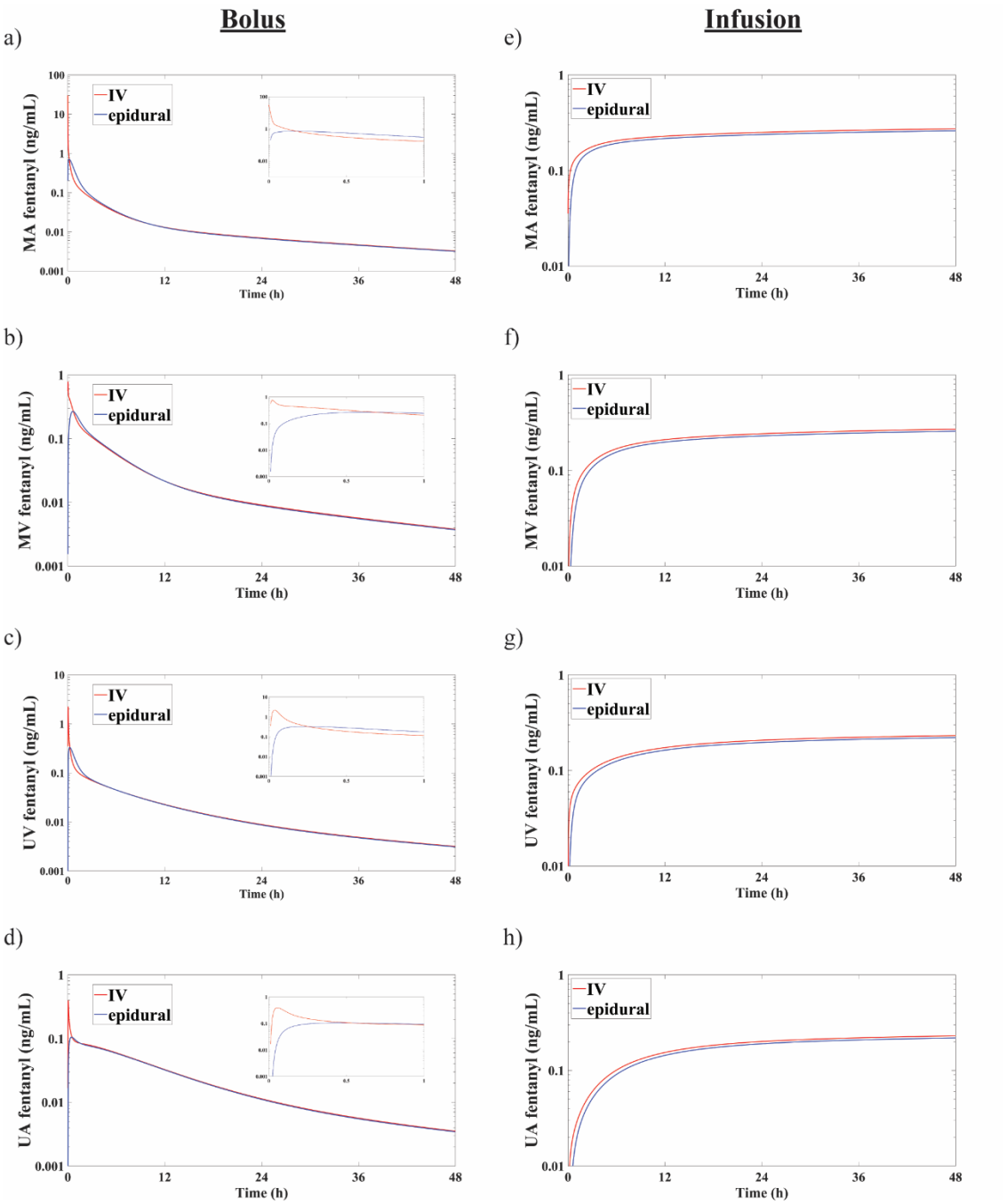

Figure 5.7 Simulated maternal and fetal fentanyl plasma concentration-time curves using the optimized mf-PBPK model. The simulated plasma concentration-time profiles (0-48 h) from a) maternal artery (MA), b) maternal arm vein (MV), c) umbilical vein (UV), and d) umbilical artery (UA) following single IV (red lines) or epidural (blue lines) bolus dose of 100 µg fentanyl. The C_{max} following IV dose was 42-fold, 3-fold, 7-fold, and 4-fold higher than following epidural dose for MA, MV, UV, and UA plasma, respectively. The insets show the data for the first hour after dosing. The simulated plasma concentrations (0 - 48 h) from e) maternal arterial (MA), f) maternal arm vein (MV), g) umbilical vein (UV), and h) umbilical artery (UA) following continuous IV (red lines) or epidural (blue lines) infusion of fentanyl at 20 µg/h.

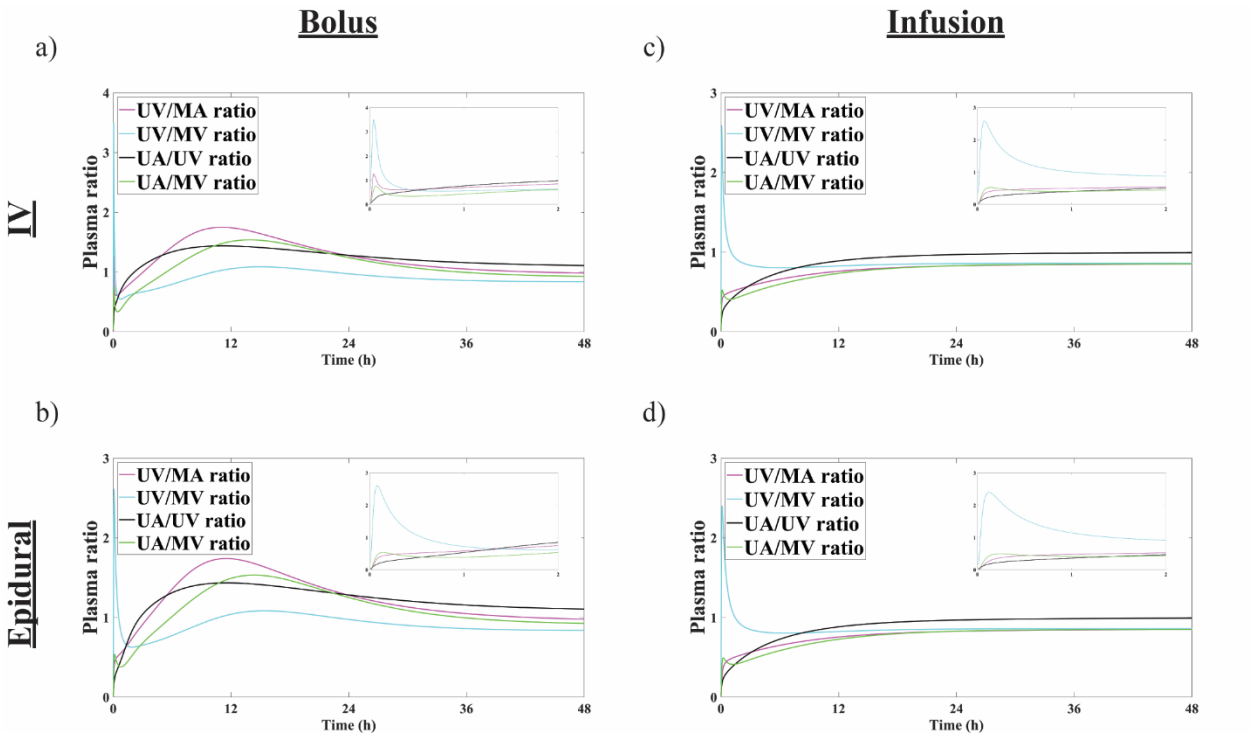

Figure 5.8 The fentanyl plasma concentration ratios between umbilical vein (UV), maternal artery (MA), maternal vein (MV), and umbilical artery (UA) as a function of time simulated using the optimized mf-PBPK model. The simulated UV/MA, UV/MV, UA/UV, and UV/MV concentration ratios (0 - 48 h) following a) an IV bolus dose of 100 µg fentanyl, b) an epidural bolus dose of 100 µg fentanyl, c) IV infusion of fentanyl at 20 µg/h, and d) epidural infusion of fentanyl at 20 µg/h. The insets show the first 2 hours of the data.

Chapter 6.

Discussion and future directions

It is well recognized that disposition of xenobiotics can be substantially different in pregnant women when compared to nonpregnant individuals. Also, the knowledge of fetal disposition of drugs taken by the mom is an indispensable piece of information to determine safe and efficacious drug use or to establish a safe exposure limit of xenobiotics in pregnant women. However, despite the recent efforts to study maternal-fetal disposition of xenobiotics,[17,48] it remains an understudied area in pharmaceutical research.[256,257] One major reason is that clinical research in pregnant women is hampered by ethical concerns.[46] Limited information (e.g. maternal PK and single timepoint umbilical cord concentration at birth) can be ascertained from restricted opportunistic studies where sampling is performed in pregnant women already taking medications for therapeutic reasons. The physiological changes (e.g. increased GFR, CYP3A4 induction, and P-gp induction) and their effects on the maternal PK of xenobiotics over the gestational period have been defined through clinical studies of probe drugs (e.g. metformin, midazolam, digoxin) in pregnant women.[14,16] Fetal disposition, on the other hand, is difficult to capture through a single umbilical cord sampling at birth. The transplacental clearance, via passive and active processes governs the rate and extent of fetal disposition of xenobiotics and is a major determining factor of the maternal-fetal distribution kinetics. The amniotic fluid has been proposed to increase the residence time and alter the plasma concentration-time profile of hydrophilic xenobiotics in the fetus because these compounds are likely to be 'trapped' in the amniotic fluid. The fetal liver has been shown to metabolize xenobiotics which may contribute to maternal-fetal disposition and limit fetal exposure to xenobiotics. These attributes of fetal disposition of xenobiotics cannot be fully elucidated in clinical studies unless fetal plasma is also sampled, which would involve invasive procedures and as such is unethical. Therefore, various

in vivo, *in vitro*, and *in silico* methodologies have been established to study maternal-fetal disposition of xenobiotics.

In this dissertation, the maternal-fetal disposition of DA was studied *in vivo* in cynomolgus monkeys employing a novel LC-MS method for DA quantification (**Chapter 2**). The effect of pregnancy on the disposition of DA was determined, and a PK model was built to kinetically describe the fetal disposition of DA (**Chapter 3**). The fetal liver metabolism of oxycodone was studied *in vitro* using FLM and recombinant CYP3A7 to quantitatively predict the contribution of fetal liver in maternal-fetal disposition of oxycodone as a model compound (**Chapter 4**). Finally, these concepts were integrated in an *in silico* study of the maternal-fetal disposition of fentanyl following IV and epidural dosing to parturient women using mf-PBPK modeling built based on the known physiology of pregnant women (**Chapter 5**).

6.1 MATERNAL-FETAL DISPOSITION OF DA IN CYNOMOLGUS MONKEYS

The renal clearance of DA was shown to be increased during pregnancy proportionally to the increased GFR by about 30-90% when compared to the individual pre-pregnancy baseline. In contrast, the AUC of DA was not altered during pregnancy because of the presence of alternative elimination pathways in monkeys (f_e = 0.4-0.7) and the variability of bioavailability following oral doses which limits the power of this study to detect a small change (<40%) in AUC.[260] This observation, when extrapolated to human, suggested that pregnant women are not at risk of higher DA exposure during pregnancy. However, based on the observed dose-dependent increase in tremor frequency in the adult female monkeys,[165] the current TDI (0.075 mg/kg/day) is insufficient to protect human from chronic toxicity. These findings suggest that the TDI for DA has to be lowered to 10% of the current TDI (0.0075 mg/kg/day) or even lower, especially for people who include DA containing seafood in their regular diet.[95,133,134] In fact, a recent study

proposed a new TDI of 167 ng/kg/day (0.2% of the current TDI) based on the impaired memory associated with DA consumption in the coastal population who are chronically exposed to DA through their diet.[261] One major research gap to protect human exposure to toxic level of DA is a reliable method to estimate human exposure since DA was not detected in the plasma collected from subjects who are chronically exposed through their diet.[155] A recent discovery of a serum DA antibody might shed light for a reliable method to determine chronic DA exposure in humans.[155]

The infant plasma DA concentration at birth together with the maternal-fetal PK modeling suggested that the placenta is partially limiting fetal disposition of DA, likely through active processes (i.e. placental efflux transporters), resulting in a fetal/maternal AUC ratio of 0.35. This lower fetal AUC may explain why the fetus did not display sign of tremors while the mom did. Nevertheless, delay in cognitive development was observed in infants born to the monkeys in the high dose group (0.15 mg/kg/day) suggesting that the fetus is not completely protected from DA toxicity.[100] Moreover, despite a <1 fetal/maternal ratio, DA has a longer apparent residence time in the fetus compared to the mom.[260] The maternal-fetal PK model suggested that the long fetal residence time is due to the long residence time of DA in the amniotic fluid. The long residence time and long apparent half-life of DA in the fetus may increase the risk of fetal toxicity following repeated exposure.

Future research on maternal-fetal disposition of DA should focus on the mechanisms of transplacental clearance, for example, to identify the efflux transporters responsible for DA transport in the placenta. Since species differences exist in the expression and localization of drug transporters in the placenta, the mechanisms of placental transport can be used to better and

more confidently predict the function of the human placenta in the maternal-fetal disposition of DA and the risks of fetal toxicity in humans.

6.2 FETAL LIVER METABOLISM AND ITS CONTRIBUTION TO THE MATERNAL-FETAL DISPOSITION OF OXYCODONE

Consistent with the abundant CYP3A7 and minimal CYP2D6 expression in the fetal liver as shown previously through gene expression, protein quantification, and enzyme activity,[38,53,61] the fetal liver was shown to metabolize oxycodone to form noroxycodone (a reaction mediated by CYP3A7) but not oxymorphone (a reaction mediated by CYP2D6). Despite a higher CYP3A7 expression in FLM compared to CYP3A4 expression in HLM, the FLM capacity (i.e. CL_{int}) in metabolizing oxycodone is about 10% of that of the HLM suggesting a significantly lower metabolic capacity of CYP3A7 in metabolizing oxycodone compared to CYP3A4. An ISEF was established in this dissertation to predict FLM activity from CYP3A7 activity which provides a convenient way to predict fetal liver metabolism without FLM.

Theoretically, fetal liver metabolism can contribute to maternal-fetal disposition of oxycodone and other xenobiotics in two ways. First, it may contribute to the total body clearance in pregnant women (although it is unlikely because of the size difference between the adult and fetal livers). Second, it may decrease fetal exposure by acting as a first pass organ or clearing oxycodone within the fetal compartment. These potential contributions of fetal liver to the maternal-fetal disposition of oxycodone were addressed quantitatively using IVIVE, and it was shown that the fetal liver does not quantitatively contribute to the maternal-fetal disposition of oxycodone. The low FLM capacity in metabolizing oxycodone compared to that in HLM together with the significantly smaller fetal liver compared to the adult liver in size (fetal liver at term: 0.13 kg vs adult liver: 1.8 kg) predicted an insignificant contribution of fetal hepatic

clearance to the total body clearance of oxycodone in pregnant women. The small extraction ratio of the fetal liver (<1%) predicted that the fetal liver does not provide first pass metabolism to limit fetal exposure to oxycodone. These results highlight the importance and provided a framework to quantitatively predict the fetal hepatic clearance of xenobiotics from FLM and recombinant enzyme activity.

6.3 PREDICTION OF MATERNAL-FETAL DISPOSITION OF FENTANYL FOLLOWING IV AND EPIDURAL ADMINISTRATION TO PARTURIENT WOMEN

The development and verification of the mf-PBPK model of fentanyl demonstrated that the maternal-fetal disposition of xenobiotics can be reliably predicted *in silico* using PBPK modeling built using a hybrid middle-out approach. Importantly, the predicted maternal (MV and MA) and fetal (UV and UA) plasma concentration-time profiles of fentanyl using the mf-PBPK model illustrated that the F/M plasma concentration ratio of fentanyl is dependent on the maternal, fetal, and transplacental distribution kinetics. Depending on the sampling site and sampling time, a single sample of the umbilical cord plasma at birth could lead to over-estimation or under-estimation of fetal exposure. The simulations using the mf-PBPK model demonstrated that the transplacental and fetal distribution of fentanyl is relatively slow. Also, the simulations showed that both the mother and the fetus are exposed to significantly higher C_{max} following an IV bolus dose compared to that following an epidural bolus dose which may increase the risks of undesirable fentanyl effects for both the mother and the fetus. In contrast, the C_{max} following IV and epidural infusion are similar.

Future mf-PBPK model development should focus on verification of the physiology in pregnant women and fetus as PBPK modeling has been increasingly used to predict maternal-fetal disposition of xenobiotics. Ideally, a mf-PBPK model would be built ‘bottom-up’ based on

the known physiology of pregnant women and the fetus, and the ADME properties of the xenobiotics of interest. However, the incomplete knowledge of the physiology of pregnant women and fetus limits the possibilities to build a mf-PBPK model using the 'bottom-up' approach. Therefore, improvement of knowledge in this area is critical to the future development of mf-PBPK models. Moreover, pregnancy is a dynamic process, and the temporal physiological changes will have a gestational-age-dependent impact on maternal-fetal disposition. Future research should focus on characterization of the time course of these physiological changes (e.g. time course of CYP enzyme induction or downregulation, ontogeny of drug metabolizing enzymes in the fetal liver) to allow prediction of maternal-fetal disposition at different gestational age.

6.4 CONCLUSION

In conclusion, the maternal-fetal disposition of DA, oxycodone, and fentanyl was quantitatively studied using *in vivo* preclinical study, *in vitro* FLM incubations, and *in silico* PBPK modeling. These studies demonstrated that maternal-fetal disposition can be studied using nonclinical methodologies which yield information that is otherwise difficult to obtain through clinical studies. The knowledge from this dissertation can be used to inform future regulatory and clinical decisions in protecting pregnant women, a vulnerable population. And the framework established in this dissertation to study maternal-fetal disposition using these methodologies can be applied to other xenobiotics in the future.

BIBLIOGRAPHY

1. Mellin, G. W. & Katzenstein, M. The saga of thalidomide (concluded) Neuropathy to embryopathy with case reports of congenital anomalies. *New Engl. J. Med.* **267**, 1238–1244 (1962).
2. Vargesson, N. Thalidomide-induced teratogenesis: History and mechanisms. *Birth Defects Res. Part C - Embryo Today Rev.* **105**, 140–156 (2015).
3. Hill, L. M. & Kleinberg, F. Effects of drugs and chemicals on the fetus and newborn (second of two parts). *Mayo Clin. Proc.* **59**, 755–765 (1984).
4. Briggs, G. G. Drug effects on the fetus and breast-fed infant. **45**, 6–21 (2002).
5. Thompson, B. L., Levitt, P. & Stanwood, G. D. Prenatal exposure to drugs: Effects on brain development and implications for policy and education. *Nat. Rev. Neurosci.* **10**, 303–312 (2009).
6. Gotlib, D., Ramaswamy, R., Kurlander, J. E., DeRiggi, A. & Riba, M. Valproic Acid in Women and Girls of Childbearing Age. *Curr. Psychiatry Rep.* **19**, 1–7 (2017).
7. Robert, E. & Guibaud, P. Maternal Valproic Acid and Congenital Neural Tube Defects. *Lancet* **320**, 937 (1982).
8. Cooper, W. O. *et al.* Major congenital malformations after first-trimester exposure to ACE inhibitors. *Obstet. Gynecol. Surv.* **354**, 2443–51 (2006).
9. Haas, D. M. *et al.* Prescription and Other Medication Use in Pregnancy. *Obstet. Gynecol.* **131**, 789–798 (2018).
10. Ornoy, A., Reece, E. A., Pavlinkova, G., Kappen, C. & Miller, R. K. Effect of maternal diabetes on the embryo, fetus, and children: Congenital anomalies, genetic and epigenetic changes and developmental outcomes. *Birth Defects Res. Part C - Embryo Today Rev.*

105, 53–72 (2015).

11. Tomson, T. *et al.* Valproate in the treatment of epilepsy in girls and women of childbearing potential. *Epilepsia* **56**, 1006–1019 (2015).
12. Razaz, N., Tomson, T., Wikström, A. K. & Cnattingius, S. Association between pregnancy and perinatal outcomes among Women with epilepsy. *JAMA Neurol.* **74**, 983–991 (2017).
13. Soma-Pillay, P., Nelson-Piercy, C., Tolppanen, H. & Mebazaa, A. Physiological changes in pregnancy. *Cardiovasc. J. Afr.* **27**, 89–94 (2016).
14. Hebert, M. F. Impact of pregnancy on pharmacokinetics of medications. *J. Popul. Ther. Clin. Pharmacol.* **20**, 350–357 (2013).
15. Lockitch, G. Clinical biochemistry of pregnancy. *Crit. Rev. Clin. Lab. Sci.* **34**, 67–139 (1997).
16. Hebert, M. F. *et al.* Effects of pregnancy on CYP3A and P-glycoprotein activities as measured by disposition of midazolam and digoxin: A University of Washington specialized center of research study. *Clin. Pharmacol. Ther.* **84**, 248–253 (2008).
17. Isoherranen, N. & Thummel, K. E. Special Section on Pregnancy — Commentary Drug Metabolism and Transport During Pregnancy : How Does Drug Disposition Change during Pregnancy and What Are the Mechanisms that Cause Such Changes ? 256–262 (2013).
18. Pariente, G. *et al.* Pregnancy-Associated Changes in Pharmacokinetics: A Systematic Review. *PLoS Med.* **13**, 1–36 (2016).
19. Liao, M. Z. *et al.* Effects of pregnancy on the pharmacokinetics of metformin. *Drug Metab. Dispos.* **48**, 264–271 (2020).

20. Högstedt, S., Lindberg, B. & Rane, A. Increased oral clearance of metoprolol in pregnancy. *Eur. J. Clin. Pharmacol.* **24**, 217–220 (1983).

21. Tracy, T. S., Venkataramanan, R., Glover, D. D. & Caritis, S. N. Temporal changes in drug metabolism (CYP1A2, CYP2D6 and CYP3A Activity) during pregnancy. *Am. J. Obstet. Gynecol.* **192**, 633–639 (2005).

22. Koerner, M., Yerby, M., Friel, P. & McCormick, K. Valproic acid disposition and protein binding in pregnancy. *Ther. Drug Monit.* 228–230 (1989).

23. Reisinger, T. L., Newman, M., Loring, D. W., Pennell, P. B. & Meador, K. J. Antiepileptic drug clearance and seizure frequency during pregnancy in women with epilepsy. *Epilepsy Behav.* **29**, 13–18 (2013).

24. Otake, Y., Kanazawa, H., Takahashi, H., Matsubara, S. & Sugimoto, H. Magnetic resonance imaging of the human placental cotyledon: Proposal of a novel cotyledon appearance score. *Eur. J. Obstet. Gynecol. Reprod. Biol.* **232**, 82–86 (2019).

25. Poulsen, M. S., Rytting, E., Mose, T. & Knudsen, L. E. Modeling placental transport: Correlation of in vitro BeWo cell permeability and ex vivo human placental perfusion. *Toxicol. Vitr.* **23**, 1380–1386 (2009).

26. Dickinson, R. G., Fowler, D. W. & Kluck, R. M. Maternaofetal transfer of phenytoin, p-hydroxy-phenytoin and p-hydroxy-phenytoin-glucuronide in the perfused human placenta. *Clin. Exp. Pharmacol. Physiol.* **16**, 789–97 (1989).

27. Han, L. W., Gao, C. & Mao, Q. An update on expression and function of P-gp/ABCB1 and BCRP/ABCG2 in the placenta and fetus. *Expert Opin. Drug Metab. Toxicol.* **14**, 817–829 (2018).

28. Cerveny, L. *et al.* Equilibrative nucleoside transporter 1 (ENT1, SLC29A1) facilitates

transfer of the antiretroviral drug abacavir across the placenta. *Drug Metab. Dispos.* **46**, 1817–1826 (2018).

29. Cygalova, L. H., Hofman, J., Ceckova, M. & Staud, F. Transplacental pharmacokinetics of glyburide, rhodamine 123, and BODIPY FL prazosin: Effect of drug efflux transporters and lipid solubility. *J. Pharmacol. Exp. Ther.* **331**, 1118–1125 (2009).

30. Lee, N. *et al.* Organic cation Transporter 3 facilitates fetal exposure to metformin during pregnancy. *Mol. Pharmacol.* **94**, 1125–1131 (2018).

31. Zhang, Y., Wang, H., Unadkat, J. D. & Mao, Q. Breast cancer resistance protein 1 limits fetal distribution of nitrofurantoin in the pregnant mouse. *Drug Metab. Dispos.* **35**, 2154–2158 (2007).

32. Ellfolk, M. *et al.* Placental transporter-mediated drug interactions and offspring congenital anomalies. *Br. J. Clin. Pharmacol.* **86**, 868–879 (2020).

33. Kiserud, T. Fetal venous circulation - An update on hemodynamics. *J. Perinat. Med.* **28**, 90–96 (2000).

34. Kiserud, T. & Acharya, G. The fetal circulation. *Prenat. Diagn.* **24**, 1049–1059 (2004).

35. Murayama, K. *et al.* Significant correlations between the flow volume of patent ductus venosus and early neonatal liver function: Possible involvement of patent ductus venosus in postnatal liver function. *Arch. Dis. Child. Fetal Neonatal Ed.* **91**, 175–179 (2006).

36. Hakkola, J. *et al.* Expression of xenobiotic-metabolizing cytochrome P450 forms in human adult and fetal liver. *Biochem. Pharmacol.* **48**, 59–64 (1994).

37. Hines, R. N. The ontogeny of drug metabolism enzymes and implications for adverse drug events. *Pharmacol. Ther.* **118**, 250–267 (2008).

38. Stevens, J. C. *et al.* Developmental Expression of the Major Human Hepatic CYP3A

Enzymes. **307**, 573–582 (2003).

39. Court, M. H. *et al.* Quantitative distribution of mRNAs encoding the 19 human UDP-glucuronosyltransferase enzymes in 26 adult and 3 fetal tissues. *Xenobiotica* **42**, 266–277 (2012).

40. Saint-Faust, M., Boubred, F. & Simeoni, U. Renal development and neonatal adaptation. *Am. J. Perinatol.* **31**, 773–780 (2014).

41. Veille, J., Hanson, R. A., Tatrum, K. & Kelley, K. Quantitative assessment of human fetal renal blood flow. *Am. J. Obstet. Gynecol.* **169**, 1399–1402 (1993).

42. Arant, B. S. Developmental patterns of renal functional maturation compared in the human neonate. *J. Pediatr.* **92**, 705–712 (1978).

43. Brace, R. A., Cheung, C. Y. & Anderson, D. F. Regulation of amniotic fluid volume: insights derived from amniotic fluid volume function curves. *Am. J. Physiol. Regul. Integr. Comp. Physiol.* **315**, R777–R789 (2018).

44. Reynolds, F. & Knott, C. *Pharmacokinetics in pregnancy and placental drug transfer*. (1989).

45. Bennetto-Hood, C. *et al.* Zidovudine, lamivudine, and nelfinavir concentrations in amniotic fluid and maternal serum. *HIV Clin. Trials* **10**, 41–47 (2009).

46. Domínguez, V., Ramos, N., Torrents, A., García, D. & Carné, X. Clinical trials during pregnancy: What has been done. *Eur. J. Clin. Pharmacol.* **68**, 455–458 (2012).

47. Emanuela Voinescu, P. *et al.* Antiepileptic drug clearances during pregnancy and clinical implications for women with epilepsy. *Neurology* **91**, E1228–E1236 (2018).

48. Bouazza, N. *et al.* Methodological Approaches to Evaluate Fetal Drug Exposure. *Curr. Pharm. Des.* **25**, 496–504 (2019).

49. Garland, M., Abildskov, K. M., Kiu, T. W., Daniel, S. S. & Stark, R. I. The contribution of fetal metabolism to the disposition of morphine. *Drug Metab. Dispos.* **33**, 68–76 (2005).

50. Georgiades, P., Fergyson-Smith, A. C. & Burton, G. J. Comparative developmental anatomy of the murine and human definitive placentae. *Placenta* **23**, 3–19 (2002).

51. Garland, M. *et al.* Fetal morphine metabolism and clearance are constant during late gestation. *Drug Metab. Dispos.* **34**, 636–646 (2006).

52. Ladona, M., Lindstrom, B., Thyr, C., Dun-Ren, P. & Rane, A. Differential foetal development of the O- and N-demethylation of codeine and dextromethorphan in man. *Br. J. Clin. Pharmacol.* **32**, 295–302 (1991).

53. Treluyer, J.-M., Jacqz-Aigrain, E., Alvarez, F. & Cresteil, T. Expression of CYP2D6 in developing human liver. *Eur. J. Biochem.* **202**, 583–588 (1991).

54. Ladona, M. G., Spalding, D. J. M., Ekman, L., Lindström, B. & Rane, A. Human fetal and adult liver metabolism of ethylmorphine. *Biochem. Pharmacol.* **38**, 3147–3155 (1989).

55. Pacifici, G. M., Säwe, J., Kager, L. & Rane, A. Morphine glucuronidation in human fetal and adult liver. *Eur. J. Clin. Pharmacol.* **22**, 553–558 (1982).

56. Shuster, D. L. *et al.* Identification of CYP3A7 for glyburide metabolism in human fetal livers. *Biochem. Pharmacol.* **92**, 690–700 (2014).

57. Topletz, A. R., Zhong, G. & Isoherranen, N. Scaling in vitro activity of CYP3A7 suggests human fetal livers do not clear retinoic acid entering from maternal circulation. *Sci. Rep.* **9**, 1–11 (2019).

58. Li, H. & Lampe, J. N. Neonatal cytochrome P450 CYP3A7: A comprehensive review of its role in development, disease, and xenobiotic metabolism. *Arch. Biochem. Biophys.* **673**,

108078 (2019).

59. Klees, T. M., Sheffels, P., Dale, O. & Kharasch, E. D. Metabolism of alfentanil by CYP3A enzymes. *Drug Metab. Dispos.* **33**, 303–311 (2005).

60. Wilkinson, G. R. & Shand, D. G. A physiological approach to hepatic drug clearance. *Clin. Pharmacol. Ther.* **18**, 377–390 (1975).

61. Leeder, J. S. *et al.* Variability of CYP3A7 Expression in Human Fetal Liver. **314**, 626–635 (2005).

62. Proctor, N. J., Tucker, G. T. & Rostami-Hodjegan, A. Predicting drug clearance from recombinantly expressed CYPs: Intersystem extrapolation factors. *Xenobiotica* **34**, 151–178 (2004).

63. Kuepfer, L. *et al.* Applied Concepts in PBPK Modeling: How to Build a PBPK/PD Model. *CPT Pharmacometrics Syst. Pharmacol.* **5**, 516–531 (2016).

64. Brown, R. P., Delp, M. D., Lindstedt, S. L., Rhomberg, L. R. & Beliles, R. P. Physiological parameter values for physiologically based pharmacokinetic models. *Toxicol. Ind. Health* **13**, 407–483 (1997).

65. Huang, W. & Isoherranen, N. Development of a Dynamic Physiologically Based Mechanistic Kidney Model to Predict Renal Clearance. *CPT Pharmacometrics Syst. Pharmacol.* **7**, 593–602 (2018).

66. Rostami-Hodjegan, A. Reverse Translation in PBPK and QSP: Going Backwards in Order to Go Forward With Confidence. *Clin. Pharmacol. Ther.* **103**, 224–232 (2018).

67. Jones, H. M. *et al.* Physiologically based pharmacokinetic modeling in drug discovery and development: A pharmaceutical industry perspective. *Clin. Pharmacol. Ther.* **97**, 247–262 (2015).

68. Sager, J. E., Yu, J., Ragueneau-Majlessi, I. & Isoherranen, N. Physiologically based pharmacokinetic (PBPK) modeling and simulation approaches: A systematic review of published models, applications, and model verification. *Drug Metab. Dispos.* **43**, 1823–1837 (2015).

69. Barrett, J. S., Della Casa Alberighi, O., Läer, S. & Meibohm, B. Physiologically Based Pharmacokinetic (PBPK) modeling in children. *Clin. Pharmacol. Ther.* **92**, 40–49 (2012).

70. Kostewicz, E. S. *et al.* PBPK models for the prediction of in vivo performance of oral dosage forms. *Eur. J. Pharm. Sci.* **57**, 300–321 (2014).

71. Varma, M. V. S. *et al.* Physiologically based modeling of pravastatin transporter-Mediated hepatobiliary disposition and Drug-Drug interactions. *Pharm. Res.* **29**, 2860–2873 (2012).

72. Corley, R. A., Mast, T. J., Carney, E. W., Rogers, J. M. & Daston, G. P. Evaluation of physiologically based models of pregnancy and lactation for their application in children's health risk assessments. *Crit. Rev. Toxicol.* **33**, 137–211 (2003).

73. Abduljalil, K., Furness, P., Johnson, T. N., Rostami-hodjegan, A. & Soltani, H. Anatomical , Physiological and Metabolic Changes with Gestational Age during Normal Pregnancy. *Clin. Pharmacokinet.* **51**, 365–396 (2012).

74. Gaohua, L., Abduljalil, K., Jamei, M., Johnson, T. N. & Rostami-hodjegan, A. A pregnancy physiologically based pharmacokinetic (p-PBPK) model for disposition of drugs metabolized by CYP1A2 ,. (2012). doi:10.1111/j.1365-2125.2012.04363.x

75. Ke, A. B. *et al.* A physiologically based pharmacokinetic model to predict disposition of CYP2D6 and CYP1A2 metabolized drugs in pregnant women. *Drug Metab. Dispos.* **41**, 801–813 (2013).

76. Ke, A. B., Nallani, S. C., Zhao, P., Rostami-Hodjegan, A. & Unadkat, J. D. Expansion of a PBPK model to predict disposition in pregnant women of drugs cleared via multiple CYP enzymes, including CYP2B6, CYP2C9 and CYP2C19. *Br. J. Clin. Pharmacol.* **77**, 554–570 (2013).

77. Zhang, Z. *et al.* Development of a novel maternal-fetal physiologically based pharmacokinetic model I: Insights into factors that determine fetal drug exposure through simulations and sensitivity analyses. *Drug Metab. Dispos.* **45**, 920–938 (2017).

78. Abduljalil, K., Jamei, M. & Johnson, T. N. Fetal Physiologically Based Pharmacokinetic Models: Systems Information on the Growth and Composition of Fetal Organs. *Clin. Pharmacokinet.* **58**, 235–262 (2019).

79. Zhang, Z. & Unadkat, J. D. Verification of a Maternal-Fetal Physiologically Based Pharmacokinetic Model for Passive Placental Permeability Drugs. *Drug Metab. Dispos.* 939–946 (2017).

80. Stiles, J. & Jernigan, T. L. The basics of brain development. *Neuropsychol. Rev.* **20**, 327–348 (2010).

81. Schlotz, W. & Phillips, D. I. W. Fetal origins of mental health: Evidence and mechanisms. *Brain. Behav. Immun.* **23**, 905–916 (2009).

82. Ross, E. J., Graham, D. L., Money, K. M. & Stanwood, G. D. Developmental consequences of fetal exposure to drugs: What we know and what we still must learn. *Neuropsychopharmacology* **40**, 61–87 (2015).

83. Hunt, R. W., Tzioumi, D., Collins, E. & Jeffery, H. E. Adverse neurodevelopmental outcome of infants exposed to opiate in-utero. *Early Hum. Dev.* **84**, 29–35 (2008).

84. Bunikowski, R. *et al.* Neurodevelopmental outcome after prenatal exposure to opiates.

Eur. J. Pediatr. **157**, 724–730 (1998).

85. Castoldi, A. F., Coccini, T., Ceccatelli, S. & Manzo, L. Neurotoxicity and molecular effects of methylmercury. **55**, 197–203 (2001).

86. Vrijheid, M., Casas, M., Gascon, M., Valvi, D. & Nieuwenhuijsen, M. Environmental pollutants and child health — A review of recent concerns. *Int. J. Hyg. Environ. Health* **219**, 331–342 (2016).

87. Lefebvre, K. A. & Robertson, A. Domoic acid and human exposure risks: A review. *Toxicon* **56**, 218–230 (2010).

88. Hampson, D. R., Huang, X., Wells, J. W., Walter, J. A. & Wright, J. L. C. Interaction of domoic acid and several derivatives with kainic acid and AMPA binding sites in rat brain. **218**, 1–8 (1992).

89. Novelli, A., Kispert, J., Fernandez-Sanchez, M. T., Torreblanca, A. & Zitko, V. Domoic acid-containing toxic mussels produce neurotoxicity in neuronal cultures through a synergism between excitatory amino acids. **577**, 41–48 (1992).

90. Todd, E. C. D. Domoic acid and amnesic shellfish poisoning - a review. *J. Food Prot.* **56**, 69–83 (1993).

91. Scholin, C. A. *et al.* Mortality of sea lions along the central California coast linked to a toxic diatom bloom. *Nature* **403**, 80–84 (2000).

92. Madl, J. E., Duncan, C. G., Stanhill, J. E., Tai, P. & Spraker, T. R. ScienceDirect Oxidative Stress and Redistribution of Glutamine Synthetase in California Sea Lions (Zalophus californianus) with Domoic Acid Toxicosis. *J. Comp. Pathol.* **150**, 306–315 (2014).

93. Lefebvre, K. A. *et al.* Chronic low-level exposure to the common seafood toxin domoic

acid causes cognitive deficits in mice. *Harmful Algae* **64**, 20–29 (2017).

94. Cook, P. F., Berns, G. S., Colegrove, K., Johnson, S. & Gulland, F. Postmortem DTI reveals altered hippocampal connectivity in wild sea lions diagnosed with chronic toxicosis from algal exposure. *J. Comp. Neurol.* **526**, 216–228 (2018).

95. Grattan, L. M. *et al.* Repeated Dietary Exposure to Low Levels of Domoic Acid and Problems with Everyday Memory : Research to Public Health Outreach. *Toxins (Basel).* **10**, 1–10 (2018).

96. Dakshinamurti, K., Sharma, S. K. & Watanabe, T. Hippocampal Changes in Developing Postnatal Intrauterine Exposure to Domoic Acid Mice following. **13**, (1993).

97. Zuloaga, D. G. *et al.* Fetal domoic acid exposure affects lateral amygdala neurons, diminishes social investigation and alters sensory-motor gating. *Neurotoxicology* **53**, 132–140 (2016).

98. Shiotani, M. *et al.* Neurobehavioral assessment of mice following repeated oral exposures to domoic acid during prenatal development. *Neurotoxicol. Teratol.* **64**, 8–19 (2017).

99. Levin, E. D., Pizarro, K., Pang, W. G., Harrison, J. & Ramsdell, J. S. Persisting behavioral consequences of prenatal domoic acid exposure in rats. *Neurotoxicol. Teratol.* **27**, 719–725 (2005).

100. Grant, K. S. *et al.* Preclinical modeling of exposure to a global marine bio-contaminant: Effects of in utero Domoic acid exposure on neonatal behavior and infant memory. *Neurotoxicol. Teratol.* **73**, 1–8 (2019).

101. Walter, J. A., Leek, D. M. & Falk, M. NMR study of the protonation of domoic acid. *Can. J. Chem.* **70**, 1156–1161 (1992).

102. Truelove, J., Iverson, F. Serum domoic acid clearance and clinical observations in the

cynomolgus monkey and sprague-dawley rat following a single IV dose. *Entironmental Contam. Toxicol.* **52**, 479–486 (1994).

103. Jing, J. *et al.* Toxicokinetics and physiologically based pharmacokinetic modeling of the shellfish toxin domoic acid in nonhuman primates. *Drug Metab. Dispos.* **46**, 155–165 (2018).

104. Lefebvre, K. A. *et al.* Domoic acid in California sea lion fetal fluids indicates continuous exposure to a neuroteratogen poses risks to mammals. *Harmful Algae* 0–1 (2018). doi:10.1016/j.hal.2018.06.003

105. Price, H. R. & Collier, A. C. Analgesics in Pregnancy: An Update on Use, Safety and Pharmacokinetic Changes in Drug Disposition. *Curr. Pharm. Des.* **23**, 6098–6114 (2017).

106. Epstein, R. A. *et al.* Incrasing pregnancy-related use of prescribed opioid analgesics. **23**, 498–503 (2013).

107. Black, E. *et al.* Medication Use and Pain Management in Pregnancy: A Critical Review. *Pain Pract.* **19**, 875–899 (2019).

108. Kokki, M. *et al.* Intravenous Oxycodone for Pain Relief in the First Stage of Labour - Maternal Pharmacokinetics and Neonatal Exposure. *Basic Clin. Pharmacol. Toxicol.* **111**, 182–188 (2012).

109. Kinnunen, M., Kokki, H., Hautajärvi, H., Tuovinen, K. & Kokki, M. Oxycodone for pain management in the latent phase of labour – A pragmatic trial. *Acta Anaesthesiol. Scand.* **64**, 685–690 (2020).

110. Lalovic, B. *et al.* Pharmacokinetics and pharmacodynamics of oral oxycodone in healthy human subjects: Role of circulating active metabolites. *Clin. Pharmacol. Ther.* **79**, 461–479 (2006).

111. Lalovic, B., Phillips, B., Risler, L. L., Howald, W. & Shen, D. D. Quantitative contribution of CYP2D6 and CYP3A to oxycodone metabolism in human liver and intestinal microsomes. **32**, 447–454 (2004).

112. Williams, J. A. *et al.* Comparative metabolic capabilities of CYP3A4, CYP3A5, and CYP3A7. *Drug Metab. Dispos.* **30**, 883–891 (2002).

113. Vella, L. M. *et al.* Epidural fentanyl in labour. *Anaesthesia* **40**, 741–747 (1985).

114. Fleet, J., Jones, M. & Belan, I. Non-axial administration of fentanyl in childbirth: A review of the efficacy and safety of fentanyl for mother and neonate. *Midwifery* **27**, e106–e113 (2011).

115. Kesavan, R., Rajan, S. & Kumar, L. Effect and safety of labor epidural analgesia with intermittent boluses of 0.1% bupivacaine with fentanyl on fetal and maternal outcomes and wellbeing. *Anesth. Essays Res.* **12**, 349–354 (2018).

116. Haidl, F., Rosseland, L. A., Spigset, O. & Dahl, V. Effects of Adrenaline on maternal and fetal fentanyl absorption in epidural analgesia: A randomized trial. *Acta Anaesthesiol. Scand.* **62**, 1267–1273 (2018).

117. Bader, A. M. *et al.* Maternal and neonatal fentanyl and bupivacaine concentrations after epidural infusion during labor. *Anesth. Analg.* **81**, 829–832 (1995).

118. Rodgers, T. & Rowland, M. Mechanistic approaches to volume of distribution predictions: Understanding the processes. *Pharm. Res.* **24**, 918–933 (2007).

119. Ziesenitz, V. C. *et al.* Pharmacokinetic interaction of intravenous fentanyl with ketoconazole. *J. Clin. Pharmacol.* **55**, 708–717 (2015).

120. Perl, M. Trish, Bedard, Lucie, Kosatsky, Tom, Hockin, C. James, Todd, C.D. Ewen, Remis, S. R. An outbreak of toxic encephalopathy caused by eating mussels contaminated

with domoic acid. *N. Engl. J. Med.* **322**, 1775–1780 (1990).

121. He, Y. *et al.* Analytical approaches for an important shellfish poisoning agent: Domoic acid. *J. Agric. Food Chem.* **58**, 11525–11533 (2010).

122. Frame, E. & LeFebvre, K. *ELISA Methods for Domoic Acid Quantification in Multiple Marine Mammal Species and Sample Matrices. U.S. Dept. Commer., NOAA Tech. Memo. NMFS-NWFSC-122, 20 p.* (2013).

123. Wang, Z. *et al.* Optimization of solid-phase extraction and liquid chromatography-tandem mass spectrometry for the determination of domoic acid in seawater, phytoplankton, and mammalian fluids and tissues. *Anal. Chim. Acta* **715**, 71–79 (2012).

124. Barbaro, E. *et al.* Domoic acid at trace levels in lagoon waters: assessment of a method using internal standard quantification. *Anal. Bioanal. Chem.* **405**, 9113–9123 (2013).

125. Zendong, Z. *et al.* High resolution mass spectrometry for quantitative analysis and untargeted screening of algal toxins in mussels and passive samplers. *J. Chromatogr. A* **1416**, 10–21 (2015).

126. Barbaro, E., Zangrando, R., Barbante, C. & Gambaro, A. Fast and Sensitive Method for Determination of Domoic Acid in Mussel Tissue. *Sci. World J.* **2016**, 1–6 (2016).

127. Zhang, W., Lin, M., Tong, P., Lu, Q. & Zhang, L. Ferrite nanospheres-based magnetic solid-phase extraction for determination of domoic acid in seawater samples using high-performance liquid chromatography with tandem mass spectrometry. *J. Chromatogr. A* **1443**, 54–61 (2016).

128. Greer, B. *et al.* A validated UPLC-MS/MS method for the surveillance of ten aquatic biotoxins in European brackish and freshwater systems. *Harmful Algae* **55**, 31–40 (2016).

129. Rodriguez, I. *et al.* Monitoring of freshwater toxins in European environmental waters by

using novel multi-detection methods. *Environ. Toxicol. Chem.* **36**, 645–654 (2017).

130. Zervou, S. K., Christophoridis, C., Kaloudis, T., Triantis, T. M. & Hiskia, A. New SPE-LC-MS/MS method for simultaneous determination of multi-class cyanobacterial and algal toxins. *J. Hazard. Mater.* **323**, 56–66 (2017).

131. Riccardi, C. *et al.* Liquid Chromatography–Tandem Mass Spectrometry Method for the Screening of Eight Paralytic Shellfish Poisoning Toxins, Domoic Acid, 13-Desmethyl Spirolide C, Palytoxin and Okadaic Acid in Seawater. *Chromatographia* **81**, 277–288 (2018).

132. Beach, D. G. *et al.* Laser ablation electrospray ionization high-resolution mass spectrometry for regulatory screening of domoic acid in shellfish. *Rapid Commun. Mass Spectrom.* 2379–2387 (2016). doi:10.1002/rcm.7725

133. Ferriss, B. E., Marcinek, D. J., Ayres, D., Borchert, J. & Lefebvre, K. A. Acute and chronic dietary exposure to domoic acid in recreational harvesters: A survey of shellfish consumption behavior. *Environ. Int.* **101**, 70–79 (2017).

134. Grattan, L. M. *et al.* The association between razor clam consumption and memory in the CoASTAL cohort. *Harmful Algae* **57**, 20–25 (2016).

135. Goldstein, T. *et al.* Novel symptomatology and changing epidemiology of domoic acid toxicosis in California sea lions (Zalophus californianus): an increasing risk to marine mammal health. *Proc. R. Soc. B Biol. Sci.* **275**, 267–276 (2008).

136. Mariën, K. Establishing tolerable dungeness crab (Cancer magister) and razor clam (Siliqua patula) domoic acid contaminant levels. *Environ. Health Perspect.* **104**, 1230–1236 (1996).

137. Tryphonas, L., Truelove, J., Todd, E. C. D., Nera, E. & Iverson, F. Experimental oral

toxicity of domoic acid in cynomolgus monkeys (Macaca fascicularis) and rats. *Food Chem. Toxicol.* **28**, 707–715 (1990).

138. Truelove, J. *et al.* 30-day oral toxicity study of domoic acid in cynomolgus monkeys: Lack of overt toxicity at doses approaching the acute toxic dose. *Nat. Toxins* **5**, 111–114 (1997).

139. Toyofuku, H. Joint FAO/WHO/IOC activities to provide scientific advice on marine biotoxins (research report). *Mar. Pollut. Bull.* **52**, 1735–1745 (2006).

140. Tor, E. R., Puschner, B. & Whitehead, W. E. Rapid determination of domoic acid in serum and urine by liquid chromatography-electrospray tandem mass spectrometry. *J. Agric. Food Chem.* **51**, 1791–1796 (2003).

141. Hesp, B. R., Harrison, J. C., Selwood, A. I., Holland, P. T. & Kerr, D. S. Detection of domoic acid in rat serum and brain by direct competitive enzyme-linked immunosorbent assay (cELISA). *Anal. Bioanal. Chem.* **383**, 783–786 (2005).

142. Seubert, E. L. *et al.* Development, comparison, and validation using ELISAs for the determination of domoic acid in California sea lion body fluids. *J. AOAC Int.* **97**, 345–355 (2014).

143. Zhang, Y., Chen, D. & Hong, Z. A rapid LC-HRMS method for the determination of domoic acid in urine using a self-assembly pipette tip solid-phase extraction. *Toxins (Basel).* **8**, 1–13 (2015).

144. Beach, D. G., Hollingdale, C. & Quilliam, M. A. Isotope-labelling derivatisation: A broadly applicable approach to quantitation of algal toxins by isotope dilution LC-MS/MS. *Anal. Methods* **8**, 2872–2879 (2016).

145. Lawrence, J. F., Lau, B. P., Cleroux, C. & Lewis, D. Comparison of UV absorption and

electrospray mass spectrometry for the high-performance liquid chromatographic determination of domoic acid in shellfish and biological samples. *J. Chromatogr. A* **659**, 119–26 (1994).

146. Walter, J. A., Falk, M. & Wright, J. L. C. Chemistry of the shellfish toxin domoic acid: characterization of related compounds. *Can. J. Chem.* **72**, 430–436 (1994).

147. Justice, N. I. of. Color Test Reagents/Kits for Preliminary Identification of Drugs of Abuse. *NIJ Stand.* 19 (2000).

148. Cullis, C. F. & Waddington, D. J. The colorimetric determination of secondary amines. *Anal. Chim. Acta* **5**, 158–163 (1956).

149. Validation, B. M. Guidance for Industry Bioanalytical Method Validation Guidance for Industry Bioanalytical Method Validation. *Fda* 1–22 (2018).

150. Thibault, P., Quilliam, M.A., Jamieson, W.D., Boyd, R. K. Mass Spectrometry of Domoic Acid, a Marine Neurotoxin. *Biomed. Environ. Mass Spectrom.* **18**, 373–386 (1989).

151. Furey, A. *et al.* Determination of domoic acid in shellfish by liquid chromatography with electrospray ionization and multiple tandem mass spectrometry. *J. Chromatogr. A* **938**, 167–174 (2001).

152. Berman, F. W., Lepage, K. T. & Murray, T. F. Domoic acid neurotoxicity in cultured cerebellar granule neurons is controlled preferentially by the NMDA receptor Ca 2 1 influx pathway. **924**, 20–29 (2002).

153. Bates, S. S. *et al.* Pseudo-nitzschia , Nitzschia , and domoic acid : New research since 2011. *Harmful Algae* **79**, 3–43 (2018).

154. Wekell, J. C., Lefebvre, K. A. & Hurst, J. The origin of the regulatory limits for PSP and ASP toxins in shellfish. *J. Shellfish Res.* **23**, 927–930 (2004).

155. Lefebvre, K. A. *et al.* Discovery of a Potential Human Serum Biomarker. *Toxins (Basel).* **11**, (2019).

156. Moyer, C. E., Hiolski, E. M., Marcinek, D. J., Lefebvre, K. A. & Smith, D. R. Repeated low level domoic acid exposure increases CA1 VGluT1 levels , but not bouton density , VGluT2 or VGAT levels in the hippocampus of adult mice. *Harmful Algae* **79**, 74–86 (2018).

157. Hiolski, E. M. transcription and impairs mitochondrial function in the CNS. 151–159 (2014). doi:10.1016/j.aquatox.2014.06.006.Chronic

158. Lefebvre, K. A. *et al.* A Novel Antibody-Based Biomarker for Chronic Algal Toxin Exposure and Sub-Acute Neurotoxicity. **7**, 1–7 (2012).

159. Cook, P. F. *et al.* Algal toxin impairs sea lion memory and hippocampal connectivity, with implications for strandings. **350**, 2013–2016 (2015).

160. Costa, L. G., Giordano, G. & Faustman, E. M. Domoic acid as a developmental neurotoxin. *Neurotoxicology* **31**, 409–423 (2010).

161. Tanemura, K. *et al.* Intrauterine environment-genome interaction and Children ' s development (2): Brain structure impairment and behavioral disturbance induced in male mice offspring by a single intraperitoneal administration of domoic acid (DA) to their dams. (2009).

162. Brodie, E. C., Gulland, F. M. D. & Greig, D. J. DOMOIC ACID CAUSES REPRODUCTIVE FAILURE IN CALIFORNIA SEA LIONS (ZALOPHUS CALIFORNIANUS). **22**, 700–707 (2006).

163. Simeone, C. *et al.* Clinical signs and mortality of non- released stranded California sea lions housed in display facilities : the suspected role of prior exposure to algal toxins.

(2019).

164. Walker, B. Pediatric environmental health. *J. Natl. Med. Assoc.* **97**, 262–269 (2005).

165. Burbacher, T. M. *et al.* Effects of oral domoic acid exposure on maternal reproduction and infant birth characteristics in a preclinical nonhuman primate model. *Neurotoxicol. Teratol.* #pagerange# (2019). doi:10.1016/J.NTT.2019.01.001

166. Petroff, R. *et al.* Neurotoxicology Chronic , low-level oral exposure to marine toxin , domoic acid , alters whole brain morphometry in nonhuman primates. *Neurotoxicology* 1–11 (2019). doi:10.1016/j.neuro.2019.02.016

167. Grant, K. S. *et al.* Neurotoxicology and Teratology Preclinical modeling of exposure to a global marine bio-contaminant : Effects of in utero Domoic acid exposure on neonatal behavior and infant memory. *Neurotoxicol. Teratol.* **73**, 1–8 (2019).

168. Maucher, J. M. & Ramsdell, J. S. Maternal-fetal transfer of domoic acid in rats at two gestational time points. *Environ. Health Perspect.* **115**, 1743–1746 (2007).

169. Maucher Fuquay, J., Muha, N., Wang, Z. & Ramsdell, J. S. Toxicokinetics of domoic acid in the fetal rat. *Toxicology* **294**, 36–41 (2012).

170. Shum, S. *et al.* Validated HPLC-MS/MS Method To Quantify Low Levels of Domoic Acid in Plasma and Urine after Subacute Exposure. (2018). doi:10.1021/acsomega.8b02115

171. Kimura, O., Kotaki, Y., Hamaue, N., Haraguchi, K. & Endo, T. Transcellular transport of domoic acid across intestinal Caco-2 cell monolayers. *Food Chem. Toxicol.* **49**, 2167–2171 (2011).

172. Teasdale, F. & Jean-Jacques, G. Morphometry of the Microvillous Membrane of the H u m a n Placenta in Maternal Diabetes Mellitus. 81–88 (1986).

173. Fujiwara, T., Suzaki, Y. & Honjo, S. Weight and size of the placenta in cynomolgus monkeys (Macaca Fascicularis). (1978).

174. Guignard, J. P., Torrado, A., Cunha, O. Da & Gautier, E. Glomerular filtration rate in the first three weeks of life. *J. Pediatr.* **87**, 268–272 (1975).

175. WILSON, C., SARKAR, P., MAZUMDAR, J. & BHARADHWAJ, B. Study of Glomerular Functions in Neonates. *Med. J. Armed Forces India* **55**, 183–186 (1999).

176. Otukesh, H., Hoseini, R., Rahimzadeh, N. & Hosseini, S. Glomerular function in neonates. *Iran. J. Kidney Dis.* **6**, 166–172 (2012).

177. Jansen, R. S., Mahakena, S., De Haas, M., Borst, P. & Van De Wetering, K. ATP-binding cassette subfamily C member 5 (ABCC5) functions as an efflux transporter of glutamate conjugates and analogs. *J. Biol. Chem.* **290**, 30429–30440 (2015).

178. Meyer Zu Schwabedissen, H. E. U. *et al.* Expression, localization, and function of MRP5 (ABCC5), a transporter for cyclic nucleotides, in human placenta and cultured human trophoblasts: Effects of gestational age and cellular differentiation. *Am. J. Pathol.* **166**, 39–48 (2005).

179. Ni, Z. & Mao, Q. ATP-Binding Cassette Efflux Transporters in Human Placenta. *Curr. Pharm. Biotechnol.* **12**, 674–685 (2011).

180. Patrick, S. W. *et al.* Prescription Opioid Epidemic and Infant Outcomes. *Pediatrics* **135**, 842–850 (2015).

181. Martins, F., Oppolzer, D., Santos, C. & Barroso, M. Opioid Use in Pregnant Women and Neonatal Abstinence Syndrome — A Review of the Literature. 1–17 (2019). doi:10.3390/toxics7010009

182. Desai, Rishi J.; Hernandez-Diaz, Sonia; Bateman, Brain T.; Huybrechts, K. F. Increase in

Prescription Opioid Use During Pregnancy Among Medicaid-Enrolled Women. **123**, 997–1002 (2014).

183. Yazdy, M. M., Desai, R. J. & Brogly, S. B. Prescription Opioids in Pregnancy and Birth Outcomes: A Review of the Literature. *J. Pediatr. Genet.* **4**, 56–70 (2015).

184. Patrick, S. W. *et al.* Neonatal abstinence syndrome and associated health care expenditures: United States, 2000-2009. *JAMA - J. Am. Med. Assoc.* **307**, 1934–1940 (2012).

185. Conradt, E. *et al.* Prenatal opioid exposure: Neurodevelopmental consequences and future research priorities. *Pediatrics* **144**, (2019).

186. Jones, H. E., Jansson, L. M., Grady, K. E. O. & Kaltenbach, K. Neurotoxicology and Teratology The relationship between maternal methadone dose at delivery and neonatal outcome : Methodological and design considerations. *Neurotoxicol. Teratol.* **39**, 110–115 (2013).

187. Jones, H. E. *et al.* Neonatal outcomes and their relationship to maternal buprenorphine dose during pregnancy. *Drug Alcohol Depend.* **134**, 414–417 (2014).

188. Liao, M. Z. *et al.* P-gp/ABCB1 exerts differential impacts on brain and fetal exposure to norbuprenorphine. *Pharmacol. Res.* **119**, 61–71 (2017).

189. Stevens, J. C. New perspectives on the impact of cytochrome P450 3A expression for pediatric pharmacology. **11**, (2006).

190. Pearce, R. E., Vakkalagadda, G. R. & Steven Leeder, J. Pathways of carbamazepine bioactivation in vitro I. Characterization of human cytochromes P450 responsible for the formation of 2- and 3-hydroxylated metabolites. *Drug Metab. Dispos.* **30**, 1170–1179 (2002).

191. Peng, C. C. *et al.* Evaluation of 6B-hydroxycortisol, 6β-hydroxycortisone, and a combination of the two as endogenous probes for inhibition of CYP3A4 in vivo. *Clin. Pharmacol. Ther.* **89**, 888–895 (2011).

192. Zhang, Z. *et al.* Development of a novel maternal-fetal physiologically based pharmacokinetic model I: Insights into factors that determine fetal drug exposure through simulations and sensitivity analyses. *Drug Metab. Dispos.* **45**, 920–938 (2017).

193. Leow, K. P., Wright, A. W. E., Cramond, T. & Smith, M. T. Determination of the serum protein binding of oxycodone and morphine using ultrafiltration. *Ther drug monit* **15**, 440–447 (1993).

194. Chen, Y., Liu, L., Nguyen, K. & Fretland, A. J. Utility of intersystem extrapolation factors in early reaction phenotyping and the quantitative extrapolation of human liver microsomal intrinsic clearance using recombinant cytochromes P450. *Drug Metab. Dispos.* **39**, 373–382 (2011).

195. Kandel, S. E., Han, L. W., Mao, Q. & Lampe, J. N. Digging deeper into CYP3A testosterone metabolism: Kinetic, regioselectivity, and stereoselectivity differences between CYP3A4/5 and CYP3A7. *Drug Metab. Dispos.* **45**, 1266–1275 (2017).

196. Rane, A. & Sjoqvist, F. Drug metabolism in hte human fetus and newborn infant. *Nippon rinsho. Japanese J. Clin. Med.* **19**, 37–49 (1972).

197. Dutton, G. J. Glucuronide synthesis in foetal liver and other tissues. *Biochem. J.* **71**, 141–148 (1959).

198. Ring, J. A., Ghabrial, H., Ching, M. S., Smallwood, R. A. & Morgan, D. J. Fetal hepatic drug elimination. *Pharmacol. Ther.* **84**, 429–445 (1999).

199. Ekström, L., Johansson, M. & Rane, A. Tissue distribution and relative gene expression of

udp- glucuronosyltransferases (2B7, 2B15, 2B17) in the human fetus. *Drug Metab. Dispos.* **41**, 291–295 (2013).

200. Huang, W. *et al.* Evidence of significant contribution from CYP3A5 to hepatic drug metabolism. *Drug Metab. Dispos.* **32**, 1434–1445 (2004).

201. Arnold, S. L., Stevison, F. & Isoherranen, N. Impact of Sample Matrix on Accuracy of Peptide Quantification: Assessment of Calibrator and Internal Standard Selection and Method Validation. *Anal. Chem.* **88**, 746–753 (2016).

202. Godamudunage, M. P., Grech, A. M. & Scott, E. E. Comparison of antifungal azole interactions with adult cytochrome P450 3A4 versus neonatal cytochrome P450 3A7. *Drug Metab. Dispos.* **46**, 1329–1337 (2018).

203. Bonnardot, J. P., Maillet, M., Colau, J. C., Millot, F. & Deligne, P. Maternal and fetal concentration of morphine after intrathecal administration during labour. *Br. J. Anaesth.* **54**, 487–489 (1982).

204. Gerdin, E., Lindberg, B., Salmonson, T. & Rane, A. Maternal kinetics of morphine during labour. *J. Perinat. Med.* **18**, 479–487 (1990).

205. Fleet, J. A., Belan, I., Gordon, A. L. & Cyna, A. M. Fentanyl concentration in maternal and umbilical cord plasma following intranasal or subcutaneous administration in labour. *Int. J. Obstet. Anesth.* **42**, 34–38 (2020).

206. De Barros Duarte, L. *et al.* Distribution of fentanyl in the placental intervillous space and in the different maternal and fetal compartments in term pregnant women. *Eur. J. Clin. Pharmacol.* **65**, 803–808 (2009).

207. Gepts, E., Heytens, L. & Camu, F. Pharmacokinetics and placental transfer of intravenous and epidural alfentanil in parturient women. *Anesth. Analg.* **65**, 1155–1160 (1986).

208. Ellis, J., Millar, W. L. & Reisner, L. S. A randomized double-blind comparison of epidural versus intravenous fentanyl infusion for analgesia after cesarean section. *Anesthesiology* 981–986 (1990).

209. Baxter, A. D. *et al.* A comparison of lumbar epidural and intravenous fentanyl infusions for post-thoracotomy analgesia. *Can. J. Anaesth.* **41**, 184–191 (1994).

210. D'Angelo, R., Gerancher, J. C., Eisenach, J. C. & Raphael, B. L. Epidural fentanyl produces labor analgesia by a spinal mechanism. *Anesthesiology* 1519–23 (1998).

211. Cohen, S., Pantuck, C. B., Amar, D., Burley, E. & Pantuck, E. J. The primary action of epidural fentanyl after cesarean delivery is via a spinal mechanism. *Anesth. Analg.* **94**, 674–679 (2002).

212. Glass, P. S. A., Estok, P., Ginsberg, B., Goldberg, J. S. & Sladen, R. N. Use of patient-controlled analgesia to compare the efficacy of epidural to intravenous fentanyl administration. *Anesth. Analg.* **74**, 345–351 (1992).

213. Grangier, L., Martinez de Tejada, B., Savoldelli, G. L., Irion, O. & Haller, G. Adverse side effects and route of administration of opioids in combined spinal-epidural analgesia for labour: a meta-analysis of randomised trials. *Int. J. Obstet. Anesth.* **41**, 83–103 (2020).

214. Loftus, J. R., Hill, H. & Cohen, S. E. Placental transfer and neonatal effects of epidural sufentanil and fentanyl administered with bupivacaine during labor. *Anesthesiology* **83**, 300–308 (1995).

215. Poole, J. H. Analgesia and Anesthesia During Labor and Birth: Implications for Mother and Fetus. *J. Obstet. Gynecol. Neonatal Nurs.* **32**, 780–793 (2003).

216. Van De Velde, M. Neuraxial analgesia and fetal bradycardia. *Curr. Opin. Anaesthesiol.* **18**, 253–256 (2005).

217. Reynolds, F., Sharma, S. K. & Seed, P. T. Analgesia in labour and fetal acid-base balance: A meta-analysis comparing epidural with systemic opioid analgesia. *BJOG An Int. J. Obstet. Gynaecol.* **109**, 1344–1353 (2002).

218. Desprats, R. *et al.* Maternal and umbilical cord concentrations of fentanyl after epidural analgesia for cesarean section. *Eur. J. Obstet. Gynecol. Reprod. Biol.* **42**, 89–94 (1991).

219. Desprats, R. *et al.* Effect of adrenaline on plasma concentrations of fentanyl during epidural anaesthesia for caesarean section. *Int. J. Obstet. Anesth.* **4**, 225–229 (1995).

220. Moisés, E. C. D. *et al.* Pharmacokinetics and transplacental distribution of fentanyl in epidural anesthesia for normal pregnant women. *Eur. J. Clin. Pharmacol.* **61**, 517–522 (2005).

221. Morley-Forster, P. K., Reid, D. W. & Vandeberghe, H. A comparison of patient-controlled analgesia fentanyl and alfentanil for labour analgesia. *Can. J. Anaesth.* **47**, 113–119 (2000).

222. Stanley, T. H. The history and development of the fentanyl series. *J. Pain Symptom Manage.* **7**, 3–7 (1992).

223. McClain, D. A. & Hug, C. C. Intravenous fentanyl kinetics. *Clin. Pharmacol. Ther.* **28**, 106–114 (1980).

224. Nozari, A. *et al.* Prolonged therapy with the anticonvulsant carbamazepine leads to increased plasma clearance of fentanyl. *J. Pharm. Pharmacol.* **71**, 982–987 (2019).

225. Huang, W. & Isoherranen, N. Sampling site has a critical impact on physiologically based pharmacokinetic modelings. *J. Pharmacol. Exp. Ther.* **372**, 30–45 (2020).

226. Richardson, J. & Groen, G. J. Applied epidural anatomy. *Contin. Educ. Anaesthesia, Crit. Care Pain* **5**, 98–100 (2005).

227. Becske, T. & Nelson, P. K. The Vascular Anatomy of the Vertebro-Spinal Axis. *Neurosurg. Clin. N. Am.* **20**, 259–264 (2009).

228. Desjardins, A. E. *et al.* Epidural needle with embedded optical fibers for spectroscopic differentiation of tissue: ex vivo feasibility study. *Biomed. Opt. Express* **2**, 1452 (2011).

229. Hogan, Q. Distribution of solution in the epidural space: Examination by cryomicrotome section. *Reg. Anesth. Pain Med.* **27**, 150–156 (2002).

230. Buffington, C. W., Nichols, L., Moran, P. L. & Blix, E. U. M. Direct connections between the spinal epidural space and the venous circulation in humans. *Reg. Anesth. Pain Med.* **36**, 134–139 (2011).

231. Ummenhofer, W. C., Arends, R. H., Shen, D. D. & Bernards, C. M. Comparative spinal distribution and clearance kinetics of intrathecally administered morphine, fentanyl, alfentanil, and sufentanil. *Anesthesiology* **92**, 739–753 (2000).

232. Walker, M. A. *et al.* Volumetric evaluation of lumbar epidural fat distribution in epidural lipomatosis and back pain in patients who are obese: Introducing a novel technique (Fat Finder algorithm). *BMJ Open Diabetes Res. Care* **7**, 1–8 (2019).

233. Arslan, M. *et al.* Surgical view of the lumbar arteries and their branches: An anatomical study. *Neurosurgery* **68**, 16–22 (2011).

234. Espahbodi, S., Doré, C. J., Humphries, K. N. & Hughes, S. P. F. Color doppler ultrasonography of lumbar artery blood flow in patients with low back pain. *Spine (Phila. Pa. 1976).* **38**, (2013).

235. Bernards, C. M. *et al.* Pharmacokinetics of Epidural Opioids (Part 1) Differences among Opioids. *Anesthesiology* 455–465 (2003).

236. Reina, M. A., Franco, C. D., López, A., Dé Andrés, J. A. & van Zundert, A. Clinical

implications of epidural fat in the spinal canal. A scanning electron microscopic study. *Acta Anaesthesiol. Belg.* **60**, 7–17 (2009).

237. Bjorkman, S., Stanski, D. R., Verotta, D. & Harashima, H. Comparative tissue concentration profiles of fentanyl and alfentanil in humans predicted from tissue/blood partition data obtained in rats. *Anesthesiology* 865–873 (1990).

238. Palm, K., Luthman, K., Ros, J., Gråsjo, J. & Artursson, P. Effect of molecular charge on intestinal epithelial drug transport: pH- dependent transport of cationic drugs. *J. Pharmacol. Exp. Ther.* **291**, 435–443 (1999).

239. Bower, S. & Hull, C. J. Comparative pharmacokinetics of fentanyl and alfentanil. *Br. J. Anaesth.* **54**, 871–877 (1982).

240. Stanski, D. R. & Hug, C. C. Alfentanil - a kinetically predictable narcotic analgesic. *Anesthesiology* **57**, 435–438 (1982).

241. Ferrier, C. *et al.* Alfentanil pharmacokinetics in patients with cirrhosis. *Anesthesiology* 480–484 (1985).

242. Kharasch, E. D. *et al.* The role of cytochrome P450 3A4 in alfentanil clearance. *Anesthesiology* 36–50 (1997).

243. Phimmasone, S. & Kharasch, E. D. A pilot evaluation of alfentanil-induced miosis as a noninvasive probe for hepatic cytochrome P450 3A4 (CYP3A4) activity in humans. *Clin. Pharmacol. Ther.* 505–17 (2001).

244. Kharasch, E. D., Walker, A., Hoffer, C. & Sheffels, P. Intravenous and oral alfentanil as in vivo probes for hepatic and first-pass cytochrome P450 3A activity: Noninvasive assessment by use of pupillary miosis. *Clin. Pharmacol. Ther.* **76**, 452–466 (2004).

245. Kharasch, E. D. *et al.* Sensitivity of intravenous and oral alfentanil and pupillary miosis as

minimal and noninvasive probes for hepatic and first-pass CYP3A induction. *Clin. Pharmacol. Ther.* **90**, 100–108 (2011).

246. Abduljalil, K., Cain, T., Humphries, H. & Rostami-hodjegan, A. Deciding on Success Criteria for Predictability of Pharmacokinetic Parameters from In Vitro Studies : An Analysis Based on In Vivo Observations s. *Drug Metab. Dispos.* **42**, 1478–1484 (2014).

247. Coda, B. A., Brown, M. C., Schaffer, R. L., Donaldson, G. & Shen, D. D. A pharmacokinetic approach to resolving spinal and systemic contributions to epidural alfentanil analgesia and side-effects. *Pain* **62**, 329–337 (1995).

248. Coda, B. A., Brown, M. C., Risler, L., Syrjala, K. & Shen, D. D. Equivalent analgesia and side effects during epidural and pharmacokinetically tailored intravenous infusion with matching plasma alfentanil concentration. *Anesthesiology* 98–108 (1999).

249. Rauck, R. *et al.* Pharmacokinetics and safety of fentanyl sublingual spray and fentanyl citrate intravenous: a single ascending dose study in opioid-naïve healthy volunteers. *Curr. Med. Res. Opin.* **33**, 1915–1920 (2017).

250. Ginosar, Y., Riley, E. T. & Angst, M. S. The Site of Action of Epidural Fentanyl in Humans: The Difference Between Infusion and Bolus Administration. *Anesth. Analg.* **97**, 1428–1438 (2003).

251. Badner, N. H. *et al.* Lumbar epidural fentanyl infusions for post-thoracotomy patients: analgesic, respiratory, and pharmacokinetic effects. *J. Cardiothorac. Anesth.* **4**, 543–551 (1990).

252. Yu, C., Yuan, M., Yang, H., Zhuang, X. & Li, H. P-glycoprotein on blood-brain barrier plays a vital role in fentanyl brain exposure and respiratory toxicity in rats. *Toxicol. Sci.* **164**, 353–362 (2018).

253. Ghassabian, S. *et al.* High-throughput assay for simultaneous quantification of the plasma concentrations of morphine, fentanyl, midazolam and their major metabolites using automated SPE coupled to LC-MS/MS. *J. Chromatogr. B* **903**, 126–133 (2012).

254. Fernando, R. *et al.* Neonatal welfare and placental transfer of fentanyl and bupivacaine during ambulatory combined spinal epidural analgesia for labour. *Anaesthesia* **52**, 517–524 (1997).

255. Labroo, R. B., Paine, M. F., Thummel, K. E. & Kharasch, E. D. Fentanyl metabolism by human hepatic and intestinal cytochrome P450 3A4: Implications for interindividual variability in disposition, efficacy, and drug interactions. *Drug Metab. Dispos.* **25**, 1072–1080 (1997).

256. Ke, A. B., Rostami-Hodjegan, A., Zhao, P. & Unadkat, J. D. Pharmacometrics in Pregnancy: An Unmet Need. *Annu. Rev. Pharmacol. Toxicol.* **54**, 53–69 (2014).

257. Ke, A. B., Greupink, R. & Abduljalil, K. Drug Dosing in Pregnant Women: Challenges and Opportunities in Using Physiologically Based Pharmacokinetic Modeling and Simulations. *CPT Pharmacometrics Syst. Pharmacol.* 103–110 (2018).

258. Mazoit, J. X. & Dalens, B. J. Pharmacokinetics of Local Anaesthetics in Infants and Children. *Clin. Pharmacokinet.* **43**, 17–32 (2004).

259. Emanuelsson, B.-M. K., Persson, J., Alm, C., Heller, A. & Gustafsson, L. L. Systemic absorption and block after epidural injection of ropivacaine in healthy volunteers. *Anesthesiology* **87**, 1309–17 (1997).

260. Shum, S. *et al.* Maternal-fetal disposition of domoic acid following repeated oral dosing during pregnancy in nonhuman primate. *Toxicol. Appl. Pharmacol.* **398**, 115027 (2020).

261. Stuchal, L. D. *et al.* Dose-response assessment for impaired memory from chronic

exposure to domoic acid among native American consumers of razor clams. *Regul. Toxicol. Pharmacol.* **117**, 104759 (2020).